A survey of hot stars in the CoRoT anticentre fields:
Classification and analysis of light curves and spectra

DIPLOMA THESIS

of

Raoul Gerber

from

Erlangen, Germany

Performed at the
Dr. Karl Remeis-Observatory Bamberg & ECAP
(Astronomical Institute of the University of Erlangen-Nuremberg)
Sternwartstraße 7, 96049 Bamberg

Supervised by
Prof. Dr. Ulrich Heber

February 2012

Abstract

The diverse galactic population contains many different kinds of stars, like evolved horizontal branch stars, white dwarfs, main sequence stars, and substellar objects which could not ignite hydrogen burning (brown dwarfs). More than half of all stars reside in binary systems. Therefore, binary systems are important tools because they allow the determination of stellar masses and radii. Light curves offer the possibility to detect eclipsing binary system. Their shape gives information about the objects orbiting each other. In this thesis the nature of binary systems composed of at least one hot star are investigated by a quantitative spectral analysis and light curve analysis.

The aim of this thesis was to identify eclipsing binary systems in three observed fields of the satellite and to classify the components. Especially, it was hoped to find systems with white dwarfs, highly evolved hot stars, or even exoplanets as components. Unprecedented high quality photometry obtained by the CoRoT ("Convection, Rotation and planetary Transits") form the basis of this thesis.

The CoRoT space mission was started already in 2006 and measured over a hundred thousands of stars. In chapter 3, the classification of light curves and physics of eclipsing binary systems is introduced. The frequency analysis tool FAMIAS and the programme SPAS which was used to fit the spectra are described in Chapter 4! The main part of the work is put into chapter 5. More than 8000 spectra had to be investigated to classify the stars on the basis of the temperature. Therefore, the spectra were personally inspected and the cool stars sorted out, since I wanted to focus on hot stars. To be well prepared to investigate the light curves in more detail, a small introduction to the properties of CoRoT light curves putting special emphasis on the observational perturbations like contaminations and stray light was given in section 5.1. In the next step, 1654 hot stars were classified with the help of their light curve. The duration of up to 150 days enabled the detection of binary systems with periods of up to 75 days. On the other hand, the astonishing accuracy of CoRoT revealed transits depths of 1% and oscillating stars with high frequencies as well as binaries with very short periods. At the end of the light curve classification, 484 oscillating stars and 59 eclipsing binaries were classified. The eclipsing binary systems detected were investigated in more detail in section 5.4. Firstly, the parameters like the orbital period, eclipse depth and the duration of the eclipse were determined from the light curve. Secondly, synthetic spectra were fitted to their spectra to determine the surface gravity (g) and the effective temperature (T_{eff}). This allowed a rough approximation of the evolutionary stage of the stars with the help of the T_{eff} and $log\ g$ diagram. Unfortunately, there was no clear evidence of a hot evolved star. Nevertheless, interesting candidates, whose parameters are close to those of horizontal branch stars, were found. At the end of this chapter the systems with periods shorter than 1 day, or surface temperature higher than 15,000K and periods shorter than 2 days were selected. Their light curves were phase folded and reviewed. In total, four binary systems with orbital periods shorter than 1 day were found. The system CoRoT 110666679 with a period of 0.36 days is so close that it can not be composed of two main sequence stars of spectral type A. Moreover, the system CoRoT 102714427 with an orbital period of 1.89 days shows strong ellipsoidal deformations combined with a small primary eclipse which could result from a compact companion. Moreover, I investigated 1782 light curves during the collaboration meeting in Cologne again. We detected 13 new hot stars showing shallow transits in their light curves which may results from planetary companions.

I also participated in a project to identify hot subdwarf B stars from light curves. Chapter 6 describes the photometric observation of subdwarf B stars done by myself in October 2011 at the Calar Alto observatory in Spain. Among the four stars measured during the five days, one new rare HW Virgines system with a strong reflection effect and a period shorter than 0.17 days was discovered.

The final chapter 7 briefly summarises the results and gives a short outlook of what might follow.

Zusammenfassung

Die vielseitige galaktische Population besteht aus vielen verschiedenen Arten von Sternen. Das wären zum Beispiel entwickelte Horizontalaststerne, Weiße Zwerge, Hauptreihensterne und substellare Objekte, welche kein Wasserstoffbrennen nicht zünden konnten (Braune Zwerge). Mehr als die Hälfte der Sterne befindet sich in Doppelsternsystemen. Daher, und weil sie es erlauben, die Massen und Radien der Komponenten zu bestimmen, sind Doppelsternsysteme wichtige Wekzeuge. Lichtkurven bieten die Möglichkeit, bedeckende Doppelsternsysteme zu entdecken. Ihre Form gibt Aufschlüsse über die sich umkreisenden Objekte. In dieser Arbeit wird die Natur der Doppelsterne bestehend aus mindestens einem heißen Stern mit Hilfe einer quantitativen Spektralanalyse und einer Lichtkurvenanalyse näher untersucht.

Das Ziel dieser Diplomarbeit war die Identifizierung bedeckender Doppelsternsysteme in den drei beobachteten Feldern des Satelliten und die Klassifizierung der Komponenten. Es wurde besonders gehofft, Systeme mit Weißen Zwergen, weit entwickelten heißen Sternen oder sogar Exoplaneten als Komponenten zu finden. Die hohe photometrische Qualität, die von CoRoT ("Convection, Rotation and planetary Transits") erreicht wird, bildeten die Basis für diese Arbeit.

Die CoRoT Weltraummission startete bereits im Jahr 2006 und beobachtete bereits über hunderttausend Sterne. In Kapitel 3 wird die Klassifikation von Lichtkurven und die Physik der bedeckenden Doppelsterne eingeführt. Das Frequenzanalyse Werkzeug FAMIAS und das Programm SPAS, welches zum Fitten der Spektren benutzt wurde, werden in Kapitel 4 näher erklärt. Der Hauptteil dieser Diplomarbeit steht im Kapitel 5. Mehr als 8000 Spektren wurden untersucht, um die Sterne an Hand ihrer Temperatur zu klassifizieren. Dafür wurden die Spektren einzeln angeschaut und die kühlen Sterne aussortiert, weil die Zielobjekte dieser Arbeit die heißen Sterne waren. Um eine genaue Lichtkurvenanalyse machen zu können, wurde vorher eine kleine Einführung zu Effekten und speziell Störungen in den Lichtkurven gegeben. Im nächsten Schritt, wurden 1654 Sterne an Hand der Form ihrer Lichtkurve klassifiziert. Die Länge von über 150 Tagen ermöglichte die Entdeckung von Doppelsternsystemen mit einer Umlaufzeit von bis zu 75 Tagen. Durch die hohe Genauigkeit war es außerdem, möglich kleine Transits mit bis zu einer Tiefe von 1% zu entdecken. Dadurch konnten außerdem oszillierende Sterne mit hohen Frequenzen und Doppelsterne mit sehr kurzen Umlaufperioden entdeckt werden. Am Ende der Lichtkurvenklassifikation, wurden 484 Sterne als oszillierend und 59 Sterne als bedeckende Doppelsterne klassifiziert. Im Abschnitt 5.4 wurden die Doppelsterne näher untersucht. Zu erst wurden Parameter wie die Umlaufperiode, Bedeckungstiefe und Bedeckungsdauer aus der Lichtkurve bestimmt. Als nächstes wurden synthetische Spektren an die Spektren gefittet, um die Effektivtemperatur (T_{eff}) und die Schwerebeschleunigung an der Oberfläche (g) zu bestimmen. Dies erlaubte eine grobe Bestimmung des Entwicklungsstadiums der Sterne mit Hilfe eines T_{eff} und $log\ g$ Diagramms. Leider gab es keinen klaren Kandidaten für einen heißen entwickelten Horizontalaststerns. Trotzdem gab es ein paar interessante Kandidaten, deren Parameter nahe an den Bereich des Horizontalastes heran kamen. Am Ende dieses Kapitels wurden die Doppelsterne mit Perioden kürzer als 1 Tag, oder mit effektiv Temperaturen höher als 15000 K und Perioden kürzer als 2 Tage ausgewählt. Ihre Lichtkurven wurden phasengefaltet und nochmals untersucht. Vier Doppelsterne mit Umlaufperioden kürzer als 1 Tag wurden gefunden. Das System CoRoT 110666679 mit einer Periode von 0.36 Tagen ist so eng, dass die Komponenten keine Hauptreihensterne der Spektralklasse A sein können. Desweiteren zeigt das System CoRoT 102714427 mit einer Umlaufperiode von 1.89 Tagen eine starke Ellipsoidalverformung, kombiniert mit einer flachen Bedeckung. Dieses System könnte einen Weißen Zwerg als Begleiter besitzen. Zusätzlich wurden 1782 Lichtkurven während des Kollaborationstreffens in Köln nochmals begutachtet. Dabei wurden 13 neue heiße Sterne mit sehr flachen Bedeckungen gefunden. Die Bedeckungen könnten durch Planeten erzeugt worden sein.

Außerdem habe ich mich an einem Projekt beteiligt, in dem Unterzwerge der Sepektralklasse B mit Hilfe von Lichtkurven klassifiziert wurden. In Kapitel 6 wurde die photometrische Beobachtung eines

Unterzwerges der Spektralklasse B durch mich im Oktober 2011 am Calar Alto in Spanien durchgeführt. Unter den vier aufgenommen Sternen in den fünf Tagen befand sich ein seltenes neues HW-Virginis System mit einem starken Reflektionseffekt und einer Umlaufperiode von nur 0.17 Tagen.

Das letzte Kapitel 7 fasst die Ergebnisse dieser Arbeit kurz zusammen und gibt einen Ausblick auf weitere Untersuchungen.

Contents

1. Introduction

Currently, one of the most highly topical field of research within astronomy is the search for exoplanets. There are many articles about newly discovered exoplanets as well as websites containing exoplanet databases. Even during guided tours at the Dr. Karl Remeis-Sternwarte in Bamberg by myself, questions about planets in other solar systems appeared frequently. The search of exoplanets could answer the question whether the Earth is a unique planet, offering the environment for intelligent life to arise and evolve.
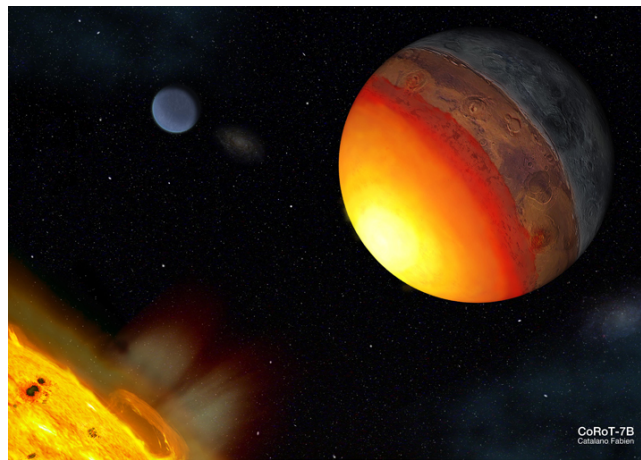

Figure 1.1.: An artist's impression[2] of the Earth-like planet CoRoT-7b

At the moment, two space missions are running and are dedicated for the search of exoplanets. The first one, launched already in 2006, is the CoRoT mission. It measures the brightness of hundred thousands of stars continuously. The aim is to detect brightness dips caused by cool objects passing in front of the stars. The other one, Kepler but of no importance for this thesis.

Until now, the exoplanet search concentrated on cool stars. Nevertheless, other small or compact objects besides planets exist which cause similar brightness variations. White dwarfs which have radii similar to the Earth will have similarly shallow depth of eclipses. This mission offers the accuracy and unique opportunity to find white dwarfs in binary systems as companions. New white dwarf candidates would help to understand the stellar evolution in more detail and to set new constraints on the white dwarf population. Moreover, substellar companions, like brown dwarfs, which are unable to ignite hydrogen burning the core, could be abundant in the huge data archive. All these objects have been ignored until now but are highly interesting and hardly detectable with other methods. In addition, main sequence hot stars as well as hot evolved stars have not been investigated yet, and offer an immense dataset containing unknown binary systems.

We decided to take the chance and to focus on the investigation of stars with spectral type O, B and A. It was expected to find new candidates of compact companions like white dwarf and substellar companions (exoplanets and brown dwarfs). Moreover, we hoped to find evolved horizontal branch stars among the hot stars, in particular subdwarf B stars. For this purpose, a collaboration with the Thüringer Landessternwarte in Tautenburg and the Institut für Geophysik und Meteorologie in Cologne was established. The colleagues provided us with spectra and light curves of the CoRoT objects. This way we had all necessary data to start the investigation of hot stars in the CoRoT field.

---

[2]`http://www.ias.u-psud.fr/`

2. The CoRoT Space mission

Every day a star rises above the horizon, it is our home star, the Sun. In principle it is not a special star, its spectral class is G2 and the surface temperature is a bit lower than 6000 Kelvin. Eight planets orbit the Sun, including our Earth. The Sun is active, eruptions throw matter into space, star spots appear and disappear. But how does the interior of the Sun and of other stars look like? Do other stars exist with planets similar to the Earth? CoRoT wants exactly to answer these questions. The name **Co**nvection, **Ro**tation and planetary **T**ransits (CoRoT) (Baglin et al., 2002) briefly describes the contents of the mission, asteroseismology and the search for exoplanets by measuring light curves. Seismology already proved to be powerful describing the interior of the Sun, with a precise instrument like CoRoT it can help to understand the physics of stars better.

The project is led by the French space agency CNES together with the space agencies of some other European countries, top space research institutes from Belgium, Brazil, Austria, Germany, Spain and the European Space Agency (ESA). The satellite weight is 630 kg, it is about 4.2 m high and has a mean diameter of 2 m. After long preparations and constructions it was finally launched on the 27th December 2006 from the Baikonour Kosmodrome into a polar low Earth orbit (LEO) with a period of 6184 s (Auvergne et al., 2009). The polar orbit has the huge advantage to allow uninterrupted observations for nearly half a year into the same direction as demonstrated in Fig. 2.1. As seen the
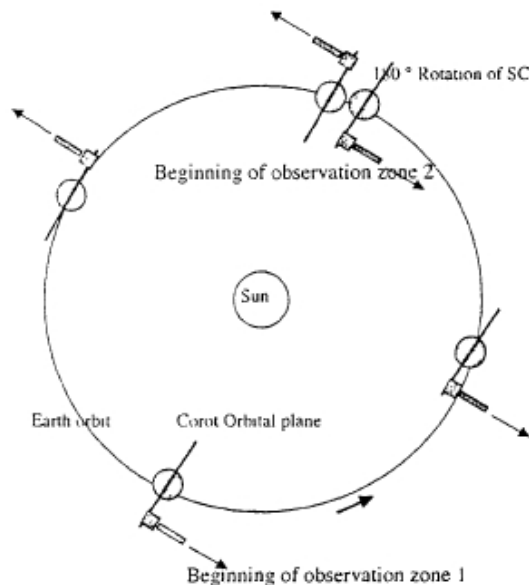

Figure 2.1.: Polar orbit of CoRoT(Baglin et al., 2002)

telescope must be turned twice during a year to avoid the Sun light entering the camera. Each half year period is divided into a long run (150 days) and 2 shorter runs (10 to 20 days) (Baglin et al., 2002). The LEO also brings up some problems, like stray light and eclipses of the Sun with the Earth which will be discussed later in chapter 5.

In the beginning the asteroseismology was the main motivation for the satellite, but this changed after 1995 when the first extrasolar giant planet was found. Therefore, the mission was divided into 2 main programmes: the seismology programme and the exoplanet programme, detailed information will be given later in their own subsections.

The satellite is equipped with four CCDs, two for each main programme. These are frame-transfer thinned, back-illuminated detectors consisting of 2048x2048 pixels in the image zone and are operated

on a temperature of -40 deg C. Unfortunately, 2 CCDs went out of operation in 2009, therefore each program has only 1 CCD left. The two scientific programmes run at the same time on nearby regions of the sky. They are separated only in the focal plane but use the same optics. To maximise the observed stars the satellite is pointed towards the centre and respectively the anti-centre of the Milky Way because the star density is very high in those regions. The field of view is 4 square degrees and up to 12000 stars are observable simultaneously. The first run started in February 2007 and the mission was scheduled for 3 years, but another 3 years were approved. At present, another extension request was submitted.

2.1. Seismology programme

As mentioned above, the seismology programme was the motivation for the satellite. The high photometric accuracy and long uninterrupted durations (150 days) of the satellite can not be achieved by ground based observations. In general, the targets are brighter than the objects for the exoplanet program and are therefore highly defocused to avoid saturation on bright objects. Because of the high time resolution (32 s exposure time) the data volume is very big and therefore approximately only 50 targets will be measured during the long runs. The data achieved are needed to understand the nature of transport processes in the interior of stars during the main sequence which represents about 90% of the stellar lifetime. Since the short programs last only 10 to 20 days it is possible to record much more stars which enables to measure wider range of oscillatory behaviour across the Hertzsprung-Russell diagram.

2.2. Planet finding programme

The targets for the planet finding programme are stars with 11-16 mag. In contrast to the seismology programme CCD, a small bi-prism is located in front of the planet finding programme CCD to allow relative broad band photometry in visible light. The aim is to find planets similar or slightly larger than the Earth, in the habitable zone and closer.

In the past, most searches for planets were performed by radial velocity measurements. As an example, the response of the Sun to the orbital motion of Jupiter is only 13 ms^{-1}. Therefore, high accuracy is needed to detect such planets via the Doppler shift. Nevertheless, in 1995 a giant planet around the solar-type star 51 Peg was discovered. The fact that the planet orbits the star at a distance of only 0.05 AU, which is even inside Mercury's orbit in our solar system, changed the ideas of planetary formation (Mayor & Queloz, 1995). Still the terrestrial exoplanets were missing and CoRoT took up the challenge to detect these planets with the transit method. During a transit, when the planet passes between the star and the observer, the received flux decreases and causes a small dip in the light curve. Of course
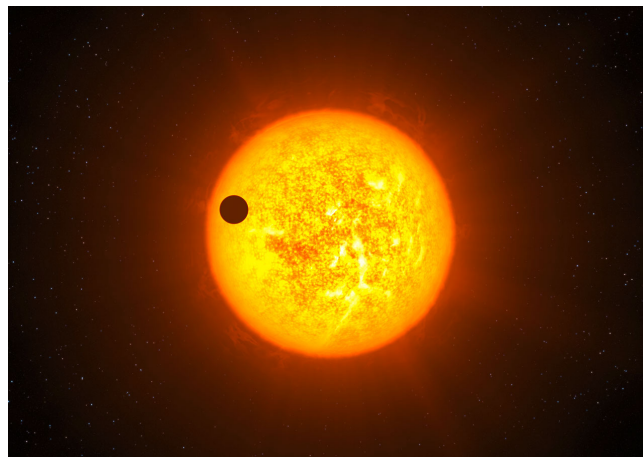

Figure 2.2.: Artistic view of a transit(eso)

these transits only occur if the line of sight lays close to the orbital plane of the planet. The geometrical probability for this is 0.5% for the Earth, 0.1% for Jupiter and 16% for 51 Peg b (Baglin et al., 2002). A large amount of stars is measured to increase the chance to detect such planets. Additionally, a high accuracy is needed to detect the small luminosity decreases of a star occulted by its planets. A Jupiter like planet has a transit event with a relative amplitude of 10^{-2} while an Earth like planet only has a relative amplitude of 8.10^{-4}. Even so CoRoT should be able to detect close-in planets similar to Earth. This was proved with the detection of CoRoT-7b. Many different results are published but all agree that the radius is smaller than 2 times the radius of the Earth and the mass lies between $2.3 \pm 1.8 M_{\text{Earth}}$ and $8.0 \pm 1.2 M_{\text{Earth}}$ (Carone et al., 2011). The uncertainties in the radial velocity, on which the mass calculation is depending, came from the host star pulsations. The pulsations scattered the radial velocity and consequently the mass derivations. Hatzes et al. (2011) specified the mass to $7.42 \pm 1.21 M_{\text{Earth}}$ by taking a corrected radial velocity curve. This mass is so far the most accurate result for CoRoT-7b. The transit depth was only 0.3 mmag with a period of 0.854 days (Pont et al., 2011). Until April 2011, 12 exoplanets have been discovered by CoRoT and approved by ground based Doppler-shift measurements (Lammer et al., 2010). At present (28.11.2011) 22 exoplanets are listed in the exoplanet catalogue which were detected by CoRoT with the transit method [1].

Besides planets, stars can eclipse each other. These systems are called eclipsing binaries and will be described in the following chapter. With lower inclination, the light curves contain only grazing eclipses and the secondary (smaller) eclipse may even disappear completely. Therefore, radial velocity measurements are needed to approve planets. Radial velocity variations constrain the companion's mass and are irreplaceable to distinguish between an eclipsing binary system or a planetary transit.

---

[1] http://exoplanet.eu

3. Binary stars

Shortly after the Sun disappears, the first shining points appear on the sky. Deep in the night the sky offers us an incredible amount of stars. Some stars seem to be very close to each other, but are probably independent. Nevertheless, around half of the stars have a companion and form a binary system. These stars are gravitationally bound and orbit around their common centre of mass. This chapter will give a short introduction to binary systems and, in particular, to eclipsing binary systems. The close binary systems, with stars so close that they distort or heat each other's surfaces through irradiation, will receive special attention. At the end, the spectral class of subdwarf B (sdB) stars will be introduced, which is closely linked to binary systems.

3.1. Introduction to binary systems

Astronomy always tried to determine stellar parameters like the mass, the radius and the surface temperature. In the case of the Sun, these parameters are well-known. But how about other stars? Our closest neighbour, the star Alpha Centauri, is located at a distance of 4.2 light years. The distance makes it difficult to investigate the stellar parameters.

The determination of masses needs observable gravitational interaction. One possibility is a planet-star interaction which could be used to specify the mass of the Sun. Another is a star-star interaction, and here it is where the binary systems take their important role. Newton demonstrated first that a spherical body with a total mass m has the equivalent gravitational field outside its sphere as a point mass m located at the centre of the sphere. Generally, stars in binary systems can be approximated by spheres (except for very close systems) and therefore treated like two point masses orbiting each other in their mutual gravitational field. This two body problem is solvable and it is the basis of Kepler's laws.

Binaries can be split into different types, the resolvable visual binaries, the spectroscopic binaries and the eclipsing binaries. Each of these types provides us with different information to determine stellar masses.

3.1.1. Visual binaries

Binaries in which the stars are resolvable are called visual binaries. They were the first sources allowing for the determination of masses of stars besides the Sun. Kepler's third law

$$G(m_1 + m_2) = \frac{4\pi^2 a^3}{P^2} \tag{3.1}$$

connects the orbital period P and the relative separation a of the stars with the sum of their stellar masses $(m_1 + m_2)$, where G is the gravitational constant. The period can be determined from examining the orbit. For the semi major axis a the distance is needed which can be measured with the parallax method. Together with the angular separation the semi major axis a is determined. The individual masses can only be determined with the knowledge of the individual absolute orbits. With a_1 and a_2 , it is possible to calculate the mass ratio from

$$a_1 * m_1 = a_2 * m_2 \; . \tag{3.2}$$

The mass ratio together with equation 3.1 lead then directly to the individual masses. Since the resolution of telescopes is limited, only a small fraction of binaries are resolvable. Despite this, their absolute separation is large which makes the determinations of the period and the orbit a long and difficult process. In the case of a faint star which is not visible, having a partner whose orbital movement is measurable, the system is called astrometric.

3.1.2. Spectroscopic binaries

By the end of the nineteenth century, the importance of spectroscopy for the astronomy rose. This technology allowed to measure the line of sight velocity V with the help of the Doppler-shift.

$$\frac{\lambda - \lambda_0}{\lambda_0} = \frac{V}{c} \ . \tag{3.3}$$

The difference of the measured wavelength λ to the wavelength in rest λ_0 gives the radial velocity V. Stars flying towards the observer have spectroscopic lines shifted to the shorter wavelengths. Apparently, single stars showed radial velocity variations and they were identified as binaries, or more precisely spectroscopic binaries. If the spectrum is composite, then the system is called a double lined spectroscopic binary, else a single lined spectroscopic binary. Recording spectra in continuous time intervals results in a radial velocity (RV) curve. Fig. 3.1 shows the RV curves of both stars of a binary with a circular orbit. RV curves from both components allow the determination of the projected
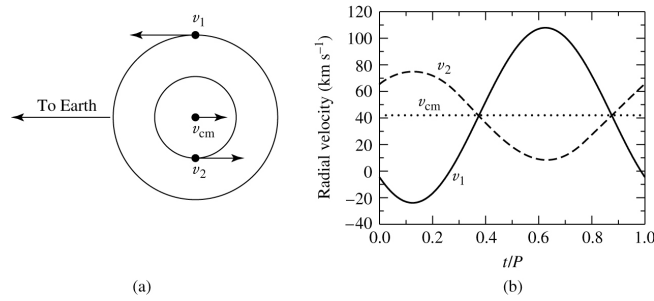

Figure 3.1.: Exemplary radial velocity curve (Caroll & Ostlie, 2006, Chapter 7). The left hand image shows the orbit and the line of sight. The complete RV curve is plotted in the right hand figure. The first star has a semi amplitude K_1 of around $65 \ \frac{km}{s}$ and the second $K_2 = 30 \ \frac{km}{s}$. When the star moves towards the Earth the velocity becomes negative, else positive. The barycentric velocity additionally shifts the sinusoidal (circular orbit) RV curve by a constant amount. In this example the system velocity v_{cm} is marked with a dotted line and equals $40 \ \frac{km}{s}$.

semi major axis $a_1 \sin i$ or $a_2 \sin i$ of the barycentric orbits from the period P, eccentricity e and the semiamplitude K_1 or K_2 through

$$a_{1,2} \sin i = \frac{(1 - e^2)^{\frac{1}{2}}}{2\pi} K_{1,2} P \ . \tag{3.4}$$

Using

$$m_1 a_1 = m_2 a_2 \tag{3.5}$$

in the left side of equation 3.1 and solving for $m_1 \sin^3 i$ leads to

$$m_1 \sin^3 i = \frac{4\pi^2}{GP^2} \frac{a^3 \sin^3 i}{1 + \frac{a_1 \sin i}{a_2 \sin i}} \ . \tag{3.6}$$

Substituting $a \sin i = a_1 \sin i + a_2 \sin i$ in equation 3.6 and using equation 3.4 for $a_{1,2}$ results in the formula for the minimum masses $m_{1,2} \sin^3 i$

$$m_{1,2} \sin^3 i = \frac{1}{2\pi G} (1 - e^2)^{\frac{3}{2}} (K_1 + K_2)^2 K_{2,1} P \ . \tag{3.7}$$

If the inclination i can be determined, it is possible to calculate the absolute masses. Double lined spectroscopic binaries provide most information and need a minimum of assumptions. They provide a lot of stellar parameters and help to understand the stellar population.

3.2. Eclipsing binary stars

As soon as the photographic plates were invented, the systematic search for variable stars started. Already in 1922 the institute in Bamberg started the search for variable stars. At that time, a section of the sky was recorded onto a photographic plate and compared to photographic plates taken at different times. This work was very time consuming but successful. Today, the brightness of stars is measured with the help of CCDs. Computers help to extract the brightness information from the two dimensional images. In a light curve, in which the brightness is plotted against time, a non constant brightness level hints at variability of the star. There are mainly 3 types of variable stars. First the eruptive variables like novae, secondly, radially and non-radially oscillating stars, and thirdly the geometrically variable stars, also known as eclipsing binary stars. The latter play the main role in this work and need special attention.

3.2.1. Light curve

As mentioned above, radial velocity curves from double lined binaries provide us with the information needed to investigate their orbital parameters and masses. Light curves also offer orbital information, like the period, the eccentricity and the inclination of the system. But this is the only overlap between radial velocity and light curves. None is basically replaceable by the other, and the information derivable is quite different. Light curves offer us the stellar radii relative to the separation a, and relative to each other. Additionally, they contain information about the surface brightness and the shape of the stars. RV curves on the other hand, deliver us absolute values of the velocity and therefore of the orbit, which leads to the masses and the separation in absolute values.

Eclipses

It is important to note that only the sum of the brightness of the stars is measurable because usually the stars in the system are so close together that the brightness is not measurable separately. The light variations from eclipsing binaries during an orbital period result from deformations, heating effects and eclipses. Since the circumstances, in which an eclipse occurs, are very restricted, and therefore very rare. For spherical stars, the condition to see an eclipse is

$$\sin\left(90° - i\right) \leq \frac{(R_1 + R_2)}{a} \ , \tag{3.8}$$

where R_1 and R_2 are the stellar radii, a is the separation and i is the inclination. As can be seen, high inclination and a close orbit increase the chances of an eclipse significantly. A schematic light curve with eclipses is shown in Fig. 3.2. The primary eclipse (A) happens when then brighter star gets occulted by the fainter star. The secondary (B) eclipse is due to the eclipse of the fainter star.

At the beginning (1), the hotter star gets occulted by the larger cooler star. Limb darkening smooths the edges of the eclipse at the ingress (1,2) phase. After the hot star has disappeared completely behind its companion (2), a constant light level is reached until the edge of the star appears on the other side (3). Again, limb darkening smooths the edges during the egress of the total eclipse (3,4). The secondary eclipse is not as deep, since the cool star's surface gets occulted by the hot star's surface, which contributes a higher fraction of the brightness. With the help of the orbital phase φ the relative stellar radii can be calculated,

$$(\varphi_2 - \varphi_1) = (\varphi_4 - \varphi_3) = \frac{2R_1}{2\pi a} \ , \tag{3.9}$$

$$(\varphi_3 - \varphi_1) = (\varphi_4 - \varphi_2) = \frac{2R_2}{2\pi a} \ . \tag{3.10}$$

R_1 is the radius of the hot star, R_2 of the cooler star and a is their separation.
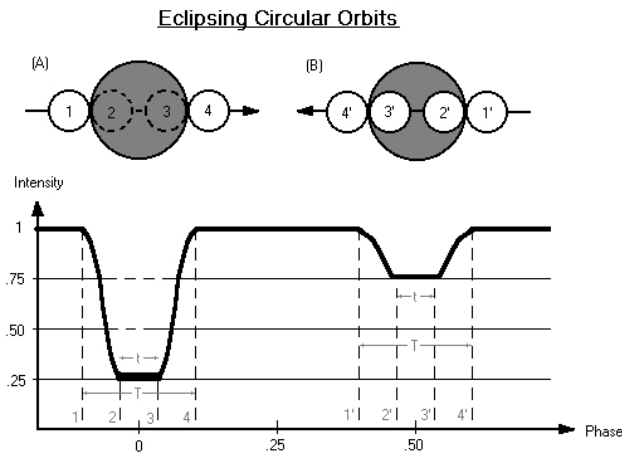
Figure 3.2.: Light curve of a total eclipse[2]. The hotter star is represented by the white circle, the grey represents the cooler star.

3.3. Close binary systems

After the introduction to binary systems and specially to eclipsing binary systems, I want to take a closer look at close binary systems. A system is close, when the components interact during their evolution at least once. Also, the stars in many of these systems are tidally locked, which leads to synchronised and circular orbits. Synchronization is achieved when the rotation of the star has the same period as the orbit. Close binary systems play an important role, they help to understand the physics of stellar interactions and the formation of peculiar stars. Additionally, the chances for an eclipsing system are higher, since the orbital separations are small. In a usual light curve analysis, one tries to fit a synthetic light curve derived from the Roche model (see below) to the measured light curve. The least squares method is used to determine the stellar parameters. The corresponding model is very complex and has on average 12+5n free parameters (n = number of light curves). Unfortunately, these parameters are correlated which complicates the problem. Without additional knowledge of the systems, it is practically impossible to find the real solution.

Roche model

The model to predict the light variations is named after the mathematician Edouard Roche (1849) and considers the deformations of the components. Originally, he investigated the mathematics of the restricted three-body problem and also found out that for a given total gravitational potential Φ, there is an equipotential surface where the third particle would feel no force in the rotating coordinate system. Since the surface of a star is a equipotential surface, the model defines the shape of stars. The following assumptions have to be made to be able to use the model:

- Because stars have most of their mass concentrated in the core, the mass distribution is approximated by a point mass.

- The rotations of the stars are assumed to be tidally locked to the orbital period. This is valid for close binary systems with convective stars, since synchronization sets in pretty fast, which is established very quickly in the formation of the binary.

- The rotation axis of the stars must be perpendicular to the orbital plane.

- Orbits need to be circular which is achieved quickly due to the tidal forces.

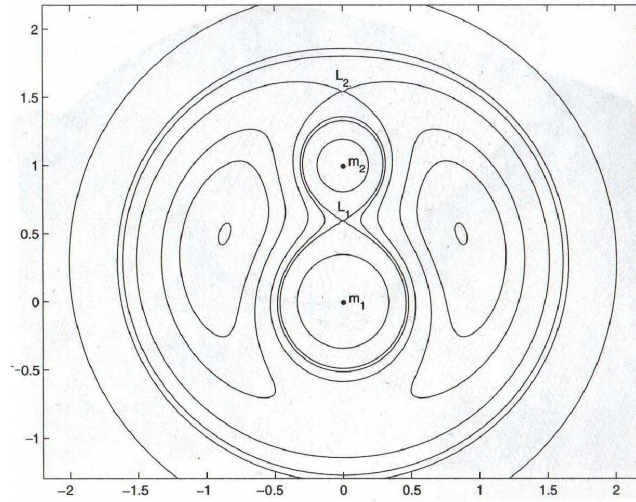[2]`https://www.msu.edu/~mckinn38/Binary_Stars/eclipsing.htm`

Figure 3.3.: A cut through equipotential surfaces in the orbital plane (x,y) for a mass ratio q= 0.4. The potential lines close to the mass points are circles. On the other hand, the lines close to the L1 point are very deformed. Therefore, stars close to filling their Roche lobe, can not be approximated with spherical surfaces. (Hilditch, 2001)

In the co-rotating coordinate system, the gravitational potential Φ only depends on the centrifugal force and the two point mass gravitational forces,

$$\Phi = -\frac{Gm_1}{r_1} - \frac{Gm_2}{r_2} - \frac{\omega^2}{2}\left(\left(x - \frac{m_2}{m_1 + m_2}\right)^2 + y^2\right) \text{ with} \tag{3.11}$$

$$r_1 = \sqrt{(x^2 + y^2 + z^2)} \text{ and } r_2 = \sqrt{(x-1)^2 + y^2 + z^2} \ .$$

The star with m_1 is set to $(x, y, z) = (0,0,0)$, the second star with m_2 to (1,0,0) and the separation a to 1. The square of the angular speed ω^2 of the system can be replaced with $\frac{G(m_1+m_2)}{a^3}$ (Kepler 3). We introduce the mass ratio $q = \frac{m_2}{m_1}$ with $(0 < q \leq 1)$ and define the normalised potential Φ_n as

$$\Phi_n = \frac{-2\Phi}{G(m_1 + m_2)} \ , \tag{3.12}$$

$$\Phi_n = \frac{2}{(1+q)r_1} + \frac{2q}{(1+q)r_2} + \left(x - \frac{q}{1+q}\right)^2 + y^2 \ . \tag{3.13}$$

The potential can be calculated now for every point (x,y,z). An example for equipotential surfaces is shown in Fig. 3.3. The Lagrangian points are labelled with L. L1 is called the inner Lagrangian point, the lobe touching it is the Roche lobe. If a star passes this lobe, it will lose mass, since all material outside this lobe is not bound to the star any more. This limiting volume depends on the separation a and the mass ratio q. Stars lying inside their Roche lobe have all their material bound. Small stars have spherical shapes and stars, the size of which comes close to the Roche lobe, are more and more distorted until they touch each other at L1.

3.3.1. Classification methods for eclipsing binary systems

It is always important to establish a classification system for objects. This makes the investigation easier and helps to understand the binaries better. There are two ways to classify the eclipsing binary systems. One is based on the shape of the light curve and the other on the morphology.

Morphology

This method depends on the position of the surfaces of the stars compared to their Roche lobes. There are the following four groups:

- **Detached system:** Both stars are well separated and their surfaces are located inside their Roche lobes.

- **Semidetached system:** One star still lies inside his Roche lobe. The other fills it's Roche lobe and can not be approximated by a sphere any more. Mass transfer is possible. The light curves show variations due to the distortion and eclipses.

- **Contact systems:** The stars are in contact and distorted. They both fill their Roche lobe.

- **Over contact system:** Both stars passed their Roche lobe and are surrounded by a common envelope.

Shape of the light curve

In this classification, the criterion is the overall shape of the light curve from the eclipsing binary. The subgroups were named after the prototype star. Light curves of the groups are shown in Fig. 3.4.

- **Algol type (EA):** The light curve has clearly defined eclipses and the variations outside the eclipses are negligible.

- **β Lyrae type (EB):** The eclipses are still well defined, but the variations outside the eclipses get stronger. The non spherical shape leads to the ellipsoidal effect.

- **W Ursae Majoris type (EW):** This light curves show variations over the whole curve. The start and ending points of the eclipses are not well defined. Both components are strongly deformed and lead to a strong ellipsoidal effect (see 3.3.2).
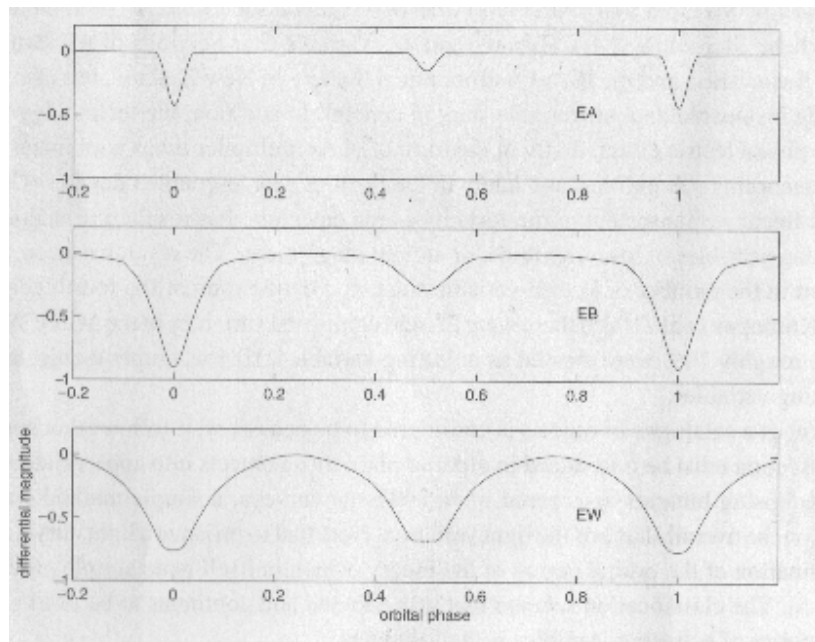

Figure 3.4.: Exemplary light curves from top to bottom: Algol type with sharp eclipses and almost no out-of-eclipse variations, β Lyrae type with small variation outside the eclipse. The W Ursae Majoris lost the sharp eclipses and the out-of-eclipse variations play an important role. The shape of the light curves within each group varies, since the shape still depends on the luminosity ratios, inclination and the sizes of the stars.(Hilditch, 2001)
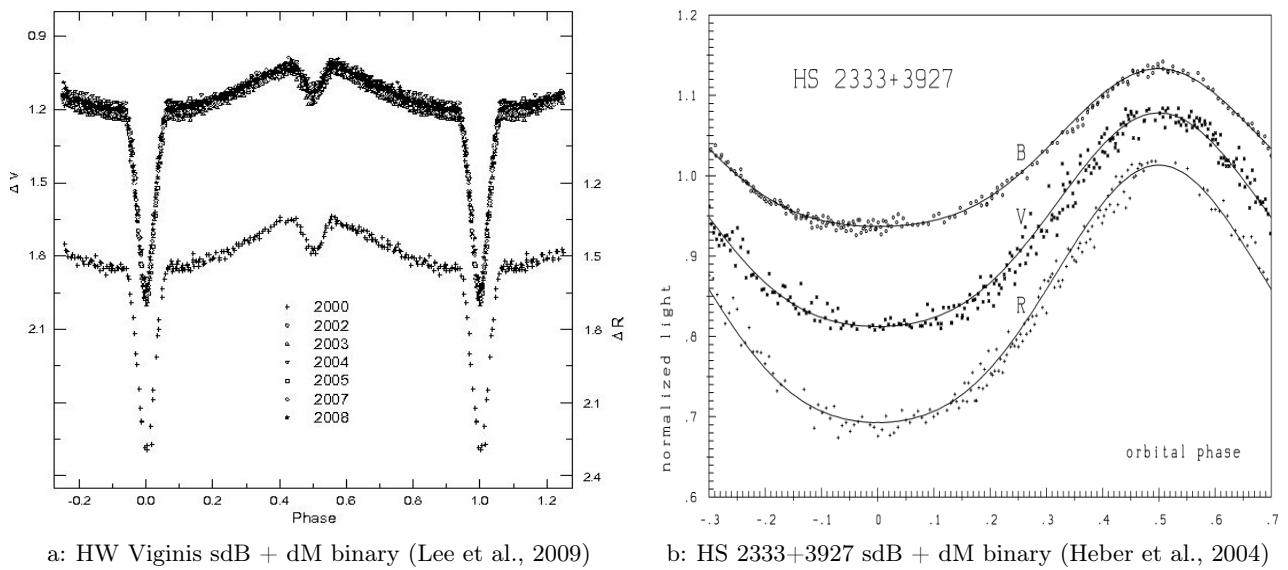
a: HW Viginis sdB + dM binary (Lee et al., 2009)   b: HS 2333+3927 sdB + dM binary (Heber et al., 2004)

Figure 3.5.: (a) HW Virginis light curve in the V and R band. This system is the prototype of HW Vir systems, which consist of a sdB primary and a M dwarf companion. The sdB star has a surface temperature of about 26000 K and the M dwarf of 4500 K. Together with the short orbital period of 2.8 h, this results in the strong reflection effect with eclipses (i= 81°). (b) shows another HW Vir system with an orbital period of 4.13 h. Since the inclination is low, the light curve contains no eclipses, but the reflection effect is still visible.

3.3.2. Reflection and ellipsoidal effect

There are two effects which affect the shape of the light curve of close binary systems besides eclipses. One was already mentioned above, it is the ellipsoidal effect. The area seen from an ellipsoidal changes with the rotation of the star. After an eclipse, the area rises and therefore, the amount of light seen rises as well. Exactly between the eclipses (Phase 0.25 in Fig. 3.4, EB and EW light curves), the light reaches a maximum, because the most deformed side faces the observer. Later, the light decreases again. The deformation gets stronger the heavier and the closer the stars are. Worth to notice is that this effect can be seen also at lower inclination, when eclipses are no longer possible. The effect has a periodicity of half the orbital period.

Another effect appearing in close binary stars is the so-called reflection effect. If the temperature difference between the stars is very large, the surface of the cooler star facing the hot star gets heated up by irradiation. Therefore, it re-radiates more light since the intensity depends on the temperature. The reflection effect disappears when the cool star is in front of the hot star and reaches its maximum, when the heated hemisphere is facing the observer, which is usually at the phase 0.5 (Fig. 3.5). Similar to the ellipsoidal effect, the reflection effect can be seen from lower inclination without any eclipses. In light curve modelling, this effect is modelled as a simple reflection described by albedo. Some binaries could be only solved with an albedo greater than 1. This means that the companion emitted more light in a wavelength area than it received. Since this effect redistributes the light in wavelength (instead of reflecting it), the law of conservation of energy is not violated. Two examples with strong reflection effect are shown in Fig. 3.5. As can be seen, the shape of a light curve contains a lot of information. The ellipsoidal and reflection effect may lead to periodic variations. Two eclipses may appear, they can be total or only grazing. To understand and model a light curve still remains very challenging and interesting.

3.4. Subdwarf B stars

After the short introduction to light curves, the shape of stars and the important role of binary systems, I want to introduce a special type of stars, the subdwarf B stars (sdB). These stars are often found in close binary systems and are interesting objects. First of all, I want to to explain their nature, the aspects which make them interesting and explain different formation models. Stars on the main sequence, which are stars burning hydrogen in their cores, are called dwarfs (see Fig. 3.6) and are luminosity class V stars . Subdwarfs are stars which lie below the main sequence in the HRD. They are underluminous compared to main sequence stars of the spectral type BV. Subdwarf B stars are therefore hot (spectral class B) underluminous stars.

If one takes a closer look, they are not at all related to the stars on the main sequence. They are helium core burning stars with an unusual thin hydrogen shell ($<0.02\ M_\odot$) (Han et al., 2002). Since the area in the HRD where stars are burning helium in their cores is called horizontal branch (see Fig. 3.6), sdB stars are often referred to as extreme horizontal branch (EHB) stars. Due to their thin hydrogen shell, the hot and dense core is located close to the surface. This leads to high surface temperatures and high surface gravity. The surface temperature usually is higher than 20000 Kelvin and the surface gravity *log g* above 5. Subdwarfs of earlier spectral types (O and OB) are called sdOB and sdO stars and are related objects. For simplicity, sdB stars will be used as collective term for sdO, sdOB and sdB stars in this work. Several facts make them to a special class of objects. First of all, their properties
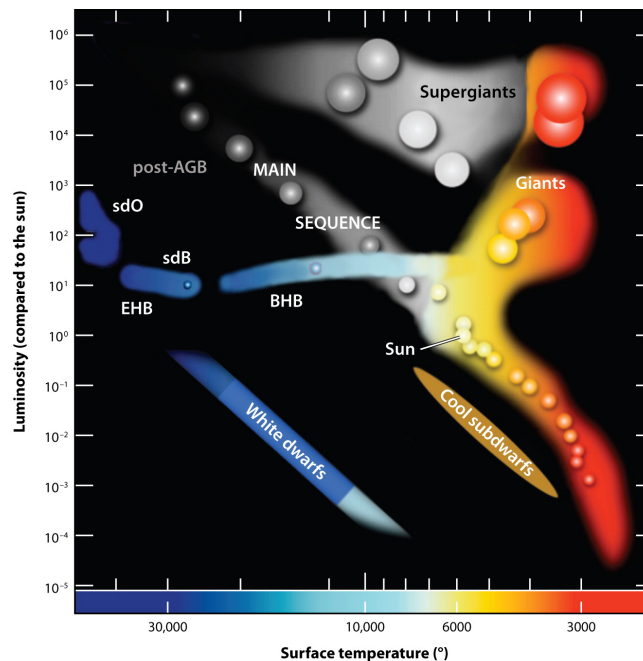
Heber U. 2009.
Annu. Rev. Astron. Astrophys. 47:211–51

Figure 3.6.: A modified Hertzsprung Russell Diagram illustrating the positions of different star classes. The sdB stars are located below the main sequence on the hot end of the horizontal branch near the white dwarf cooling area (Heber, 2009).

like the thin hydrogen-rich envelopes are not completely understood yet. Solving this issue would lead to a better understanding of the theory of stellar evolution and binary evolution. Secondly, sdB stars are the dominant population in surveys of blue objects and they seem to be the dominant source for the ultraviolet upturn in elliptical (old) galaxies. They also seem to form everywhere, sdB stars were found in the galactic field, in old (globular) and young (open) star clusters. Surveys show that the fraction of binary stars among the sdB stars is higher than 50 percent (Han et al., 2002). Especially the fraction of binaries with short periods (from hours to days) is very high. Maxted et al. (2001), Morales-Rueda et al. (2003) and Napiwotzki et al. (2004) showed that the majority of sdB stars are

short-period binaries with white dwarf (WD) and main sequence (MS) companions. Obviously, binary systems seem to be an important factor in the formation of sdB stars.

3.4.1. Origin

For long time, there was no explanation how a star could get rid of almost all its envelope during the red giant (RG) phase, which is required to form sdB stars. There were theories that stellar winds could blow away the weaker bound envelope, but they could not explain the high fraction of close binaries. Han et al. (2002) showed through binary population synthesis (BPS) that three main formation channels, explained below, could account for the observed sdB population:

Stable Roche lobe overflow

As soon as the hydrogen burning is exhausted in the core, the star evolves to a red giant. During this phase, the surface of the stars enlarges significantly. If the surface reaches the Roche lobe, mass transfer sets in. This is called Roche lobe overflow (RLOF) and it stays stable if the mass ratio q of the stars is $q < 1.2...1.5$. In this way, the red giant loses its envelope to the companion. After most of the envelope is lost, the star begins to shrink and the degenerated helium core with a thin envelope remains. If all this mass transfer occurs on the tip of the red giant branch, the core will still the critical mass of around 0.46 $M_{\odot}$, ignite the helium and the system will evolve to a sdB star with a main sequence companion. Theoretically, a second RLOF phase could occur when the smaller companion evolves to a red giant. In this case, it would result in a binary composed of a sdB and a white dwarf. The orbital periods of RLOF systems are rather large and around $\gtrsim 1000d$. The theory of mass transfer is still uncertain and requires further investigation. Nevertheless, observations show that sdB stars with long periods do exist, and that they have rather thick envelopes compared to objects formed through other channels.

Common-envelope ejection

Another channel leading to a sdB star in a binary system is via common-envelope (CE) ejection. Usually, when a star reaches its Roche lobe the mass transfer is unstable and occurs on a dynamical time scale. The accreting star is unable to bind the material and a common envelope, engulfing the degenerated core of the RG and the companion, develops. The stars begin to lose orbital energy due to the friction with the common envelope (CE). Therefore, the orbits begin to shrink until the orbital energy released is high enough to eject the CE. A close binary system remains. If the degenerated core is massive enough, helium burning will be ignited and it will become a sdB star. The companion can be a main-sequence star or an evolved white dwarf if the CE phase happens a second time. This channel leads to short periods of 0.1-10 d, thin hydrogen-rich envelopes and a mass distribution of the resulting sdB stars that sharply peaks around 0.46 $M_{\odot}$ (see Fig. 3.7a).

Double helium white dwarfs merger

In contrast to the other channels, the double helium white dwarfs (WD) merger channel results in a single sdB star. In WD binaries, the angular momentum loss by gravitational wave radiation leads to a shrinking of the orbit. When the period is sufficient low, the lighter WD can be disrupted (P < 2 min) and an accretion disc is formed. Due to the increasing mass of the heavier component, helium burning can be ignited and a single sdB star is born. This channel can produce a wide range of masses (0.4-0.65 $M_{\odot}$) with extremely thin hydrogen-rich envelopes. The BPS showed that the mass distribution of the sdB stars created in this process has its main peak around 0.5 $M_{\odot}$ however, sdB masses up to 0.7 $M_{\odot}$ are possible (see Fig. 3.7a). In general, the stars should be hotter and more compact than the stars formed in the binary channels.

These three channels are able to explain the evolution of sdB stars. An overview of 81 measured sdB orbital periods is given in Fig. 3.7b. Up to recently it was not possible to determine periods for
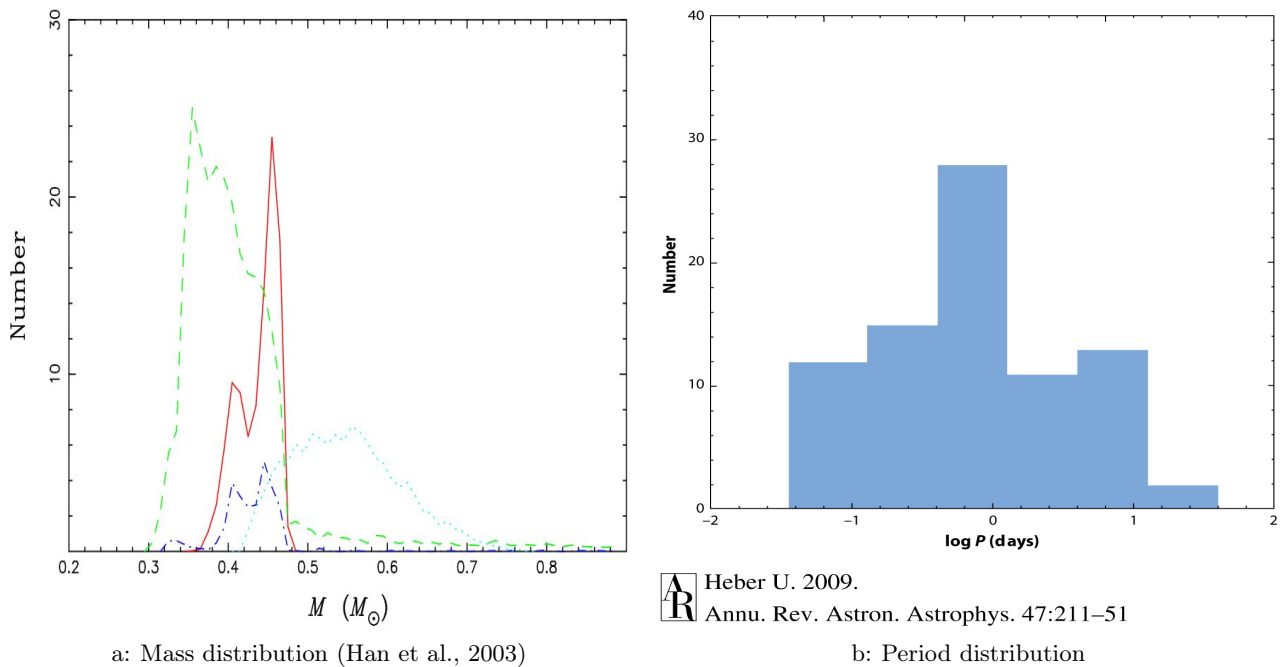
a: Mass distribution (Han et al., 2003)   b: Period distribution

Figure 3.7.: The mass distribution of the three channels observed in the the BPS . The mass distri-
bution of the BPS has 4 sharp peaks, resulting from the different channels. The solid red
line represents the first CE ejection channel, green dashed line the stable RLOF, blue
dot-dashed the second CE ejection channel and the dotted cyan the the merger channel.
The right figure shows the measured periods of 81 sdB stars from Ritter and Kolb (2002).
As one can see, short periods of sdB binaries around 1 days are very abundant.

the sdB + MS binaries of almost equal mass which are supposed to form through RLOF. Deca et al.
(2011) and Østensen & Van Winckel (2011) derived periods between 500 and 1200 days for 8 sdB +MS
systems. These periods are much longer than predicted by BPS and are creating a new puzzle. Binary
systems with larger periods are harder to detect and their RV variation is smaller than the one of close
binary systems. Unfortunately, the single sdB star population is still not explained convincingly. The
single sdB stars should have a high rotation velocity if formed by mergers due to the angular momen-
tum conversion. Despite this, the observed single sdB stars are rotating slowly. A possible explanation
for these stars could be brow dwarfs or planetary companions (Geier et al., 2009). The amplitudes of
RV variations of a sdB star with a brown dwarf or planet as companion are very small, which makes
them harder to detect. Therefore, apparently single sdB stars could have an undetected companion
which would eject the CE. Moreover, planets with masses lower than $\approx 10 M_J$ get evaporated during
the CE phase. Additional sdB binary candidates would help to clarify the origin and evolution of sdB
stars. They would also improve the understanding of mass transfer mechanisms and stellar interaction
in general. I investigated the CoRoT light curves for eclipsing binary systems and searched for new
sdB candidates.

4. Programmes used for analysis

In this chapter a short introduction to the programme SPAS (Spectrum Plotting and Analysis Suite) and FAMIAS (Frequency Analysis and Mode Identification for Asteroseismology) will be given which were used for the data analysis in this thesis. Apart from these two programmes, several small tools were applied in the data analysis, which were programmed by myself. They were used to bin light curves, to create phase plots and to remove trends from the light curves. more details on these tools can be found in chapter 5.

4.1. SPAS

SPAS was programmed by Heiko Hirsch (Hirsch, 2009). It is a reimplementation of FITSB2 (Ralf Napiwotzki) with an improved user interface and new features. SPAS was used to measure surface gravities ($log\ g$) and surface temperatures (T_{eff}) of the binary systems. As mentioned in section 3.2.1, light curves just provide information to measure relative radii. Spectral lines contain information of the surface, like $log\ g$, T_{eff} and helium and metal abundances, as well as information of rotational velocity v_{rot} and radial velocity v_{rad}. The depths of absorption lines are depended on T_{eff}, while the density has an influence on the width of lines. In particular the Balmer-lines are very sensitive to the gravity because of the Stark-effect. The Doppler shift due to v_{rad} shifts the spectral lines from their laboratory in rest wavelength. Therefore, the stellar parameters influence the shape and position of absorption lines in a known way, but unfortunately not independently. Different combinations of the stellar parameters can lead to similar line shapes. Grids of synthetic spectra (different combination of stellar parameters) are created using model atmospheres and used by SPAS. SPAS interpolates linearly in this grid and compares the stellar spectrum to a synthetic spectrum with specific parameters. Instead of comparing the whole spectrum with the synthetic spectra, the user selects a region around a specific spectral line (see Fig. 4.1), containing usually one or two spectral lines. The spectral lines are defined in a configurable file and can be edited freely. SPAS then fits the stellar parameters with the help of a downhill simplex algorithm by minimizing the deviation of the synthetic lines from the stellar lines. This fit can be done simultaneously or independently. The errors are determined with a Bootstraping algorithm at the simultaneous fit. The independent fit returns the standard deviation and the results of each line. These pieces of information allow to estimate the errors. Gaussian+Lorentzian-functions are fitted to the lines to calculate v_{rad} from the Doppler-shift.

Munari grid

To obtain comparable results, it is important to use correct synthetic spectra grids. In this work, the LTE model grid with line blanketing from Munari et al. (2005) with solar metallicity was used. The atmospheric parameters span the ranges: $5000\ K \leq T_{eff} \leq 45000\ K$, $1.5 \leq log\ g \leq 5$. The synthetic spectra have a wavelength range of $2500 - 10500$ Å and are available in different resolutions. This covers our whole spectral range ($3700 - 7400$ Å) and resolution $R = \frac{\lambda}{\triangle\lambda}$ of 1300. Predicted lines, which are calculated absorption lines, where one or two energy levels are predicted by atomic structure codes but not detected in laboratory experiments, are excluded from the computation of the spectra, since their accuracy is very low in wavelength (≥ 10 Å) and intensity. Therefore, the spectra may not contain all spectral features, especially of cool stars, where the metal lines gain strength. Since this work is focused on hot stars, the exclusion of predicted lines is irrelevant.
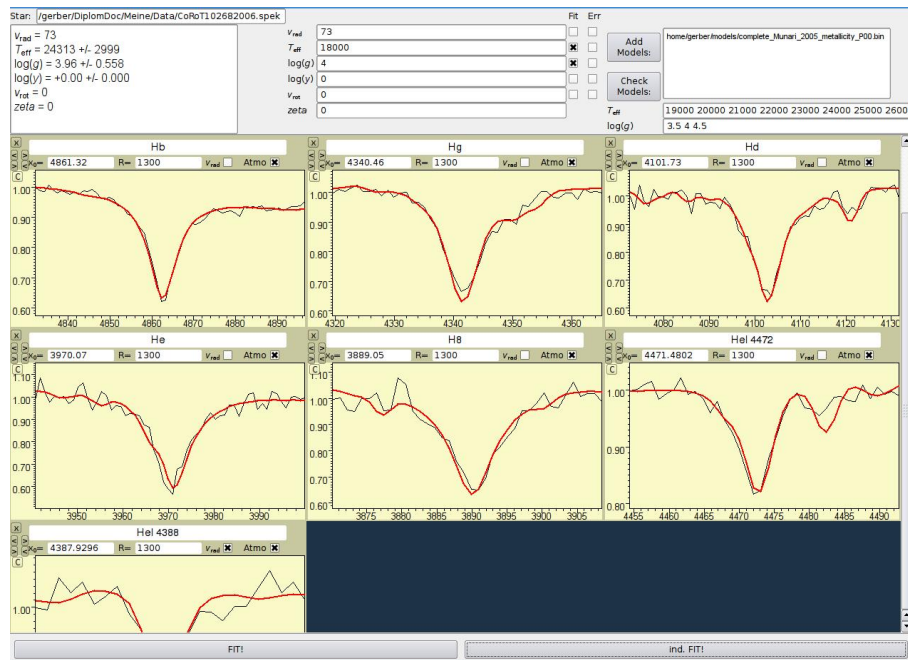
Figure 4.1.: User interface of SPAS. In this example, 7 spectral lines are selected for the determination of the stellar parameters. The black lines are the stellar lines, the red line represents the best fit.

4.2. FAMIAS

The programme was developed at the Instituut voor Sterrenkunde, K.U. Leuven (Zima, 2008) and contains tools to analyse time series of photometric and spectroscopic data. It can calculate a Fourier transform (DFT) and computes the statistical significance of detected frequency peaks which was used to find the orbital period. Another feature which was used is the Least-Squares Fitting, in which a non-linear multi-periodic least-squares fit is computed. Moreover, it is possible to pre-whiten the data by removing sinusoidal oscillations from the light curve. FAMIAS was used to determine the orbital periods of the eclipsing binary systems from the light curves. At first, a Fourier analysis was performed to determine the periodicities in the light curve (see Fig. 4.2) The frequency range is freely adjustable which saves computation time. Knowing the period, the least squares fit with the orbital period as
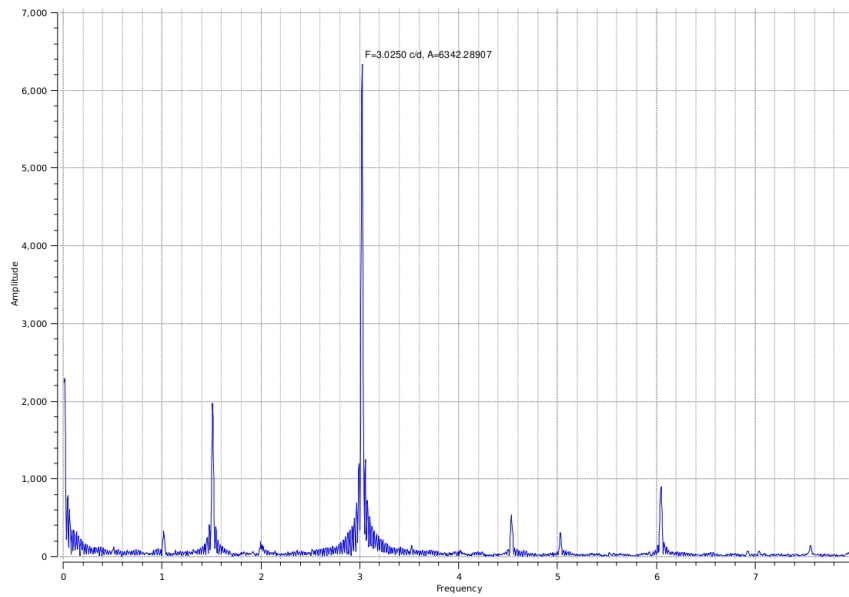
Figure 4.2.: Result of the Fourier analysis of an eclipsing binary system with a period of 0.66 days ($1.51 \frac{1}{d}$). The larger peak corresponds to the half orbital period, but since a complete period consists of two eclipses the smaller one is the real value.

start parameter improved the certainty. FAMIAS also offers the opportunity to phase the light curve, which was very useful to approve the DFT and least squares fit results.

5. Analysis of the CoRoT stars

Most of the time of the research was dedicated to look for B-type stars. In particular, it was hoped to discover new eclipsing binary systems with a sdB component. Because the fraction of close binary systems among the sdB stars is high, . To have a reliable identification, in the first step, hot targets were pre-selected with the help of AAOmega spectra in the IRa01, LRa01 and Lra02 fields, then, the corresponding light curves were investigated for eclipses and oscillations. As the final step, the stellar parameters of the eclipsing binaries were fitted to distinguish between horizontal branch and main sequence stars. Before starting the investigation, a closer look to the properties of CoRoT light curves will be taken.

5.1. CoRoT lightcurves

As mentioned in Chapter 2, CoRoT light curves offer an accuracy in photometry (10^{-4}) and long uninterrupted time series (up to 150 days), being unique at that time. Since the launch in 2006, CoRoT measures more than 100,000 stars and the mission is still going on. The CoRoT data become freely available via the web-interface. After the data acquisition, it takes 4 to 6 months to reduce them. In the following year, the data access is restricted to Co-Investigators and Guest Investigators (proprietary period). After this period, the data are available for public download (Baudin et al., 2006).
The CoRoT data are divided into different levels or evolution stages. The first stage is N0, the raw data which is not useful for scientific investigations, and therefore are not published. The next level is N1, it is corrected for the first order instrumental effects and thus can be used only with caution and is not available for the public. The N2 data represent the light curves at final stage. The perturbations are marked or removed and the light curves are accessible via the CoRoT N2 Public Archive[1]. Deduced results from scientific analysis, like frequencies of the detected modes or variable classification are collected in the N3 data and can be further interpreted. These data are also published and freely accessible. This way, many scientist can have a closer look at the light curves and use them for their projects, which assures an optimal usage of the information.

5.1.1. Field information

The mission is divided into different runs. During the winter, the telescope points to the anticentre (RA≈6h) of the Milky Way, which contains for example the stellar constellations Aquilla and Scutum. The other "eye" (RA≈18h), in the direction of the centre of the Milky Way, lies at Orion and Monoceros and is observed in the summer (Fig. 5.1a). The runs are named after their length and whether they are located in the centre (c) or anticentre (a) field in the way as it follows: The first two letters determine the length, the long runs start with LR and the short run with SR. The first run was named initial run (IR) and had an length of 60 days. The following letter encodes the position, and the last numbers are incremented after each run for each field. The runs in the anticentre field which are published at present are shown in Fig. 5.1b. The figure was created with the Alladin Sky Atlas[4]. The IRa01 and LRa01 runs overlap a bit and some stars have been observed twice in this runs.
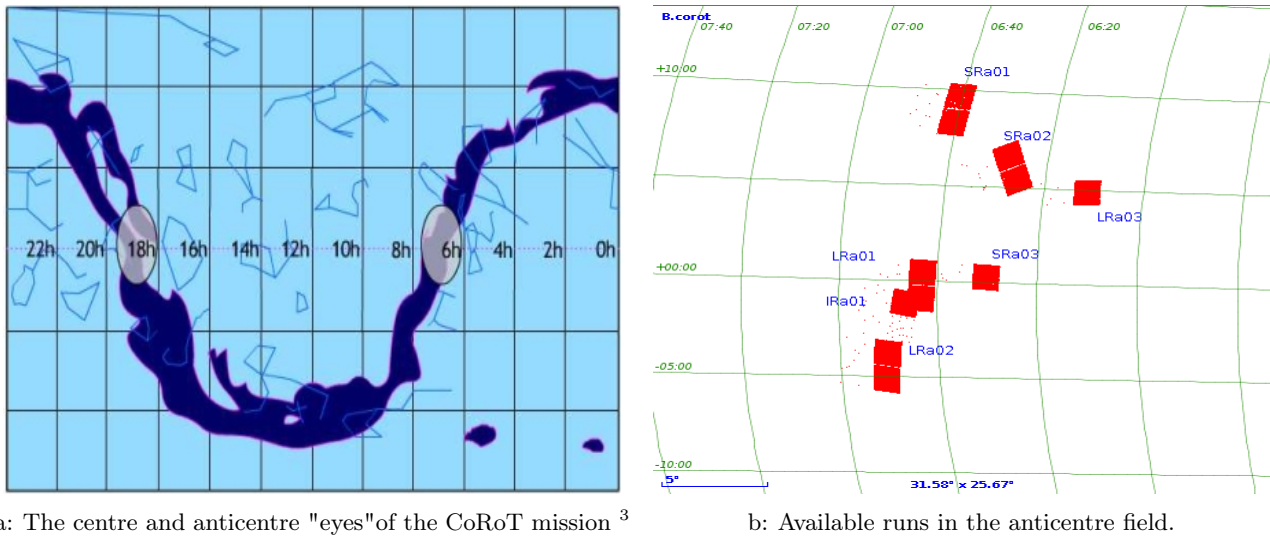
---

[1]http://idoc-corotn2-public.ias.u-psud.fr/invoquerSva.do
[3]http://www.corot.de/german/Mission/zielsterne.html
[4]http://aladin.u-strasbg.fr/

a: The centre and anticentre "eyes"of the CoRoT mission [3]   b: Available runs in the anticentre field.

Figure 5.1.: Overview of the CoRoT fields and runs

5.1.2. Contaminations

In November 2011 I had the opportunity to participate in a CoRoT workshop in Cologne. I was introduced to effects in the perturbation of light curves which result from the orbit and the properties of the satellite. To distinguish between stellar variation or contaminations it is important to know in which way the light curve is affected by environmental conditions and extern perturbations. The strongest effects and some examples of light curves are summarised below.

South Atlantic Anomaly

On the Earth, the atmosphere and the magnetic field filter out a large amount of high energy particles. In space, the telescope is exposed to high energy protons (10 keV to 300 MeV) and electrons. The South Atlantic Anomaly (SAA), a distortion of the magnetic field above South America raises the amount of particle impacts on the satellite. Above the south Atlantic the satellite passes through the Earth's magnetic field and the cosmic impacts gain strength. As protection, CoRoT has a 10 mm aluminium shielding, it absorbs all electrons but it can not stop the high energy protons. Besides this, it is not possible to shield the complete satellite, since an aperture for the telescope is needed. In collisions, the particles are able to create atomic displacements which lead to permanent hot pixels. Lower energy particles can create hot pixels which decay on time. Since the hot pixel detection is only performed at the beginning of each run, they influence the actual measured light curves and create jumps in the brightness. An automatic corrections of the flux is very difficult, since the jumps in the light curve decay on different time scales and the brightness may even remain on a higher final value. Several parts on the CCD are dedicated to measure the background, to correct out the stray light. An impact on this area leads to negative jumps in decreasing brightness, since the background flux raises. A light curve with jumps is shown in Fig. 5.2.

Eclipses

Since CoRoT orbits around the Earth ($f = 14.18\frac{1}{d}$) the Sun disappears sometimes behind the Earth. These eclipses have a variable length, depending on the date they appear. The temperature differences during the egress and ingress induce vibrations on the satellite's solar panels which disturb the pointing. Moreover, voltage fluctuations appear when the power supply switches to the battery mode (Auvergne et al., 2009). The eclipses occur more often at the beginning and at the end of a run. Therefore, the quality of the data is the best in the middle of a run.
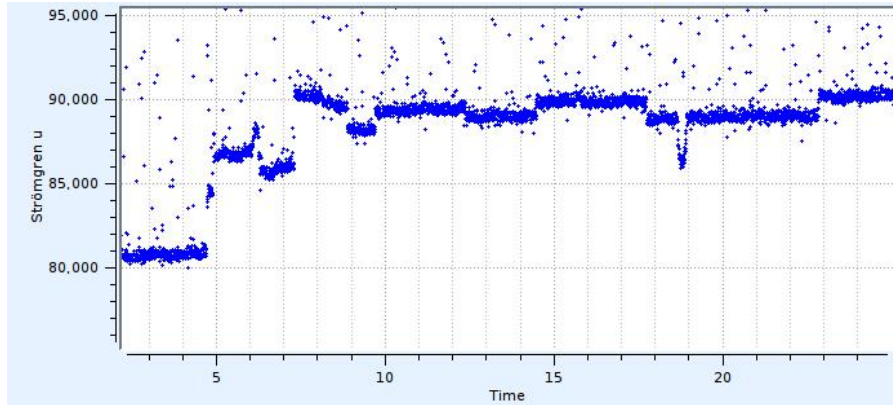
Figure 5.2.: A part of the light curve of CoRoT 102874481 in the IRa01 field. Several changes on the flux level are noticeable, at 18.80 d a small grazing eclipse occurs.

Blending

One of the reasons why CoRoT observes in the galactic field is the high density of stars. In this way, the amount of stars measurable simultaneously is very high. On the other hand, stars can be so close together that they are blended and not separable any more. Therefore, the flux of a system may be contaminated by neighbouring stars. The contamination factors have been calculated and are noted in the header of the light curves ((Deleuil et al., 2009)). Most of the targets investigated here have a contamination factor lower than 0.1. But 9 systems have a contamination factor bigger than 0.1 and the contamination reaches a level where it may not be negligible any more. The correction of the blending stars is only possible if it is assumed that the eclipses result from the observed system and not from the blending star. This assumption is reliable for systems with deep eclipses and small contaminations. At systems with contaminations above 10% and eclipse depths smaller than several percent the variation may origin from the blending star and not from the CoRoT star. A complete list of the contamination factors of the eclipsing binaries is given in Table A.3.

Other perturbations

Despite eclipses and the SAA, other perturbations influence the measurements. Temperature variations due to the changing infrared emissions of the Earth and the Sun appear on time scales of the orbital period and days. Also the albedo of the Earth is changing, dependent on clouds and the overflown region. All these effects lead to periodic changes in brightness and have to be considered when analysing frequencies close to the orbital frequency, 1 day frequency, and to their harmonics.

Conclusions

The baffle is able to reduce the scattered light from the Earth by a factor of 10^{12} (Auvergne et al., 2009). Also the temperature variations on short time scales are stabilised better than 0.01. Problems which still play a role are the effects during the ingress and egress of eclipses, the proton impacts and the temperature variations on 24 h and orbital time scales. Therefore, every measurement made during the passage of the SAA and the ingress and egress of eclipses or other perturbations is flagged. This allows bad measurements to be removed from a light curve. As an example the light curve of CoRoT 0102648472 with all measurements included and only with the unperturbed measurements is shown in Fig. 5.3.

However, the best validations of the quality of data from CoRoT are the available results. The shallowest transit detected by CoRoT in the first three runs, has a depth of $6*10^{-4}$ at a star with R-magnitude of 12 mag. This demonstrates clearly the great performance of the satellite.
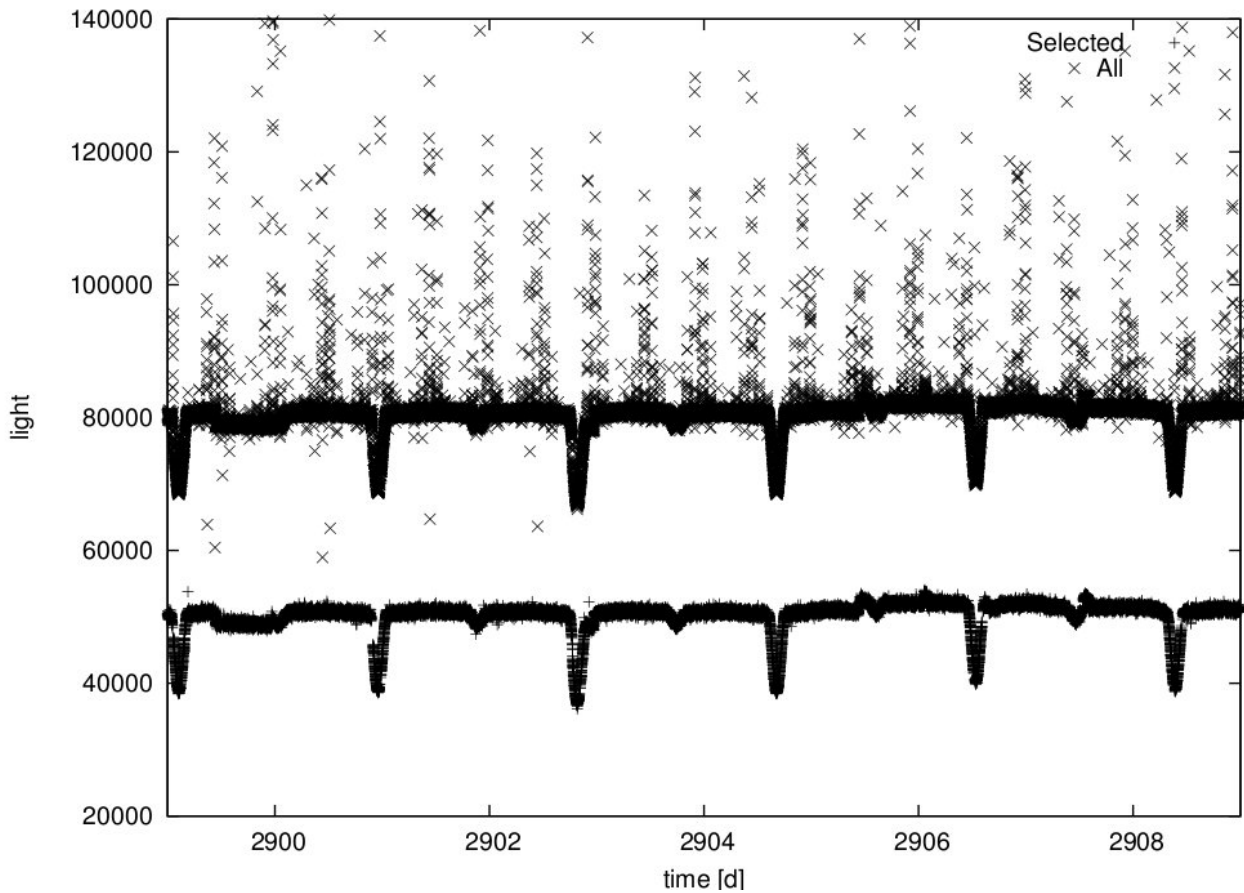
Figure 5.3.: A part of the light curve of an eclipsing binary CoRoT 0102648472. The bottom contains only the undisturbed measurements, while the top (shifted by 30000) contains all. As a consequence, the signal to noise is doubled.

5.1.3. Colours

The CoRoT light curves of stars brighter than V=14.5 mag are available in three colours: blue, green, and red. For this purpose a prism is located in front of the CCD and splits the incoming light. The wavelengths are not calibrated and the dispersion is non linear and depends on the position. Nevertheless, the chromatic light curves help to distinguish between artefacts and real transits. In doubtful cases they may help to decide whether transits are real or not.

5.2. Spectroscopic selection

In this work the runs IRa01, LRa01 and LRa02 are investigated. The long runs (LR) offer 150 days of uninterrupted observations. Another reason to choose these fields is the availability of spectra. Prior to the start of the satellite, the stars in the CoRoT fields were classified with the help of broad band photometry in the (B,V,R,I) channels. But due to the galactic reddening the photometric classification is not reliable. Therefore, spectra were taken at the Anglo-Australian Telescope/Australian Astronomical Telescope with the AAOmega multi-object-spectrograph by Dr. Eike Günter. This spectrograph can cover the field of view (FOV) of the IRa01, LRa01 and LRa02 fields completely. Moreover, it can measure up to 350 stars at the same time, which shortens the observation time. In two campaigns (January and December 2008) more than 20,000 spectra with the resolution of $R = 1300$, of stars with the V-magnitude of 10-15, were taken. The spectra are divided into blue (3740-5810Å) and red (5650-8770Å) (Sebastian & Guenther, 2011). The three fields contain around 32,000 light curves, but

only the half of them are chromatic (see Exodat[1]. To have the maximum information available of the targets, the objects with chromatic light curves were investigated primarily.

The purpose of this work is to find new B-type eclipsing binaries in particular with sdB components. Since sdB stars have surface temperatures higher than 20,000 K, the first step was to select the interesting hot stars from the fields. Instead of relying on the photometric spectral classification, the AAOmega spectra was used. The spectra could be used later to measure stellar parameters ($log\ g, T_{eff}$).

5.2.1. Selection method

Since CoRoT observes inside the Galactic plane, where large dust clouds are located, the inter-stellar reddening plays an important role. Due to the galactic reddening, where an amount of the blue light is absorbed and re-emitted at longer wavelength by the interstellar material, the energy intensity distribution of the stars may have changed a lot. The maximum of the energy emission depends on the surface temperature, and is shifted to longer wavelength due to the reddening. Therefore, we decided
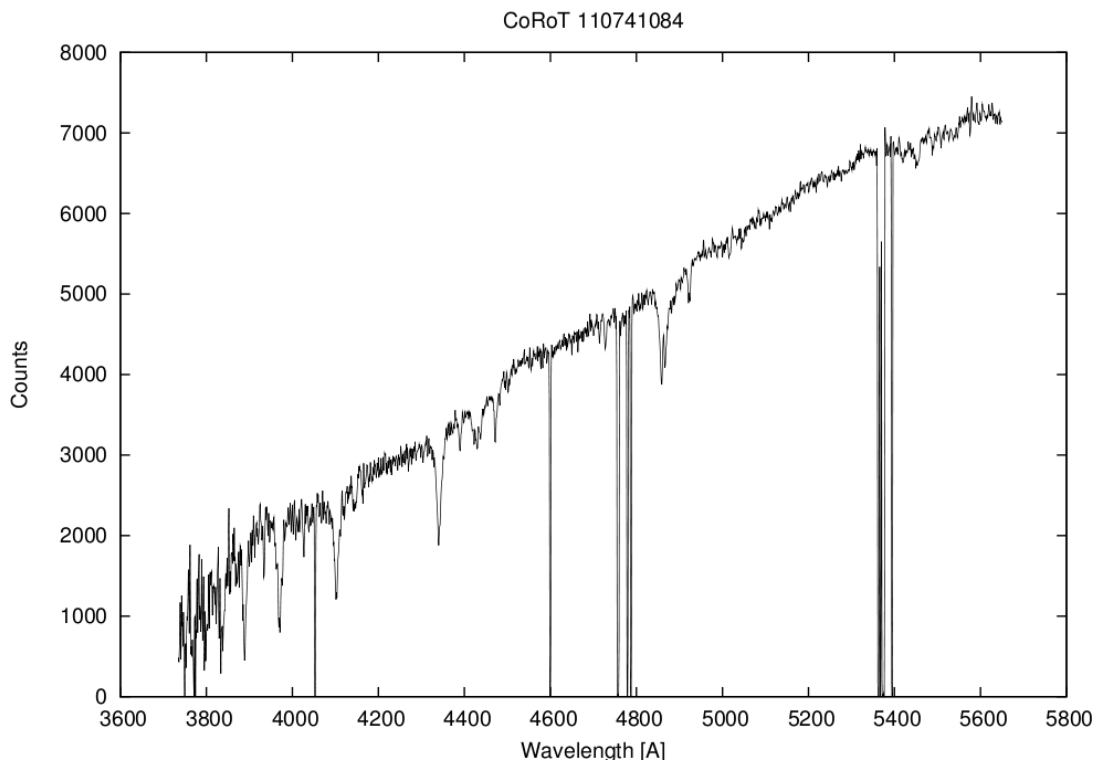
Figure 5.4.: The blue spectrum of CoRoT 110741084 shows helium lines at 4472 Å and 4388 Å and its spectral class is B. The Planck function for such hot stars would have its maximum in the blue. But in this case, the reddening redistributed the light, and the maximum lies now in the red. This reddening may lead to problems in automatic classification systems.

not to rely on automatic classification methods and all the spectra were inspected personally. The spectra were converted to postscript images and put together, allowing to navigate through them more quickly. The spectral atlas of R. O. Gray[2] was used to distinguish hot from cool stars. As seen in Fig. 5.5, the Balmer lines gain strength with temperature until the spectral class A1. For hotter stars their equivalent width decreases again. The helium lines start to appear in spectral classes earlier than A0. The appearance of He II lines separates B and O stars. The Ca II K-line at 3933.66Å dominates over the Balmer lines in spectral types later than F, while in early A and B stars it results from interstellar material, but is still much weaker than the H_ε. Around F2 the G-band appears and metal

---

[1] http://idoc-corotn2-public.ias.u-psud.fr/invoquerSva.do
[2] http://ned.ipac.caltech.edu/level5/Gray/Gray_contents.html

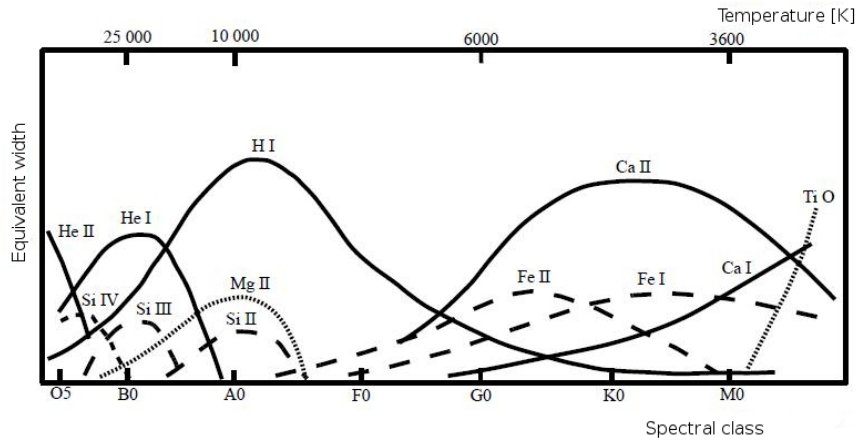lines gain strength dramatically. The stars were classified with the help of the Balmer lines, He lines

Figure 5.5.: The qualitative dependency of the equivalent width to the surface temperature and therefore spectral class (Karttunen et al)

and the Ca II K-line. Stars having dominant Balmer lines or He lines were classified as hot stars. If the Ca II K-line was stronger than the Balmer lines or the G-band appeared (around 4300 Å), the stars were sorted out. In doubtful cases, the intensity of metal lines was considered. Stars with a lot of metal lines and a strong Ca II K-line were sorted out as well. In Fig. 5.6, Fig. 5.7 and Fig. 5.8 three spectra are shown, two classified as hot and one as cold stars.
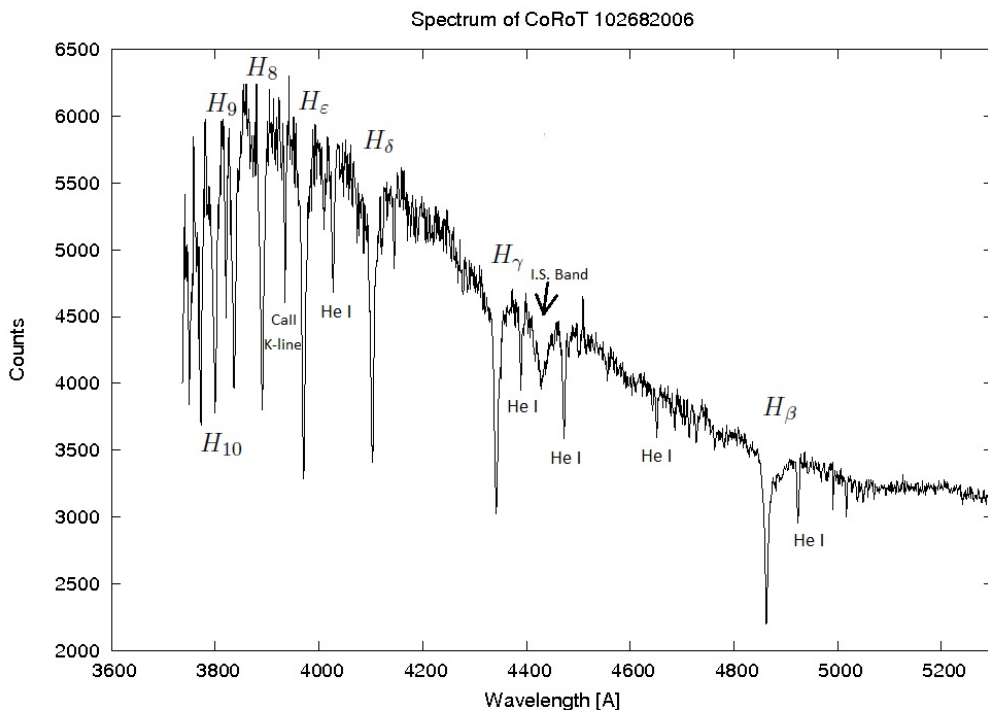
Figure 5.6.: Spectrum of a star classified as hot. The Balmer and helium lines dominate the spectrum. The Ca II K-line is very weak and probably interstellar. A strong I.S. Band is visible at 4430 Å.

Spectrum of CoRoT 110741084
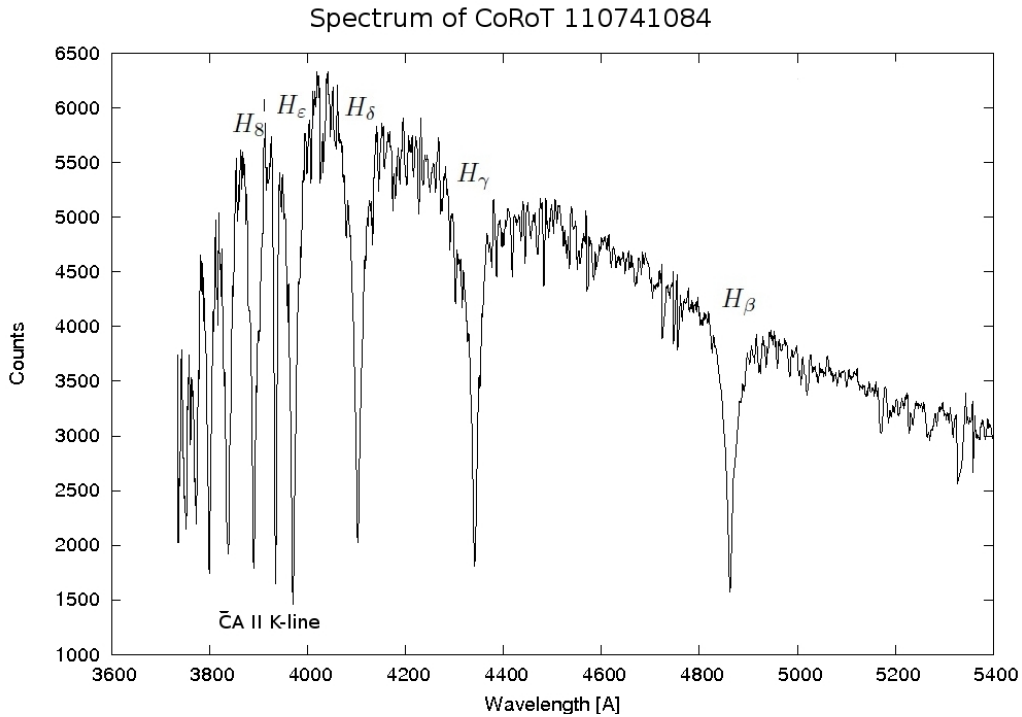
Figure 5.7.: Spectrum of a star classified still as hot. In this spectrum the Balmer lines clearly dominate, the Ca II K-line gained strength but is weaker than the H_ε. Moreover, helium lines disappeared or are not separable from the appearing metal lines.

Spectrum of CoRoT 0110743656
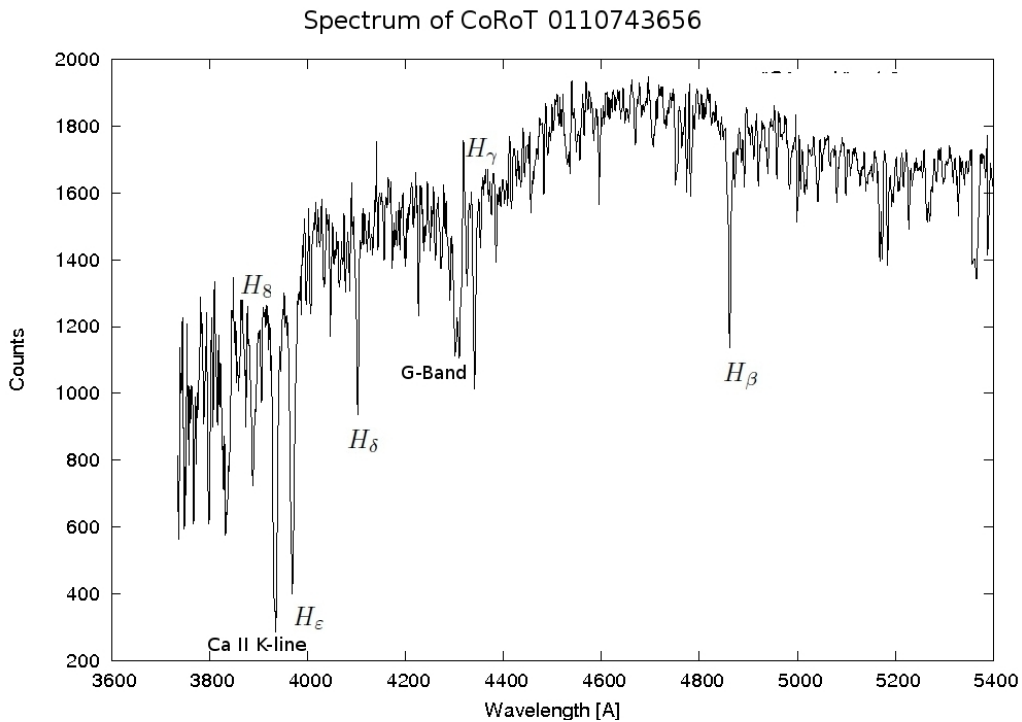
Figure 5.8.: Spectrum classified as cool. The Balmer lines are weak, the G-Band gains on strength. The Ca II K-line is stronger than the H_ε. Fe I and other metals gain significantly on strength.

5.2.2. Results of the spectral classification

In total 8809 spectra from the LRa02 field were examined and 2183 were classified as hot. These 2183 spectra corresponded to only 1215 stars because some of the stars were recorded more than once, due to the poor quality of the spectrum. Fig. 5.9a shows the distribution of spectra per star. Unfortunately only 806 of the 1215 stars had light curves available, since some stars were just selected to fill the fibers and were never observed by CoRoT. From these, the 689 chromatic were investigated while the other 117 monochromatic were investigated later in partnership in Cologne. The other 2 fields IRa01 and LRa01 were already preselected. The IRa01 field contained 436 stars and the LRa01 field 529 hot stars (Fig. 5.9b).

a: Spectra per star
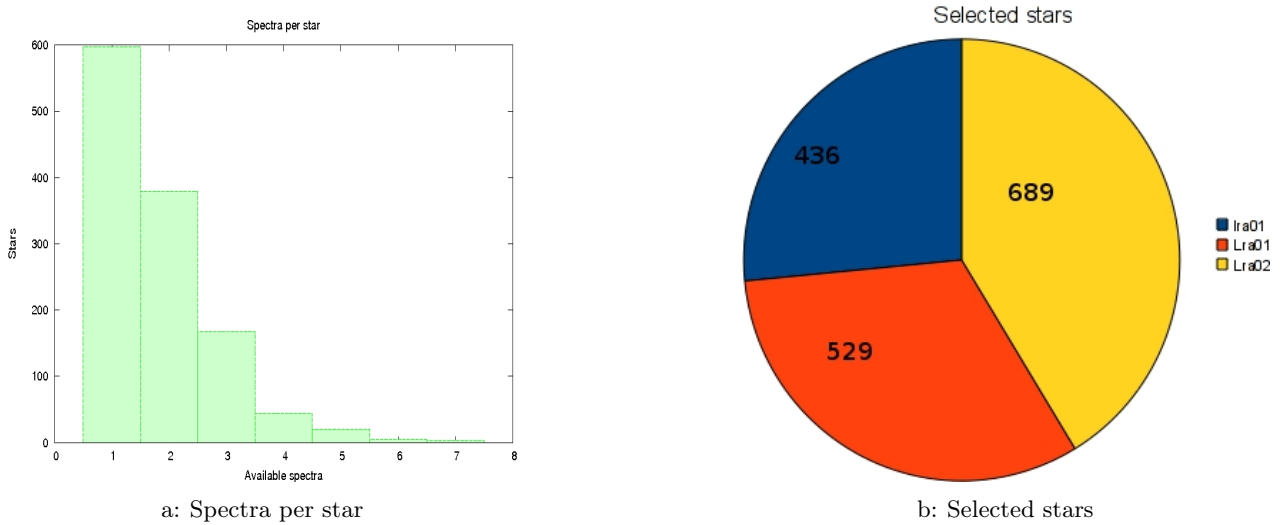
b: Selected stars

Figure 5.9.: (a) The relationship between spectra and stars in the LRa02 field. The majority of the stars were measured once, but some have up to 7 spectra. (b) The distribution of the selected stars in the fields. Most stars are located in the LRa02 field.

5.3. Classification of the variation type

In the investigation of the spectra in the three fields, 1654 stars were classified as hot and interesting. Now the main part of the work started, the observation of the corresponding light curves. The light curves were divided into 3 classes: no variance (NV), oscillation (O) and eclipsing binary (EB) The types of the EB were also classified with the help of the light curves. Systems showing ellipsoidal effects were classified as EW, stars with weak out-of-eclipse variations as EB, and stars without any variation apart from the eclipses as EA.

5.3.1. The data

The light curves were saved as Flexible Image Transport System (FITS) files. The files contain time information, blue, green and the red flux. For the classification the red flux was used, it was extracted together with the time and 3 different cut-outs were saved in a postscript image (Fig. 5.10). In this
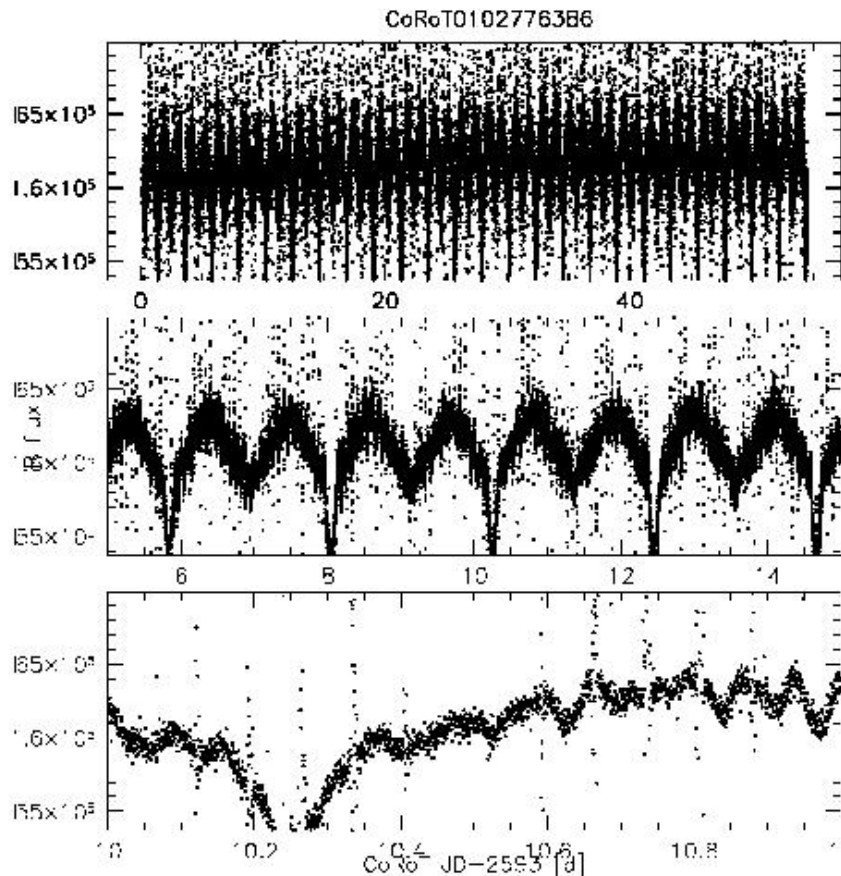
Figure 5.10.: Three differently scaled views were used to investigate the light curve. The top view covered 60 days, the middle 10 days, and the bottom 1 day of measurement. This star was classified as an eclipsing binary

way it was possible to recognise variations on different time scales. The top view, with 60 days, offered a good overview, while the 10 days middle view helped to identify the kind of the variation. The last view revealed fast variations.

5.3.2. Results of the light curve classification

In some cases it was hard to distinguish the type of variation. Since the search is focused on eclipsing binaries the doubtful stars were classified as binaries and investigated later in more detail. The IRa01

field contained 40 oscillating stars and 13 eclipsing binaries. Therefore, the frequentness in this field were 9% for oscillating stars and 3% for eclipsing binary stars. The fraction of oscillating stars in the LRa01 field was a bit lower (7%, 35 stars) while the fraction increased in the LRa02 field to 10% with 41 stars. The LRa01 field contained 10 EBs which corresponded to a fraction of 2% and the LRa02 had 22 EBs (3%). An overview of the classification is shown in Table A.1. The oscillation frequencies of the oscillating stars were determined with the help of FAMIAS. In some cases the Fourier transformation was not possible, since the sampling rate of the light curve changed, or because of the appearance of jumps and interruptions. In this cases the time difference between two maxima was accounted as the period. The incidence of the oscillating stars are summarised in Table A.5.

Detected transit systems in Cologne

During the meeting in Cologne several transits have been identified. There are several possible reasons why they were overseen during the previous classification:

1. The transit depth was smaller than several percent.

2. The stars were not included in the hot sample used in this work.

3. The oscillations of the star were dominant compared to the transit.

In Fig. 5.11 a part of 20 days of the light curves from the stars CoRoT 110853363 and CoRoT 110666175 is shown. CoRoT 110853363 has a period of 9.1 days. It has a contamination of 11% and the depth of the transit is only 3% . Therefore, the transit could result from the blending system with a transit depth of around 30% . The second system CoRoT 110666175 has a period of 8.76 days, transit depth of 1.3% , and a contamination factor of 35%. Unfortunately, it is not sure if not a blending system with an eclipse depth of 3.7% creates this small transits. All planetary candidates are listed in Table A.4.
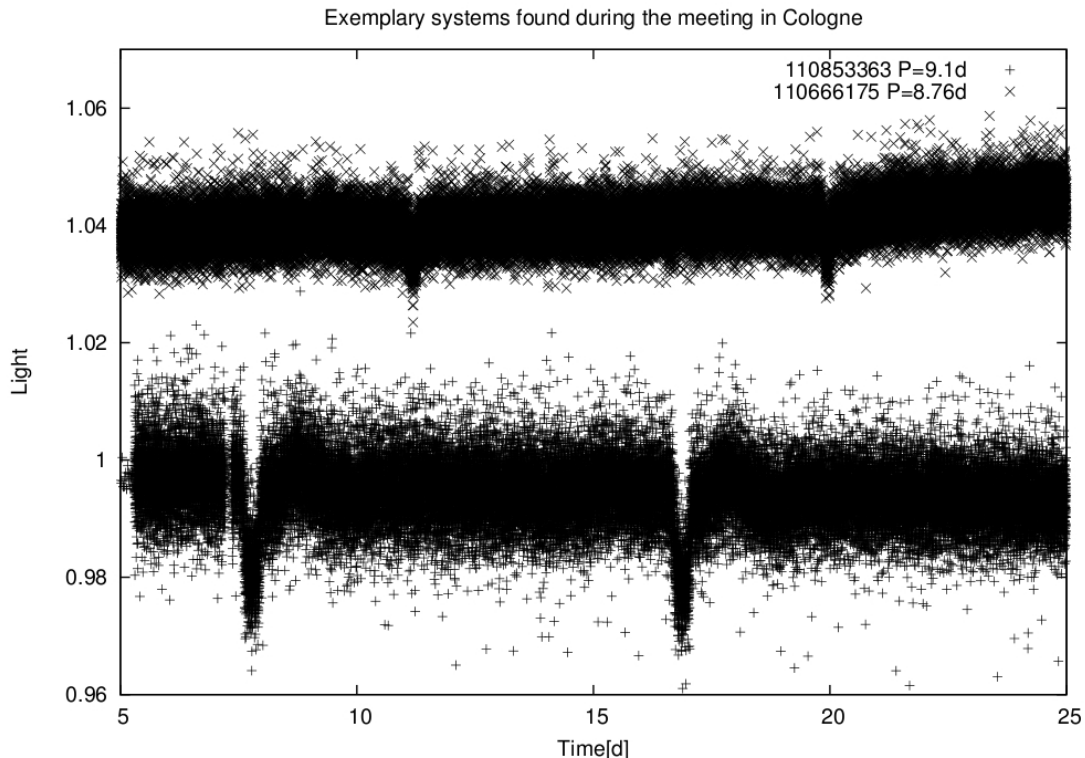

Figure 5.11.: Light curves of CoRoT 110853363 and CoRoT 110666175. Both are good planetary transit candidates and were discovered during the meeting in Cologne

5.3.3. Conclusion

The fraction of oscillating stars is a bit low but is a result of the classification method. Small amplitudes of variations were not visible in the postscript images. Therefore, small transits and low amplitude oscillations may have been overlooked. However, the aim were eclipsing binaries with sdB star components. Those were expected to be detected, since the depth of the eclipses would be several percent. A second classification of the LRa01 and LRa02 fields was done during the meeting in Cologne in November 2011. The star sample was not identical but very similar (hot stars). Sascha Grziwa programmed a tool which detrended the light curves and filtered out low frequencies with a Harmonic filter (Grziwa, priv. com.). After a box fit was performed and the light curves were phased with the detected periods. These phased images were examined by visual inspection. The results are shown in Table A.2. The fraction of detected oscillating stars is three times higher, while the binary fraction only increased by a small amount. The higher oscillation fractions resulted from the increased accuracy achieved in this way and seems more realistic. The newly detected transits were very shallow and may even result from planets, though some were not even visible in the original light curve. These new systems are interesting, and further investigations are going on, but they are unlikely to be composed of a sdB star.

In total, our binary list can be regarded as completed. Eclipsing binaries of particular interest will be examined in more detail in the next section.

5.4. Investigation of the detected eclipsing binary systems

In this section the detected EBs will be analysed in more detail. In the beginning, the orbital period will be determined with the help of FAMIAS. Furthermore, the duration and the depth of the eclipses will be measured. At the end, the stellar parameters will be fitted with SPAS and the Munari grid of synthetic spectra.

5.4.1. Light curve analysis

Among the 1654 stars, 45 have been identified as eclipsing binary systems. The fraction of 3% in the three fields agrees well with the theoretic predictions. S. Söderhjelm & J. Dischler (2005) made a large population synthesis and calculated the probability of observable eclipses. Fig ?? shows the probability
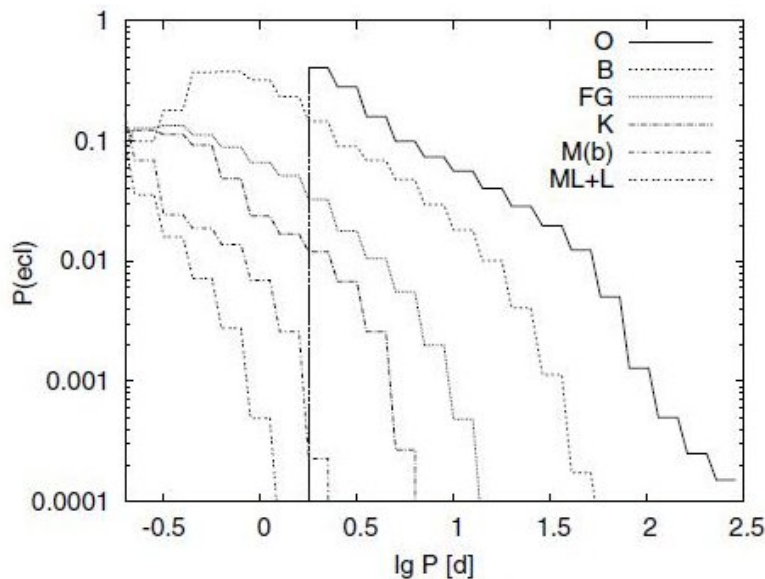

Figure 5.12.: Probability of an eclipse (S. Söderhjelm & J. Dischler, 2005).

of an eclipse with a depth of minimum 0.1 mag of main sequence stars dependent on the spectral class

and orbital period. O stars have a short period cut-off which results from their size. The large O and B stars dominate at orbital periods longer than 10 days. However, the model takes into account only main sequence stars, if one would include giants, where eclipses appear more easily due to their large size, K-giant stars would have a larger probability. For all spectral types the probability of eclipses decreases with increasing orbital period as expected.

Orbital period

The orbital period is a parameter extractable from a light curve. Already the difference between two following primary eclipses gives a rough estimation of the period. To calculate the periods more precisely, the light curves were loaded into FAMIAS and a Fourier analysis was performed. The result was confirmed with the phase plot of FAMIAS. Given that eclipses are not shaped like sinusoids, the Fourier analysis results were sometimes not precise enough to phase the whole 150 days light curve. Therefore, the frequency was varied manually until the phase plot did not improve significantly. Fig. 5.13 shows the calculated orbital periods for all eclipsing binaries. The majority (15 stars) of the EBs
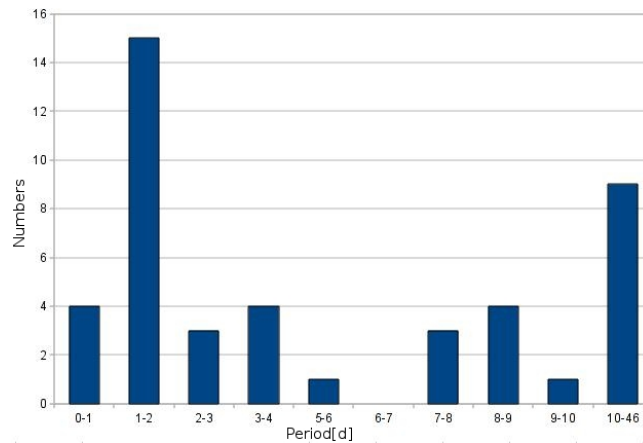
Figure 5.13.: The orbital period distribution of the identified EBs

had an orbital period between 1-2 days. Four stars even had periods shorter than 1 day. The longest orbital period detected was 45.9 days. Since the long run duration is around 150 days, the detection limit is around 75 days. The light curve of CoRoT 102874481 passed this limit and showed only one eclipse, the calculation of the orbital period was therefore not possible. All periods are listed in Table A.6.

Parameters of eclipses

The depth of an eclipse contains information about the brightness ratio of the stars. Stars with same brightness and size would have light curves with identically deep eclipses. The more different the stars are the more differ the primary and secondary eclipses. The duration of an eclipse offers information which can be used to calculate the sum of the stellar radii relative to the semi major axis. Therefore, it was decided to measure the depth and duration of eclipses. To calculate the duration, the difference between the ingress and the egress of an eclipse was measured.

The relative depth was determined on the following way: The difference of the egress brightness and the minimum of the eclipse brightness was divided by the egress brightness. Unfortunately, in light curves of the EW class binaries the ingress and the egress of an eclipse were not precisely recognizable. In such cases the brightness level between the primary and secondary eclipse was taken as the out of eclipse brightness and the duration was approximated as good as possible. In Fig. 5.14 two examples are shown to demonstrate the difficulties.

CoRoT 102717012 had the smallest measured relative depth, the primary eclipse has a relative depth of 1.8%, the secondary 0.8%. With the help of the contamination factor (see table A.3) , read from the header of the light curves, it could be checked how much flux from a star blending the system was
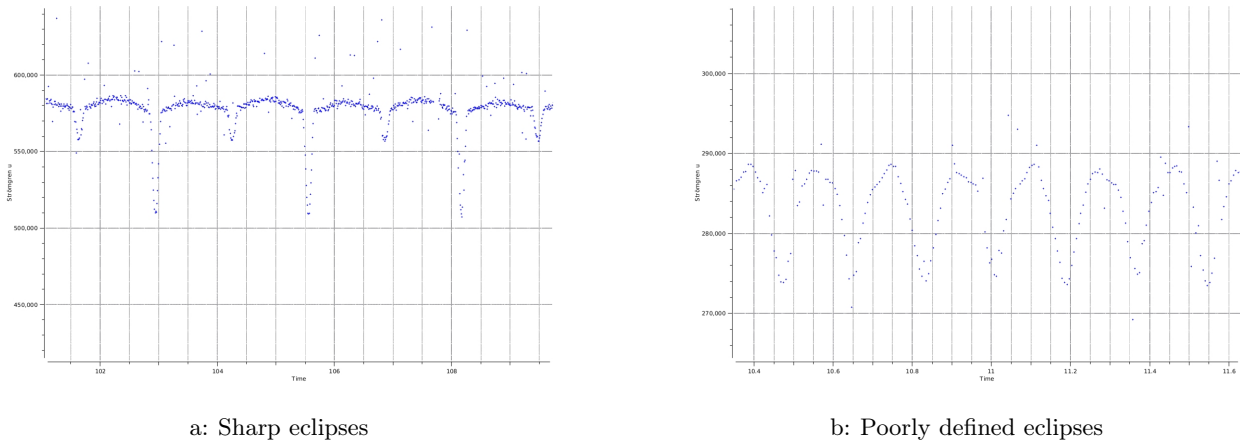
a: Sharp eclipses   b: Poorly defined eclipses

Figure 5.14.: (a) Part of the light curve of CoRoT 110764867 in which the eclipses are clearly defined. (b) Cut of the light curve of CoRoT 110666679, the eclipses have no sharp starting and ending points. The "Time" is showed in days.

measured. The deepest eclipse (47%) occurred in the light curve of CoRoT 110677259. Fig. 5.15 shows the observed distribution of the relative depths. Most stars had small eclipses, with relative depths smaller than 5%, and 10 secondary eclipses were not visible. The small relative depths may also result from small inclinations of the systems. Only 7 light curves showed total eclipses, the others were all grazing eclipses. The shortest measured duration was 0.066 days in the light curve of CoRoT 110749182
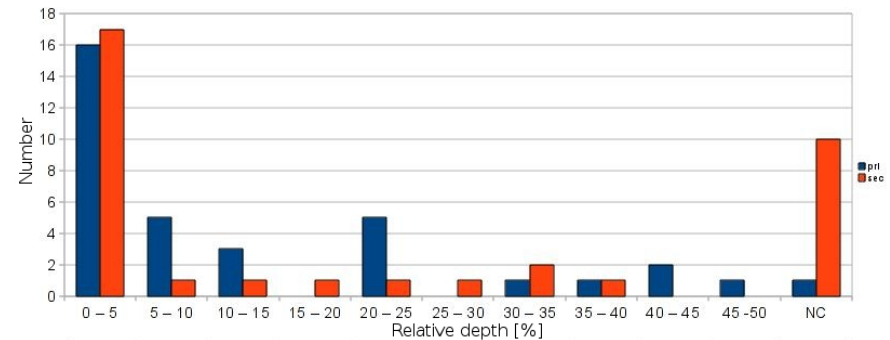
Figure 5.15.: The uncorrected relative depths of the primary (blue) and secondary (red) eclipses. Most stars had small eclipses (NC =not calculable).

(P=2.99 days). CoRoT 110857632 (P=22.08 days) has a duration of 10.8 days which is the longest measured eclipse duration in the light curves. Besides this star, CoRoT 102926060 (4 days duration) was the only star having an eclipse duration longer than 1 day. All the determined durations and depths of the binary systems are listed in Table A.6.

Classification of the eclipsing binary class

In this work the binary systems were classified with the help of the shape of the light curve. As shown in Fig. 3.4, there are 3 types of eclipsing binaries: EA, EB and EW. All binaries classified as EW had orbital periods shorter than 2.5 days. On the other hand, systems classified as EA had periods longer than 1.4 days (Fig. 5.16. In general, the shape of the light curve depends on several parameters and not only on the orbital period. In total, 23 binaries were classified as the EA type, 12 as EB type, and 10 as EW type. All EW types showed ellipsoidal deformations, none of the investigated targets had a reflection effect. All the results are shown in Fig. A.6
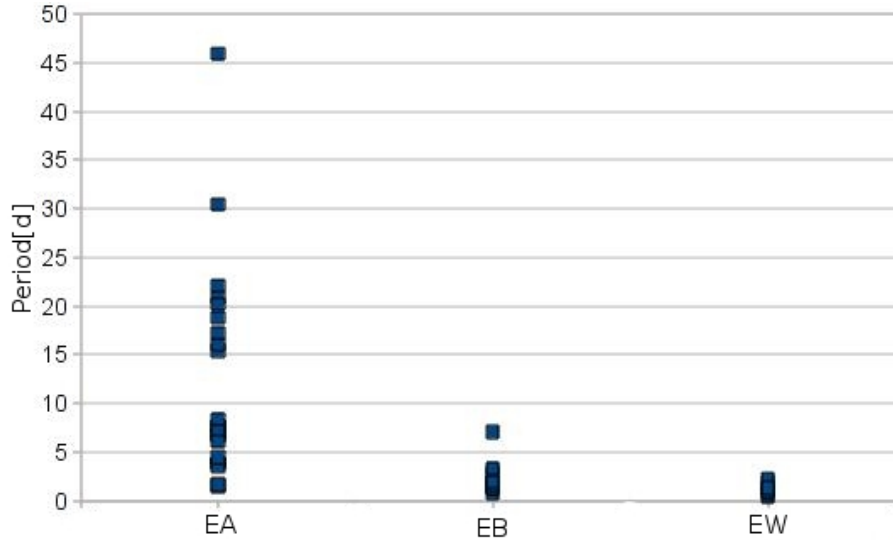
Figure 5.16.: Relationshop of the period and type.

5.4.2. Determination of stellar parameters

This section deals with the fitting of stellar parameters, in particular $log\ g$ and T_{eff}, to determine the evolution stages of the stars. The aim was to find hot stars with high surface gravity ($log\ g\ > 5$) and surface temperatures higher than 20,000 K. The following steps have been used to determine the stellar parameters:

1. The spectrum was loaded with SPAS to have an overview. This allowed to make an approximation of the spectral class and therefore, the surface temperature.

2. In this step, the usable spectral lines were chosen. Because of the resolution R=1300, it was possible to use the strong hydrogen and helium lines only to fit stellar parameters. Unfortunately, the H_β line was often unusable because of impacts on the CCD chip. In the spectra of cooler stars, it was avoided to use the H_ε line because of the blend with the Ca II H-line (Richard O. Gray, 2009). In most fits, the H_β, H_γ, H_δ, H_ε, H_8 and H_9 were used to calculate T_{eff} and $log\ g$. Helium lines were additionally used for the calculations of the radial velocity v_{rad}.

3. The first step of the fit was to determine v_{rad}. In the model fitting window the good lines were added. To minimise the errors, the used wavelength range was shortened by zooming closer into the line. In this way, only the cores of the lines were used for the fit.

4. The rough estimation of the spectral class was used to set the start values of T_{eff} and $log\ g$. Additionally, the grid points (T_{eff}, $log\ g$) to be used, had to be specified around the expected solution.

5. The wings of the lines contain information about the surface gravity and had to be clearly visible. Therefore, it was necessary to use a wider wavelength range around the lines to get reliable results.

6. In the last step it was confirmed that the results are consistent with the overall shape of the spectrum. If they were not, the start parameters were varied, and the selected range around the spectral lines was adjusted.

Problems encountered

In spectra of hot stars the Balmer series play the dominant role since only few weak metal lines are visible. With decreasing temperature the metal lines gain strength. The spectra of stars cooler than 9,000 K were difficult to fit, because some lines in the spectrum were no included in the model.

Moreover, the fit of synthetic spectral lines to the hydrogen lines always resulted in a too high unrealistic value of *log g*. A possible explanation could be the fact, that the spectra are results of binary systems and not of single stars, or that many stars in this temperature range have peculiarities which were not included in the model atmospheres. In such cases the surface gravity was fixed to the value of 4.0 dex and only the surface temperature was fitted. These results are marked with the huge *log g* error of 1 dex.

5.4.3. Results

The parameter fits with SPAS were used to determine v_{rad}, T_{eff} and *log g*. But which further information are derivable from them? Investigations of the main sequence population have shown that stars change their size during the main sequence evolution. The stars are getting bigger, and therefore the surface gravity is getting smaller with the time passed on the main sequence. Stars on the horizontal branch get hotter with their age.

The Vogt-Russell theorem says that the evolution tracks of stars depend only on their initial mass and chemical composition. Therefore, the surface gravity and the surface temperature can be derived from the age, the initial mass and the chemical composition, or they can give information about the possible evolution stage of the star. Stellar evolution calculations by Schaller et al. (1992) determined evolution tracks for stars with different masses on the main sequence.

The values of T_{eff} and *log g* for the zero age main sequence (ZAMS), when the fusion of hydrogen in the core starts, and for the terminal age main sequence (TAMS), corresponding to the exhausting of hydrogen burning in the core, were taken to mark the both evolution stages in the $log\ g\ -\ T_{eff}$ diagram. The zero age horizontal branch and the terminal age horizontal branch were constrained by the results of evolved stellar evolution calculations of Dorman et al. (1993) in the similar way, accounting the helium burning instead of the hydrogen burning. The parameter results are plotted together with the evolution stages in Fig. 5.17.

Unfortunately none of the hot stars lies on the horizontal branch. Nevertheless, CoRoT 110656145 ($T_{eff} = 21,300K$, *log g* $= 4.62dex$) and CoRoT 102714427 ($T_{eff} = 20,000K$ and *log g* $= 4.3dex$) comes close to the horizontal branch. Also CoRoT 110666679 with its short orbital period of 0.36 days is a special star. Their parameter fits and the light curves are shown as examples in the following section. All the approximated values of v_{rad}, T_{eff} and *log g* together with the errors and the number of used spectral lines are given in Table A.7.

5.4.4. Parameter fits and light curves of interesting stars

In this section, the determination of stellar parameters of three interesting stars are listed. The spectra with the fits and light curves are shown in each subsection.
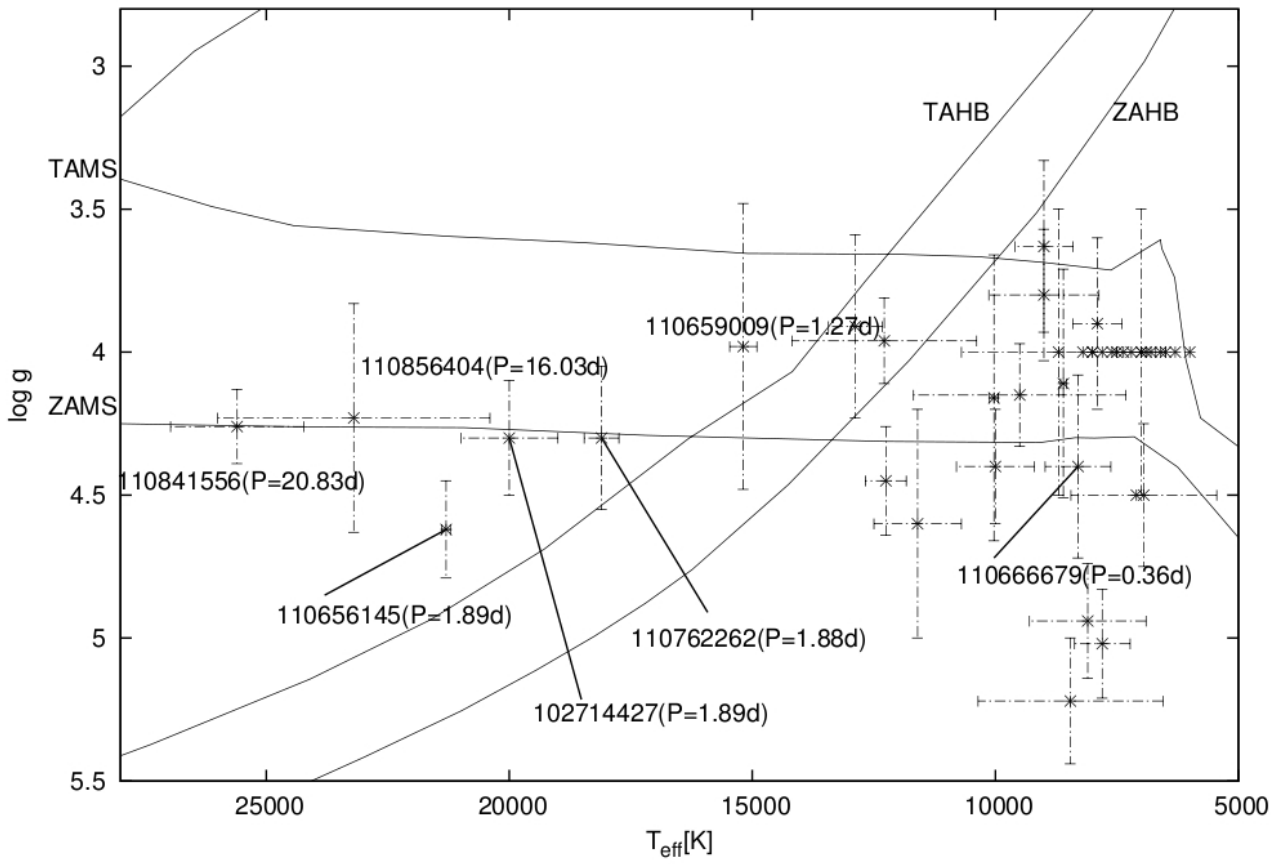
Figure 5.17.: The results plotted into the *Log g – T_{eff}* diagram. The points without error bars correspond to stars where the fit of *log g* was not possible. Additionally the ZAHB, TAHB, ZAMS, and TAMS are marked.

Analysis of the possible sdB candidate CoRoT 110656145

In the Fig. 5.18 the spectrum of the the hot star CoRoT 110656145 is shown. It contains strong helium lines and a weak Ca II K-line. The interstellar band at 4430 is very strong. This indicates a strong reddening of the spectrum. Unfortunately the H_β is strongly contaminated by cosmic impacts and could not be used in further investigations. The following 7 lines were used in the fit: H_γ, H_δ,
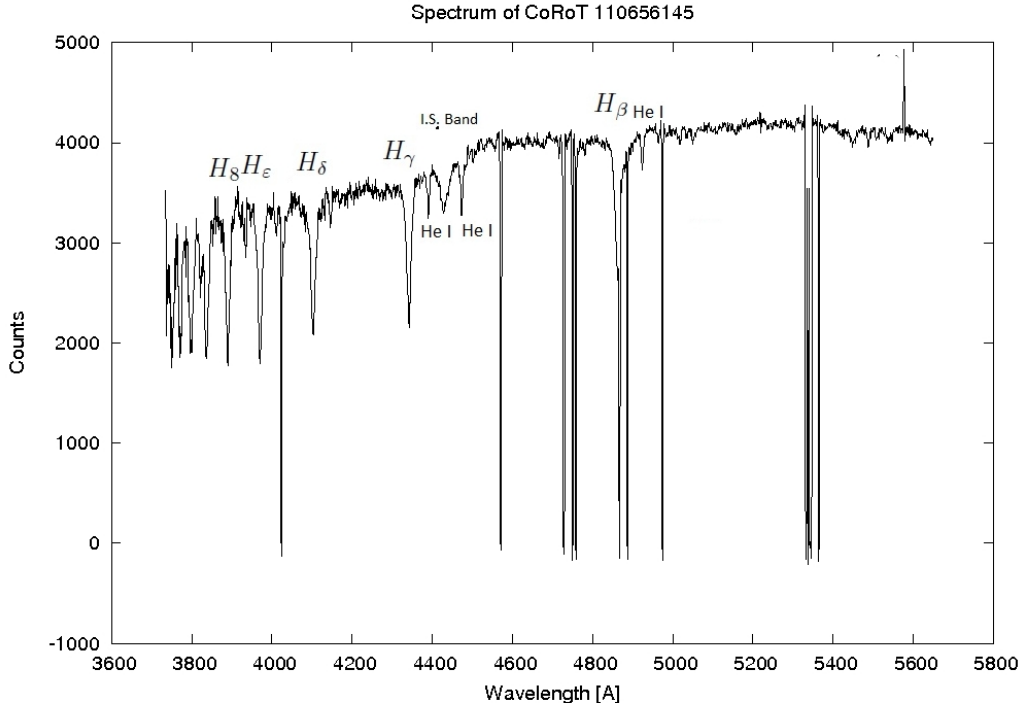
Figure 5.18.: Spectrum of CoRoT 110656145. The intergalactic reddening is very strong, since the I.S. band is strongly visible in the spectrum. Helium lines are are clearly visible and the H_β line is not usable because of cosmics impacts.

H_ε, H_8 and the He I lines at 4377 Å, 4472 Å, 4922 Å. The helium lines showed a large shift, that resulted in an radial velocity of $150 \pm 20 \frac{km}{s}$. The shift of the used Balmer lines was smaller, the radial velocity was determined to be $70 \pm 20 \frac{km}{s}$. Because of this, I decided to fit the Balmer and the helium lines separately. The parameter fit of the four Balmer lines determined $T_{eff} = 21300 \pm 1700K$ and $log \ g = 4.62 \pm 0.2 dex$.
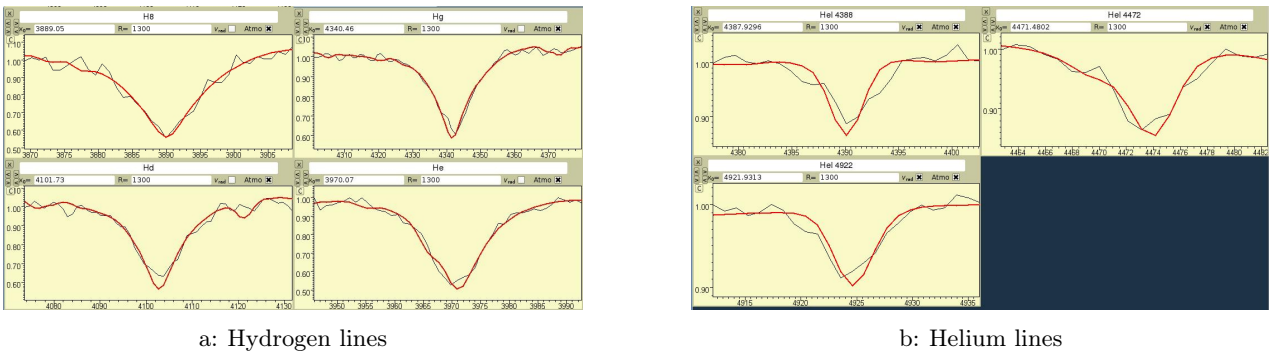
a: Hydrogen lines

b: Helium lines

Figure 5.19.: The fit of the (a) hydrogen lines and (b) helium lines. None of the fits is perfect. The solution of the hydrogen lines seemed more reliable and taken as the final result

Unfortunately, the solution of the helium lines fit did not accord with the hydrogen solution, the results were: $T_{eff} = 22300 \pm 3200K$ and $log\ g = 3.4 \pm 0.36 dex$. The reasons for this may be the composite spectrum. The parameters represent a weighted average of the parameters of each star. It is possible that the composition of the helium lines differs from the hydrogen lines which results in the different solutions. Since the hydrogen lines seemed to be more reliable, their result was noted, though it was not very convincing. The fits to the spectral lines are shown in Fig. 5.19. From the light curve of CoRoT 110656145 an orbital period of 1.89 days was derived. A part of normalised light curve in the three bands is shown in Fig. 5.20. The part was taken from the 32 seconds sampled region to achieve a good result. The secondary and primary eclipse are visible and their relative depths are
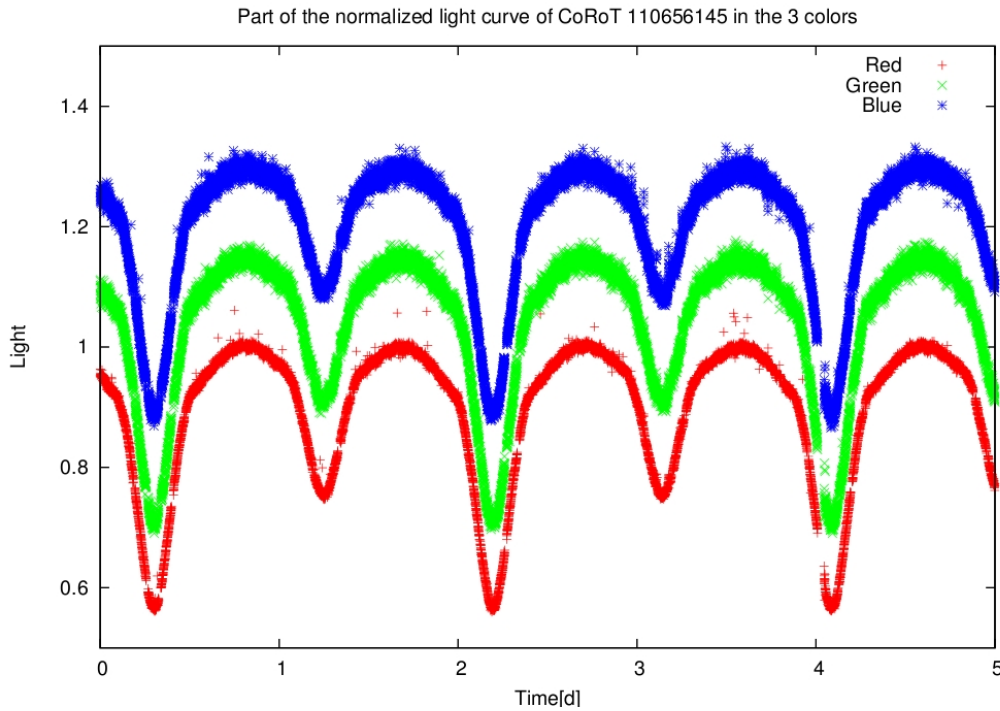
Figure 5.20.: 5 days part of the light curve of CoRoT 110656145 in the three bands. The three bands have been shifted by 0.15 respectively to each other.

44% and 25%. The contamination factor was zero for this system. Therefore, both stars may be able to contribute to the spectrum and create a composite spectrum which is not recognizable at this low resolution. Moreover, the eclipses do not change their depths in the three bands. This indicates that both stars have similar surface temperatures. The ellipsoidal effect makes a large light variation. This system remains interesting, a radial velocity curve or a spectrum with better resolution are needed to determine more accurate parameters.

Analysis of the hot system CoRoT 102714427

This star is located in the LRa01 field and was originally not included in my sample. The light curve was first seen during the meeting in Cologne. Surprisingly, it was neither mentioned in the first investigation of the hot stars in the LRa01 field. Therefore, this binary system was included into my sample. Its spectrum is shown in Fig. 5.21 The spectrum allowed me to use the following 8 lines for
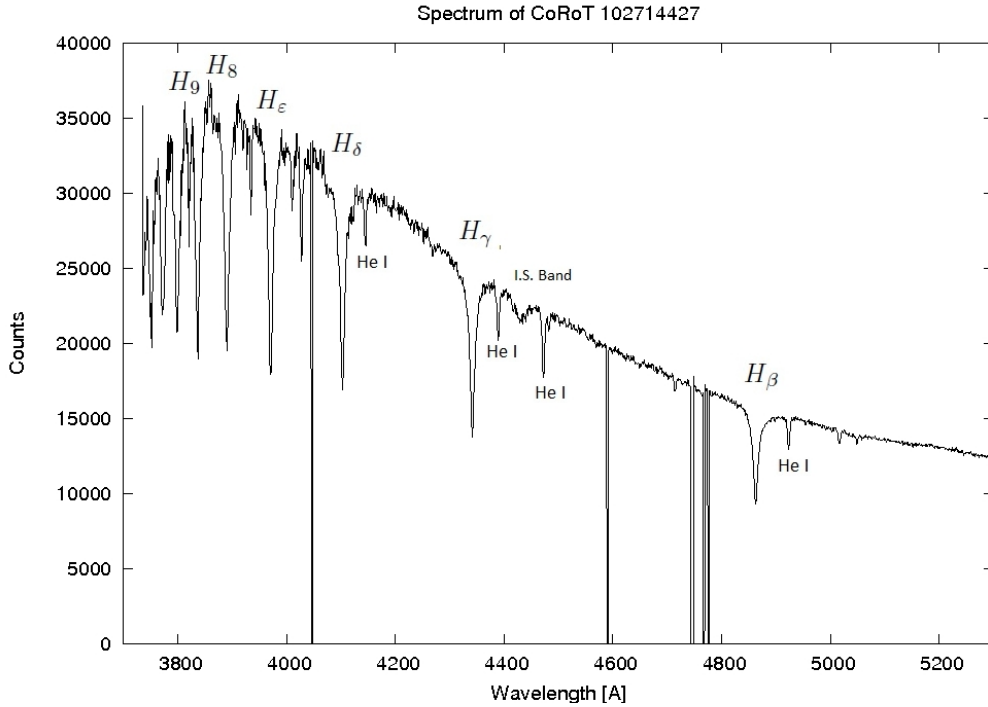

Figure 5.21.: Spectrum of CoRoT 102714427. The intergalactic reddening is weaker than of CoRoT 110656145 (see Fig. 5.18). The helium lines are are clearly visible and all Balmer lines are free of cosmic impacts.

the quantitative spectral analysis:H_β, H_γ, H_δ, H_ε, H_8 and the He I lines at 4377 Å, 4472 Å, 4922 Å. The calculated radial velocity $v_{rad} = 71 \pm 12 \frac{km}{s}$ of the helium and hydrogen lines was identical. The strong helium lines indicated an early B type star. The fit results of the lines are shown in Fig. 5.22.
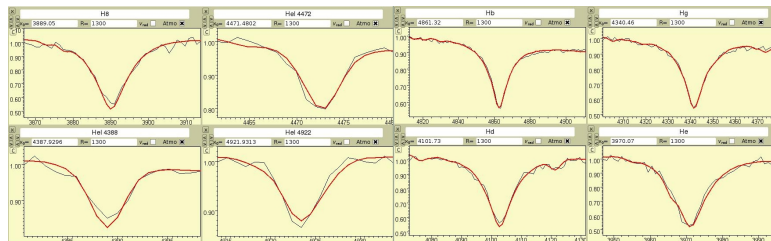
Figure 5.22.: The result of the fit of the lines from the spectrum of CoRoT 102714427: $T_{eff} = 20,000 \pm 1000K$ and $log\ g\ = 4.3 \pm 0.2dex$. Besides the H_ε all the hydrogen lines are good approximated by the fit.

The orbital period of the system is 1.89 days. The 3 colours of a 7 days long part of light curve are shown in Fig. 5.23.
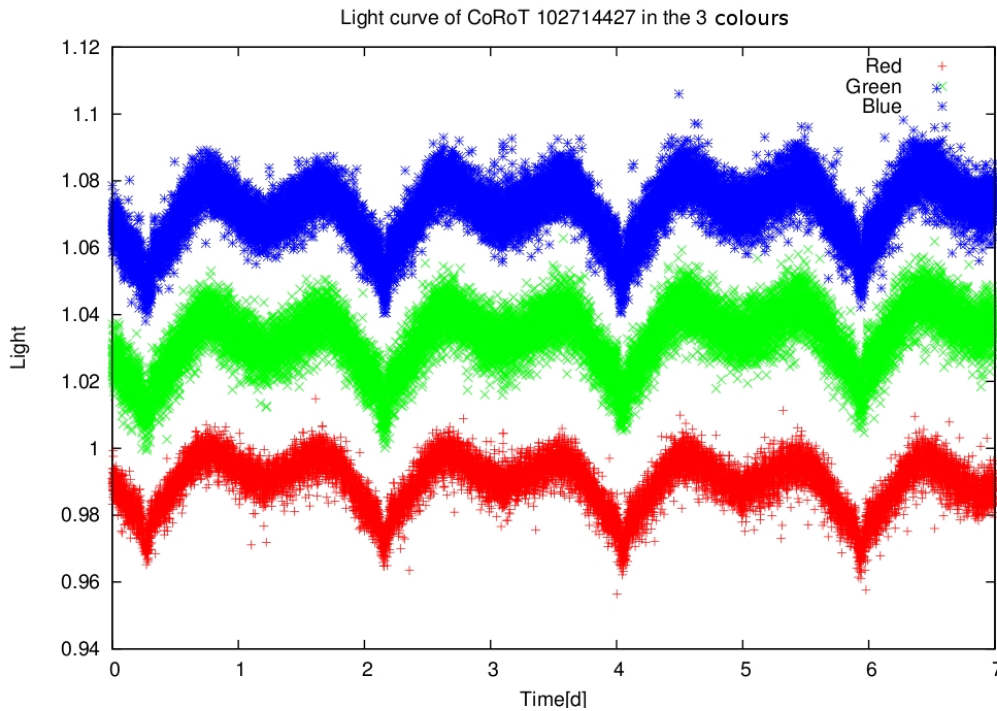
Figure 5.23.: 7 days part of the light curve of CoRoT 102714427 in the three bands. The three bands have been shifted by 0.04 respectively to each other.

The light curve shows small primary eclipses (relative depth 1%) and no secondary eclipse. The strong ellipsoidal effect has a strength of 2% at the primary eclipse. One can see that the ellipsoidal effect is weaker close to the secondary minimum. In this case the contamination is very high (29%). It is possible that the variation origins from a background star, or that the variation is larger than measured in the contaminated light curve. A possible solution would be a white dwarf (strong ellipsoidal effect hints for a compact object) and a B-type star. As seen, the light curve is very interesting, a radial velocity curve would enable to fit the light curve and to understand the shape of it. Especially, it would be possible to calculate the masses and to constrain the type of the stars.

Analysis of the short periodic system CoRoT 110666679

The CoRoT 110666679 is a promising sdB candidate, the system has the shortest orbital period (P=0.36 days) among the investigated stars. Hopefully, the stellar parameters help to set more constraints to the system. The blue spectrum is shown in Fig. 5.24.
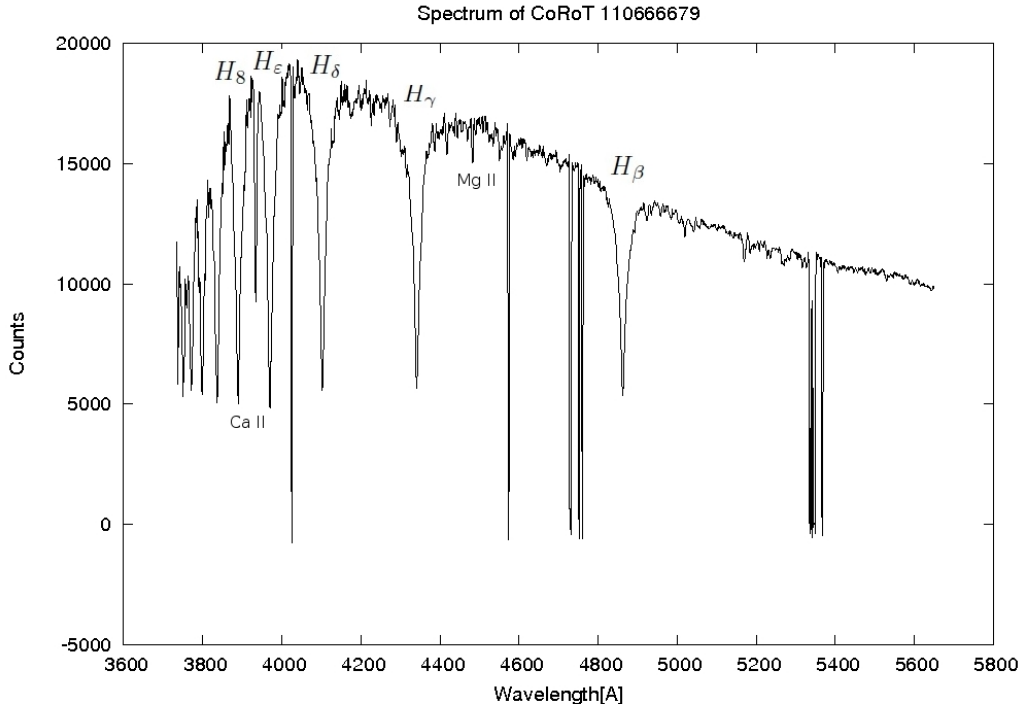
Figure 5.24.: Spectrum of CoRoT 110666679

The line Mg II at 4431 Å is too strong for a B star. Moreover, no He II lines are detectable and the Balmer lines dominate the spectrum. The Ca II K-line is almost so strong as the H_ε. All this spectral features constrain the spectral class to $A3 - A5$. The H_β, H_γ, H_δ and H_8 were used in the fit. Because of the blend with the Ca II line H_ε was excluded from the fit. The fit of the stellar parameters $log\ g$ and T_{eff} suggested 2 solutions. A Munari grid with solar metallicity lead to the first solution with $T_{eff} = 11024K$ and $log\ g = 4.5$ (Table **??** and Fig. 5.25a). The cooler solution with $T_{eff} = 8300K$ and $log\ g = 4.4$ (Table **??** and Fig. 5.25b) was determined with a lower metallicity (10^{-1} solar metallicity).

a: Hot Solution

b: Cooler Solution
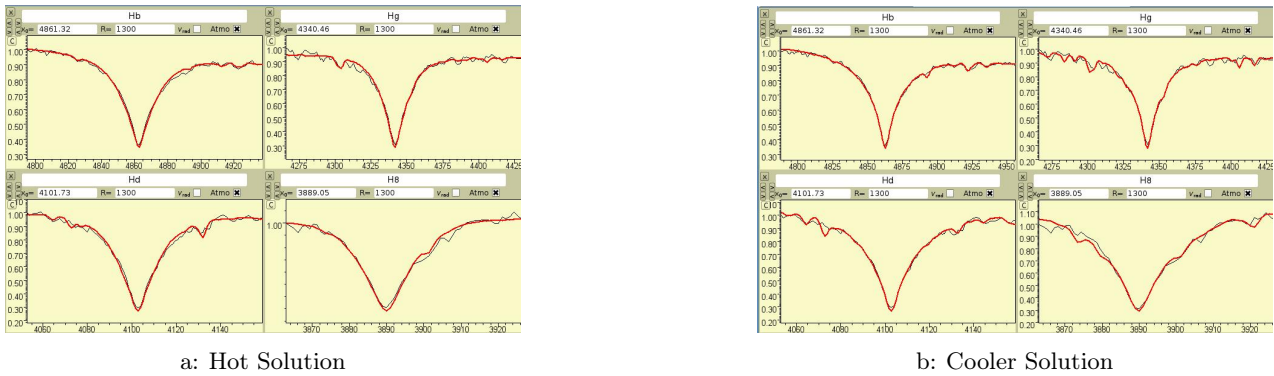
Figure 5.25.: The two fits to the spectrum. The absorption line of the spectrum is black and fitted line is red.

To assure that the Ca II K-line origins from the same star, its fitted radial velocity was compared with the v_{rad} of H_β. The radial velocities were $53\frac{km}{s}$ and $67\frac{km}{s}$ and therefore smaller than the accuracy

Line	$T_{eff}[K]$	$log\ g$
H_β	10829	4.46
H_γ	11049	4.44
H_δ	10980	4.56
H_8	11239	4.35

Line	$T_{eff}[K]$	$log\ g$
H_β	8291	4.52
H_γ	8124	4.07
H_δ	8443	4.47
H_8	8507	4.81

Table 5.1.: Hot fit solution of CoRoT 110666679

Table 5.2.: Cool fit solution CoRoT 110666679

Table 5.3.: Fit results of CoRoT 110666679.

achievable with this resolution. Since the other spectral features suggested a spectral type of A, it was decided to accept the cool solution. A 1.5 days long and 32 seconds sampled part of the light curve is shown in Fig. 5.26. The red channel shows clear characteristics of a binary system, while the green and
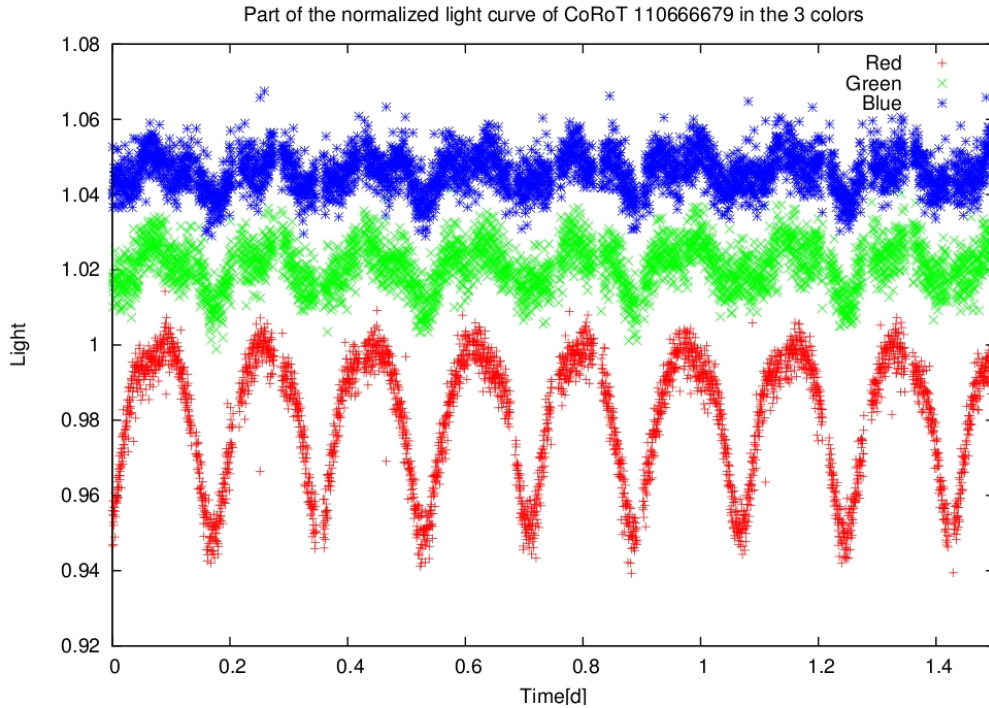
Figure 5.26.: 1.5 days long part of the light curve of CoRoT 110666679 in the three bands. The three bands have been shifted by 0.025 respectively to each other.

blue channel offer a poor quality. The depths of the secondary and primary eclipses in the red channel are almost equal. Obviously, the depths decrease with wavelength, in the red channel the primary has a relative depth of 5% , in the green channel of only 2%, and in the blue channel 1%.

The star is too cool to be a sdB candidate. Additionally, the surface gravity is to low compared to sdB stars, Nevertheless, the system remains interesting. With the help of Kepler's third law (see equation 3.1) the semi major axis is calculable with assuming a mass of 2.5 $M_\odot$ (typical mass of spectral type A star) for the primary and varying the mass of the secondary in a range of 1.8-2.4 $M_\odot$ (Spectral type A) and using the period of 0.36 days. The stellar radii were calculated with the mass radius relation for main sequence stars ($R = M^{0.57}$). Morover, the semi major axis together with masses enabled to calculate the Roche lobes. The result is shown in Fig. 5.27. It is not possible that the stars are main sequence stars, since their radii would lay outside their Roche lobes. The stars have to be more compact objects to fit inside their Roche lobes. Further investigations are going on, and now a radial velocity curve would be needed to determine the stellar masses and the evolution stage of the stars. The systems is very interesting and will be hopefully understood soon.
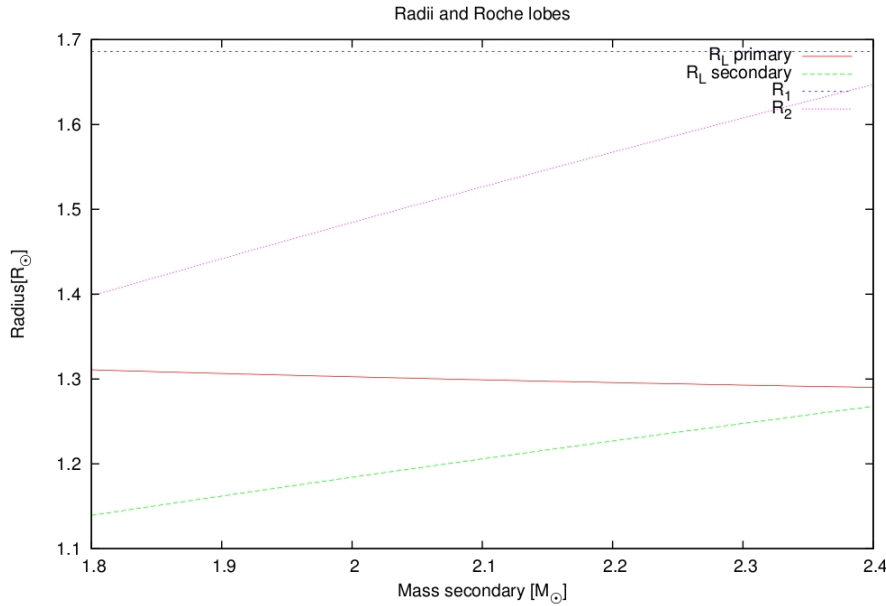
Figure 5.27.: The Roche lobes and the stellar radii plotted against the mass of the secondary (M primary is fixed at 2.5 $M_\odot$. Both stars would lay outside their Roche lobes, which excludes the solution with 2 main sequence stars of the spectral type A

5.5. Detailed determination of orbital periods

In January 2012, 20 days observation time at the McDonald observatory in Texas were received. It was planned to measure radial velocity curves of interesting CoRoT stars. As preparation, all systems with orbital periods shorter than 1 day and hot objects with periods shorter than 2 days were investigated in more detail. The goal was to determine more precise periods of the systems. This was done in the following way:

1. Removal of the bad measurements with the help of the flags in the data files (see section 5.1).

2. Removal of the linear trends in the light curve. In order to do this, the light curve was divided by a liner function which was fitted to the light curve before.

3. Performing a Fourier analysis to determine large oscillation and the orbital period. If large oscillation were visible, they would be removed. If the light curve contained empty parts (LRa01 field) or was not equally sampled (switching from 512 seconds to 32 seconds sampling time) the Fourier analysis would fail. These light curves were interpolated to a equal sampling rate. Since the results were not satisfying, a Savitzky-Golay smoothing filter was applied to smooth down the interpolated light curve without affecting the eclipses. Afterwards, the Fourier analysis worked and the periods could been calculated. Nevertheless, only the light curve without the interpolating and smoothing was used for further investigations or plots.

4. Testing of the orbital period with the phase function of FAMIAS. This test often showed that the achieved periods were not accurate enough to phase fold the full length of CoRoT light curves. In this cases, the least squares fit in FAMIAS improved the accuracy. The reason for this is the shape of the eclipses and the light curves. In contrast to oscillations, eclipses may look completely different to sinusoidal function. The Fourier analysis failed therefore to determine the exact frequency. The orbital period with the best phase fold was taken.

5. A programmed tool was used to phase the light curve since FAMIAS did not allow to set a starting point, neither to change the phase range. The primary eclipse was set to phase $\Phi = 0$

and the range to $-0.2 < \Phi < 1.2$. An additional binning of the factor 100 was applied and plotted on top of the light curve.

In total, 4 binary systems had orbital periods shorter than 1 day (CoRoT 110666679, CoRoT 110856005, CoRoT 102725895, and CoRoT 102634660) and 5 systems with periods shorter than 2 days had a high surface temperature(CoRoT 110858300, CoRoT 110659009, CoRoT 110656145, CoRoT 102648472, and CoRoT 102858100). Their light curves and results are shown in the following sections.

5.5.1. Results

- **CoRoT 110666679:** This light curve was already shown in Fig. 5.26. The phase folded light curve in Fig. 5.28 reveals more details. The starting point of the secondary eclipse is separable from the ellipsoidal variation at $\Phi \approx 0.38$ and $\Phi \approx 0.62$. But the eclipses are still equally formed and are only separable due to their different depth.

- **CoRoT 110856005:** The primary and secondary eclipse are both total (see Fig. 5.29) . The brightness at $\Phi = 0.75$ is a bit higher than at $\Phi = 0.75$ which could result from the Doppler beaming. Moreover, the light during the total primary eclipse is not constant. It increases softly. The light curve of this system looks like a light curve of a contact system. The listed contamination is 22% and not negligible. The corrected depths of the eclipses would be 19% and 13%. A radial velocity curve is needed to approve the possibility of the Doppler beaming.

- **CoRoT 102725895:** This light curve contains very small eclipses ($\approx 2\%$) and the variation outside the eclipses is small. The contamination is only 2% and therefore, negligible. The light curve is shown in Fig. 5.30, this system may be a detached system of small and cool stars.

- **CoRoT 102634660:** The eclipses are almost total, at the primary eclipse, the light still increase by a small amount during the "total" eclipse phase (Fig. 5.31). Additionally, the brightness level of $\Phi = 0.25$ is a higher than at $\Phi = 0.75$. This difference may result from the O'Connell effect since the system is very close (P=0.85d) and relative cool with ($T_{eff} = 8000K$). The two stars are probably engulfed by a circumstellar material. The side of the star which always collides with the surrounding material and gets heated up faces the observer at the phase $\Phi = 0.25$. At phase $\Phi = 0.75$ the unheated side of the star is faced to the observer and is therefore fainter as the other side. The contamination is very low (1%).

- **CoRoT 110659009:** The light curve (Fig. 5.32) has deep secondary and primary eclipses and is contaminated by a factor of 0.05. Both are total and the limb darkening is visible. Additionally a strong ellipsoidal effect is visible. The binary probably consists of two main sequence B stars.

- **CoRoT 110656145:** The eclipses in this light curve are grazing (Fig. 5.33). They are very deep (Relative depth: $\approx 45\%$ and $\approx 25\%$ and separated from the small ellipsoidal effect. The contamination is zero. The components of this system are probably two main sequence B stars.

In Table A.8 the periods and further information are listed.

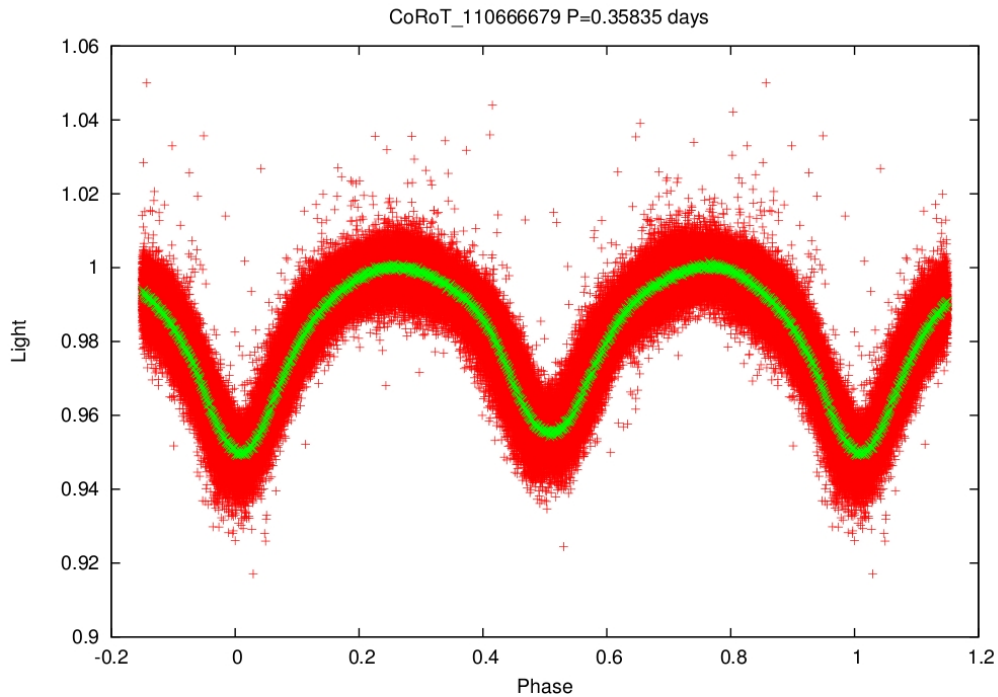## 5.5.2. Phased light curves

Figure 5.28.: Phased light curve (red channel) of CoRoT 110666679. The binned light curve is overplotted (100 data points). Mean stellar parameters: $T_{eff} = 8300K$, $log\ g\ = 4.4dex$
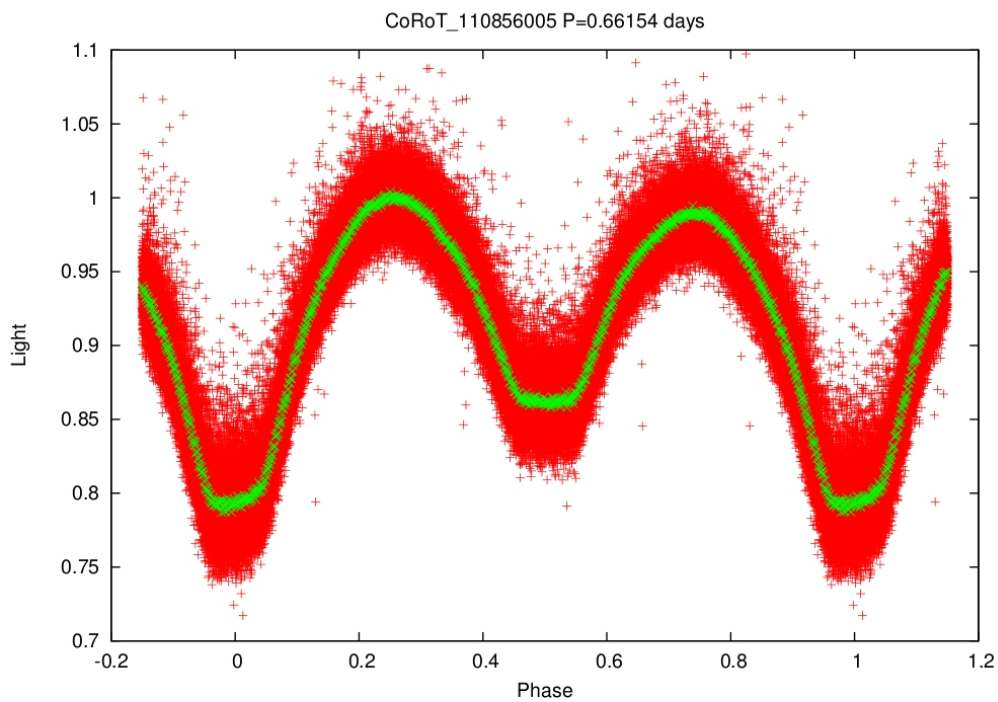

Figure 5.29.: Phased light curve (red channel) of CoRoT 110856005 with an overplotted binned light curve (100 data points). Mean stellar parameters: $T_{eff} = 7300K$, $log\ g\ = 5.9dex$ (*log g* is too high, out of model grid)
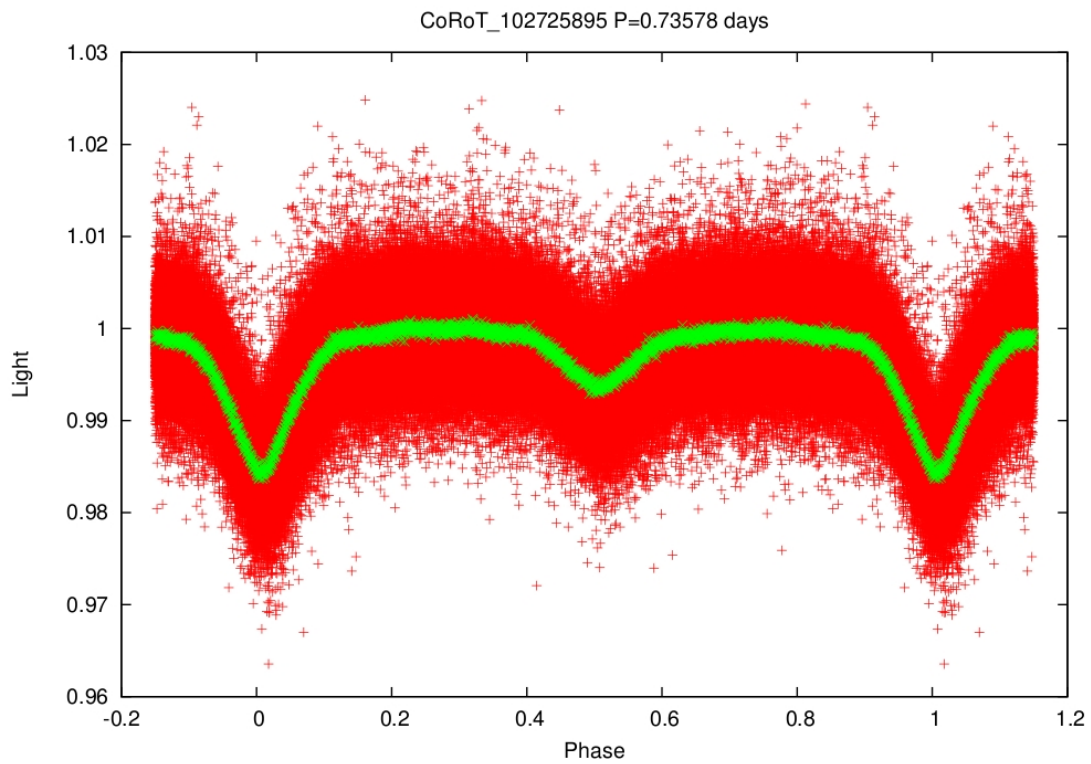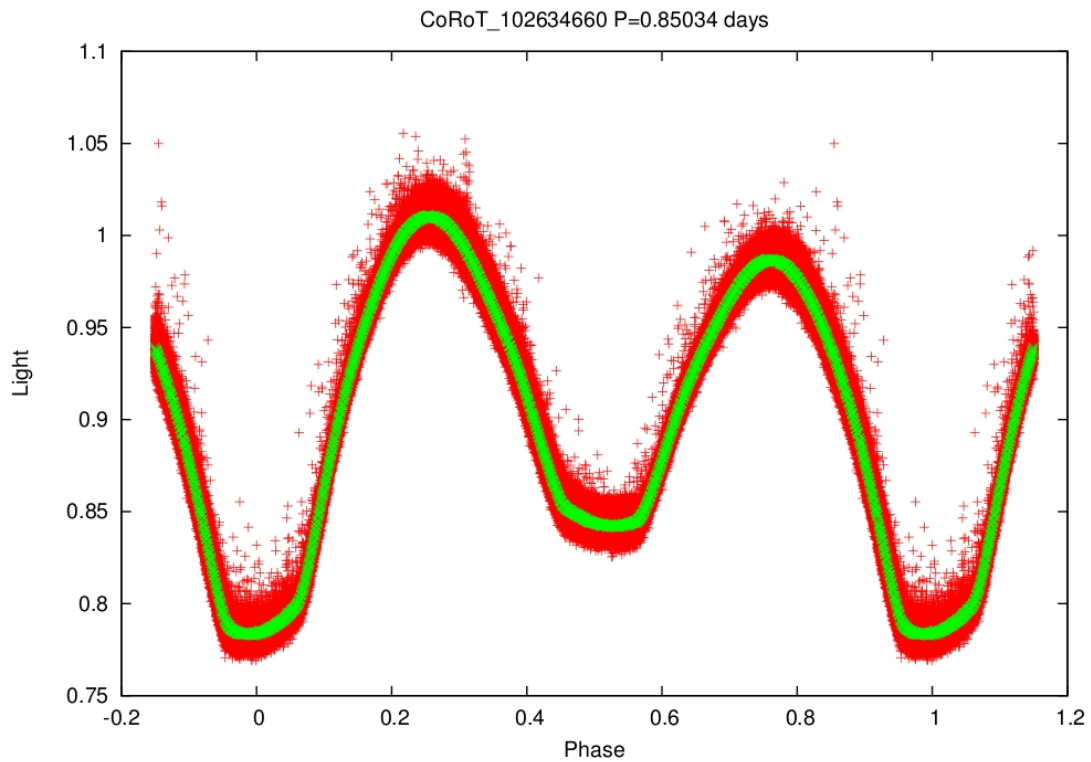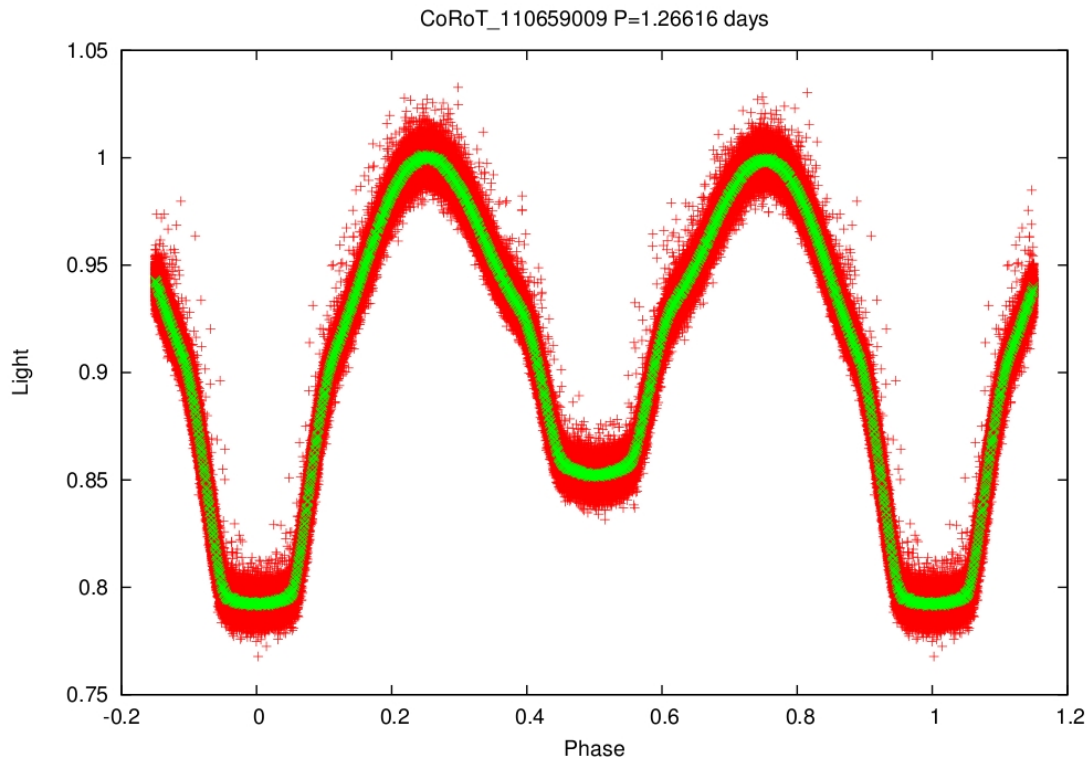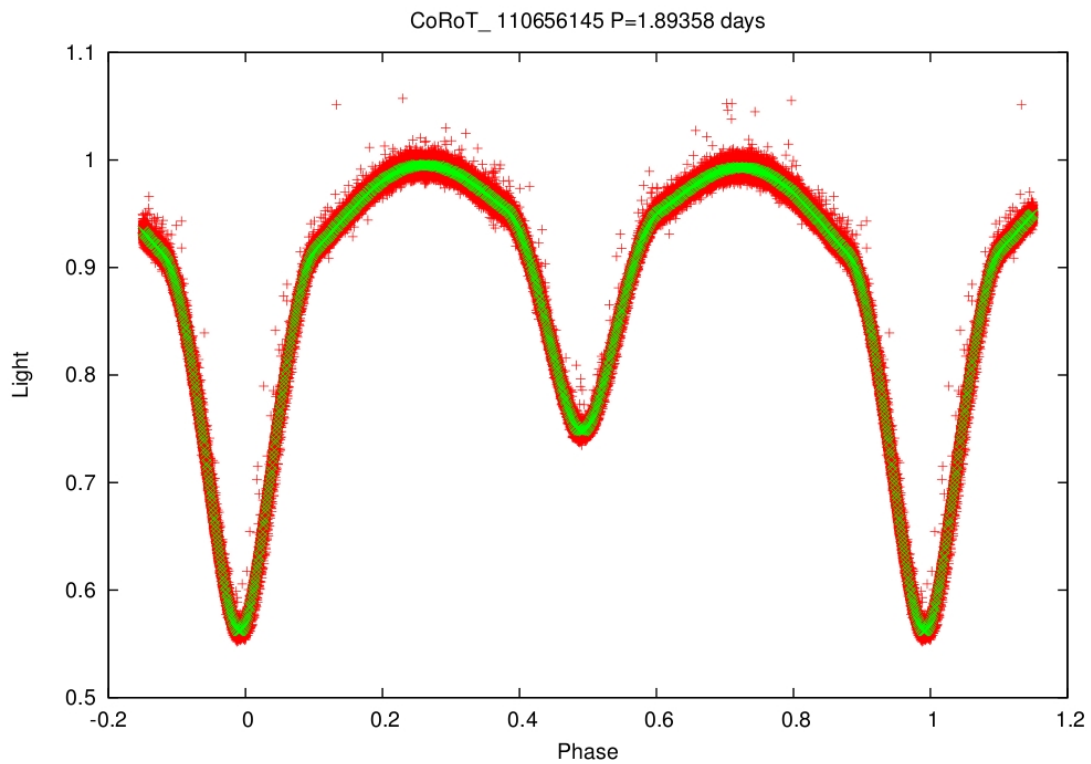
Figure 5.30.: Phased light curve (red channel) of CoRoT 102725895 (With overplotted binned light curve (100 data points). The fit of the stellar parameters was not possible (star is too cool)

Figure 5.31.: Phased light curve (red channel) of CoRoT 102634660 (With overplotted binned light curve (100 data points). Mean stellar parameters: $T_{eff} = 8000K$, $log\ g\ = 4dex$

Figure 5.32.: Phased light curve (red channel) of CoRoT 110659009 with an overplotted binned light curve (100 data points). Mean stellar parameters: $T_{eff} = 15200K$, $log\ g\ = 3.98dex$

Figure 5.33.: Phased light curve (red channel) of CoRoT 110656145 with an overplotted binned light curve (100 data points). Mean stellar parameters: $T_{eff} = 21300K$, $log\ g\ = 4.6dex$

6. Photometric campaign at Calar Alto

Unfortunately, no good sdB candidate was found in the CoRoT fields. Parallel to the investigations of the CoRoT we searched for HW Virginis systems in another campaign. In this context I had the chance to measure a light curve by myself. In October 2011, I had the opportunity to run my own observations in the German-Spanish Astronomical Center at the Calar Alto. I received 5 nights of observation time for the project Massive Unseen Companions to Hot Faint Underluminous Stars from SDSS (MUCHFUSS). The project searches for sdB stars with compact companions, like supermassive white dwarf($M > 1.0 M_\odot$), neutron stars, or black holes (Geier et al., 2011). The aim of this observation run was to identify the selected sdB star companions with the help of light curves. Since RV measurements predicted a binary, we hoped to find an eclipsing binary system to determine the inclination. This would help to solve the orbital and stellar parameters. The observatory is located above 2,000 metres in the Sierra de Los Filabres (Andalucia, Southern Spain) north of Almeria. In

Figure 6.1.: Calar Alto observatory (MPIA webpage)

figure 6.1, the four telescopes with apertures of 3.5 m (right top), 2.2 m (left top), 1.5 m and 1.23 m are visible. The fifth telescope is not used for science any more. The observatory is operated jointly by the Max-Planck-Institute für Astronomie (MPIA) in Heidelberg, Germany, and the Instituto de Astrofisica de Andalucia (CSIC).

6.1. Instrument

For the observation, the 2.2 m telescope equipped with the Bonn University Simultaneous Camera (BUSCA) was used. Most information in this section is from the BUSCA manual (Cordes, priv. com.) and the dissertation "Simultaneous Multichannel Photometry with BUSCA" by Cordes (2004). The camera allows simultaneous photometry in 4 bands, which saves a lot of time since the complete optical spectrum is observed at the same time and therefore with identical conditions. To achieve this, a beam splitter divides the incoming light beam in four different colours, ultraviolet, blue-green, yellow-red

and visual infrared. The main components of the beam splitter are three dichroic plates, each splitting the incoming light into a blue totally reflected and a red transmitted beam. In Fig 6.2, the optical path of the light through BUSCA is shown. Additionally, a filter wheel with four positions for each
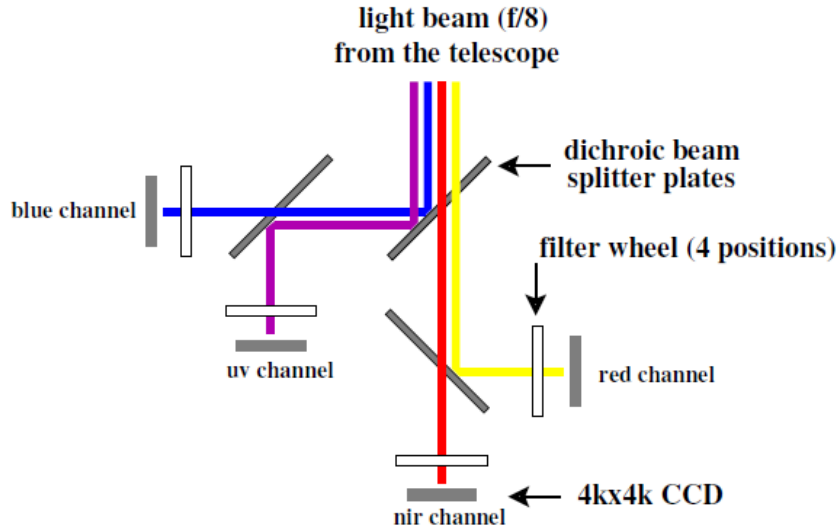

Figure 6.2.: Schematic view of the light path through the BUSCA beam splitter(Cordes, 2004)

BUSCA-band is installed. For this, several filter sets are available like the Strömgren filter system (u, v, b, y, $H\beta_{small}$ and $H\beta_{wide}$). An additional Cousins-I filter is added to match the infrared channel of BUSCA. Furthermore, BUSCA has its intrinsic filter system (UV_B, B_B, R_B and NIR_B) which is defined by the transmission curves of the beam splitter (see Fig. 6.3) and enables broad band photometry. Moreover, the glass filters protect the beam splitter from dust and mechanical impact during the Dewar mounting and demounting. Also, their thickness is the same as the thickness of the Strömgren filters, which avoids a changing of the focal plane when switching the filters and makes refocusing unnecessary. All together, BUSCA is a great instrument and makes use of all of the optical bandwidth when used with the intrinsic filter.
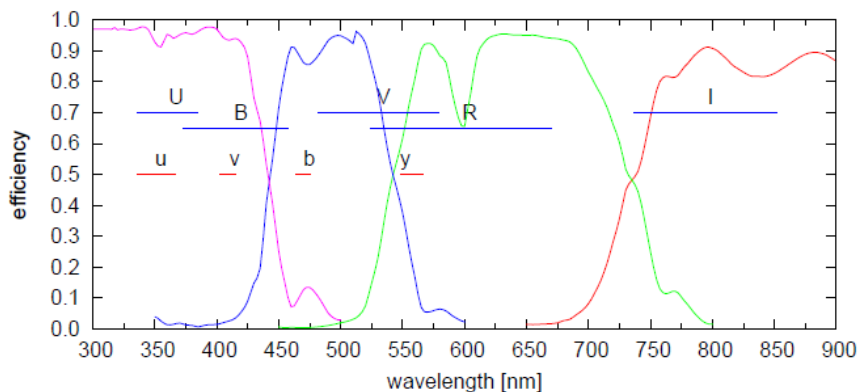
Figure 6.3.: Characteristics of the BUSCA channel transmissions(curve) and the Strömgren (u, v, b, y) and Johnson-Cousins(U, B, V, R, I) filter positions (Cordes, 2004). The use of the Johnson-Cousins filters is not possible because their bands do not lie inside the BUSCA bands(V is partly in B_B and R_B)

6.2. Observing

Before heading off to Spain, a lot preparation had to be done. For this purpose, Veronika Schaffenroth, introduced me to the BUSCA system. Additionally, information for the reduction and preparation was taken from Hilditch 2001, chapter 5.

6.2.1. Preparation

To assure an efficient usage of the time during the observation, it was necessary to prepare the target list and the finding charts.

Target list

All started with the selection of the targets. The starting point was a list of 238 sdB stars which are known to show significant radial variations at short time scales. As preselection, I searched for the observable targets and afterwards picked out the scientific interesting objects.

1. *Observational aspects:* The first selection criterion was that all targets should reach at least 60° altitude during the night. This avoided high extinction, especially in the ultraviolet channel, due to the increasing air mass with lower altitude. The list of interesting objects contained 88 stars. As a next step, the faint stars (>17.5 mag) were sorted out and put on a backup list. Practical experience showed that the conditions for such faint objects must be very good to achieve valuable light curves in the four bands. Additionally, the long exposure time would not allow sufficient sampling. Secondary it was important to have stars well distributed over the night. Therefore, it was tried to have stars culminating at different times to assure observable targets for the complete night. In this way, 190 stars were removed and a primary list of visible, bright and homogeneously spread stars remained.

2. *Scientific aspects:* The final step of the selection was to separate the interesting targets (final list) from the normal targets (primary list). This was done by reviewing their RV measurements, in some cases a tentative orbital period was available and the stars with periods shorter than 5 hours were put onto the final list. Due to the fact that only few systems had a preliminary period, stars with small RV variability were preferred.

3. *Additional aspects:* Additionally, a few very bright objects (< 15 mag) joined the list, even if they did not match the previous criteria. This assured the availability of observable targets in the case of bad conditions. Moreover, stars which were observed in the previous five runs by Veronika Schaffenroth were sorted out as well.

I the end, the final list (see table A.9) consisted of 25 stars. Three stars are brighter than 16 mag to be observable during bad conditions. On the other hand, two stars were picked with 17.5 mag in the case of excellent photometric nights. The right ascensions and declinations are well spread over the sky. With this targets I could adapt to the conditions and observe the 5 nights without the leak of stars.

Position charts

After the selection was done, for each star on the final list an altitude diagram was created, in which the altitude of the star was plotted against time. Also a figure which showed the star track on the sky was created. This information could have been useful in the case of strong wind when the telescope was allowed to point only in a specific direction or during a partially cloudy sky. With this information, it was assured that during the observation a fast selection of the target was possible, to ensure a good time management and high quality of data.

Finding charts and comparison stars

Finally, finding charts were created with the help of the SDSS database (SDSS, DR7 data release). The database allowed to choose the reference stars which are necessary for differential photometry in advance, since it provided brightness information of each star in different bands. The finding charts were scaled to $12' \times 12'$, which is nearly the astronomical field of view of BUSCA in combination with the 2.2 metre telescope. To avoid overexposures, it is important that the reference stars do not differ more than 2 magnitudes in the ultraviolet (u) and less than 1 magnitude in the near infrared (i) band in the SDSS filter system. This requirement was not always possible to fulfil, because the sdB stars are very bright in the u band. It was impossible to find enough stars with the same colour, the comparison stars were much brighter in the infrared band and fainter in the ultraviolet band. Therefore, the constraints were weakened to find enough reference stars. In the end for each target 7 reference stars were selected to overcome problems which might occur later during the observation.

6.2.2. The observation

Before starting the measurement, the weather conditions had to be checked. Strong wind or high humidity may damage the telescope and it is forbidden to open the dome under such conditions. Since a very precise pointing is necessary, the tracking has to be supported by a guiding star to correct the telescope pointing against the earth rotation. Next, the focus was set up by a sequence of 9 measurements, each with a small change of the focus. The control software offered this automated measurement and only the start focus, value of the change and the number of measurements had to be defined. To determine the best value a parabola was fit to the full widths at half maximum of a star with different foci and the minimum was taken. Since the focus depends on the tube temperature, which varied slightly during the night, small corrections had to be applied during observations, usually every 1-2 hours.

Window mode

BUSCA provides the option to read out only specified rectangular areas from the CCD. With this option, the readout time of the data could be shortened significantly. It was decided to use 5 windows to assure enough working reference stars. Problems which make a reference star unusable are for example overexposure and intrinsic variability. The windows were neither allowed to overlap, nor to touch the border of the chip. Therefore, the size of the windows was adapted to this restrictions and to the seeing conditions. A size of 60 x 60 pixels was used which contained enough sky background to reduce the data efficiently and to keep the readout time still low compared to the exposure time. For example, J1920 was exposed for 25 seconds with 5 windows each with a size of 60 x 60 pixels. The readout time was only 18 seconds which lead to a time resolution of 43 seconds.

To calibrate the windows, a full CCD image in the R_B *channel* was taken and compared with the finding chart (see Fig. 6.4) The software transferred the coordinates automatically to the other channels. The huge white lines are results of an overexposure of some stars which saturated the CCD pixels. After locating the target and its reference stars, the windows were set around those coordinates and finally the measurement could be started.

Exposure time

Since BUSCA measures the flux in the 4 channels simultaneously, the same exposure time had to be used in all channels. This made the selection of the exposure time tricky. The main criteria was to avoid saturation of any star in the most sensitive red channel by keeping the counts of the pixels below 25,000. Sometimes, when the seeing got better the counts raised dramatically. In this case a small defocusing was performed to lower them again.
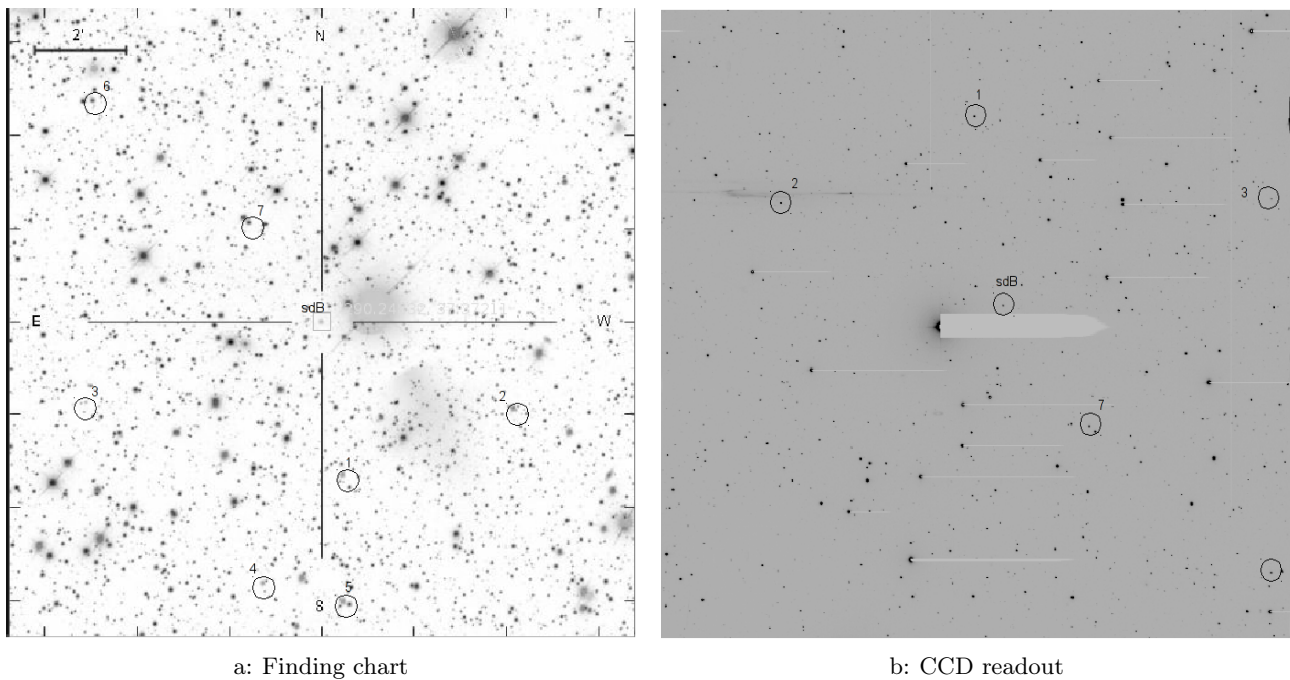
a: Finding chart   b: CCD readout

Figure 6.4.: Comparison of the finding chart and real colour-inverted image from the CCD of J1920 (marked star). The CCD image is rotated by 180° and the FOV is a bit smaller than of the finding chart.

The nights

The first observing night (26.10.11) was very humid and it was impossible to make any observations. Sadly, the two following nights were foggy as well. The end of the third and the fourth night had conditions which allowed observations. Fortunately, the fifth night was completely clear and offered perfect conditions. In total, 5 stars could be observed from which one was measured in very cloudy conditions, another one with seeing above 2.5 and the last three with clear sky and seeing below 1.5.

Additional measurements: Bias and Flatfield images

After each observation, a bias frame, which is a zero second exposure with closed shutters, and a flat field, where the telescope points to homogeneous illuminated area, were needed. The bias frame defines an offset for every pixel, while the flat field calibrates each pixel's sensitivity. Basically, this is done during the time before sunrise or after the sunset and called sky flat. Another way is to point to a foil which is illuminated by halogen lamps inside the dome, these flats are called dome flats. For this work, the dome flats were sufficient and were taken together with the bias during the following day with the same window configurations as the measurements.

6.2.3. Reduction

The reduction of the data was done with the astronomical package IRAF[1] (Image Reduction and Analysis Facility). In the following section, a small description of the reduction steps are given, which are needed to extract a light curve from the raw data.

First of all, two corrections have to be applied to receive scientific data from the raw CCD images. As mentioned above, for every observation a corresponding bias and a flat field were recorded. These data are now needed to apply corrections on the raw data files.

---

[1] http://iraf.noao.edu/

Bias correction

Each electronic device has electric noise, so does the CCD. While reading out the CCD, a small voltage is applied to avoid negative values due to the noise. This pretends a higher flux per pixel as was really measured and this offset is called bias signal. Exactly this offset is measured with a bias measurement. To minimise statistical errors, at least 15 exposures were done and averaged after. This so called masterbias is then subtracted from each measurement.

Flat field correction

The flat field correction is important to determine the sensitivity of each pixel. Individual pixels do not have the same sensitivity due to thickness or manufacture differences. Additionally, dust grains can enhance the opacity which changes the response in an unevenly distributed way. To overcome this issue, the flat field is used. To create the masterflat, a minimum of 15 flats for each target were taken, and corrected for the bias signal. Accordingly, all bias corrected images were divided through the normalised masterflat. These images represent the scientific data and are used for the following photometric reduction.

Photometric reduction

After these corrections, the data is still in a two dimensional image format (fits file). The photometric reduction transforms these data into brightness information. The starting point is the corrected CCD image, the image of J1920 is shown in figure 6.5. In this case the target is the third from the left, the other windows contain the reference stars. To extract the image information, the IRAF function
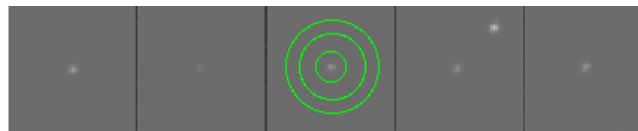
Figure 6.5.: CCD image of J1920 with the aperture (inner circle and sky annulus area between second and third circle))

"phot" was used. This function centres a circle called aperture (inner circle in figure 6.5) on the star and sums up the counts inside it. Since the "empty" sky is not perfectly dark, these counts additionally contain the stray light which has to be subtracted. Phot determines the average sky value inside the sky annulus (area between the second and third circle in figure 6.5) by summing up the counts and dividing by the corresponding area, any stars located inside the sky annulus are detected and excluded. The radius of the aperture depends on the seeing and the focus, in this work it was set to the triple of the mean half width at half maximum of the star. The aperture and the sky annulus were separated by at least 5 pixels to avoid any flux from the star. Setting the sky annulus width to around 10 pixels led to good results. To determine the brightness, the area where the flux was integrated is multiplied with the average sky value and subtracted from the star flux. In this way, the brightness for each of the windows was extracted and this process was repeated for all exposures. The corresponding observing time was read out respectively from the header of the images.
Another problem are the changing photometric conditions, like the the changing of the airmass. Since the airmass depends on the length of the way the light travels through, it changes with the altitude of the star. This leads to brightness differences in the light curve. Also clouds or the moon can appear which significantly change the conditions. For this purpose, the reference stars are recorded. They also contain these perturbations and by dividing the targets flux through their flux, these perturbations are corrected out and only the relative light changes of the target remain.

6.3. Results

Since CCDs are most sensitive to red light, the most attention was given to light curves in the R_B *channel*. To demonstrate the importance of reference stars, figure 6.6 shows the uncorrected light curve of J0650. The brightness increases in the light curve, which may be interpreted as a reflection effect. In truth, the star ascends during the observation and therefore the atmospheric absorption decreases. Since the reference stars behave similar, this effect gets corrected out and the result is the flat light curve in Fig. 6.7. A complete overview of the observation is available in table A.10.
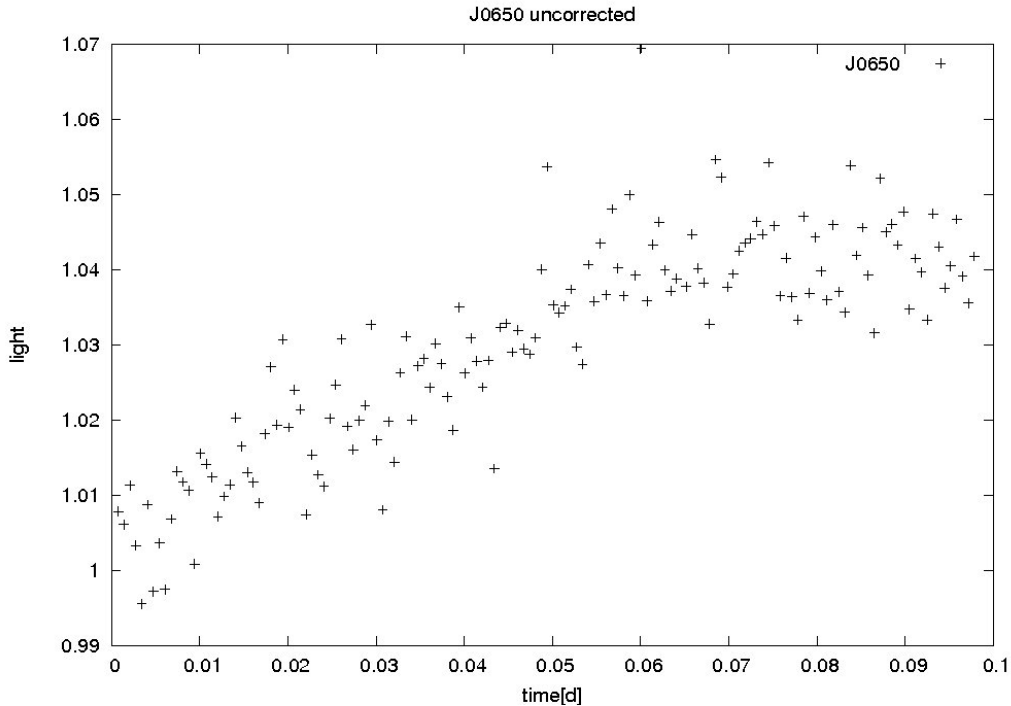
Figure 6.6.: Uncorrected light curve of J0650 in the R_B *channel*. Changing atmospheric conditions induce the light variation.

J0306, J0748, J2345 and J0650 light curves

The target J0306 was measured with a signal to noise (S/N) of 251 and a sampling rate of 104.5 seconds for 1.74 hours. The highest frequency detectable, called Nyquist frequency is therefore 0.0048 Hz. We can exclude an eclipsing binary system with orbital period shorter than 3.4 hours (assuming two visible eclipses).

J2345 was recorded with an exposure time of 55 seconds for 1.67 hours. This resulted in an effective time sampling of 71.6 seconds (Nyquist frequency 0.0070 Hz). The S/N of 179 was a bit lower than the S/N of the J2345 light curve. At this accuracy, no light variations were detectable. With the same restrictions as above, an eclipsing binary with orbital period shorter than 3.3 hours can be excluded.

The light curve of J0650 has a length of 2.33 hours with a sampling rate of 57.6 seconds. The Nyquist frequency equals 0.0087 Hz. If we assume a visible primary and secondary eclipse, we can exclude an eclipsing binary system with period shorter than 4.6 hours. Because of the worse conditions, the S/N is with 123 lower than the one for the others. At this scale no time variations are visible.

All the light curves are shown in figure 6.7. Unfortunately, the weather during the measurement of J0748 was very bad. A lot of clouds passed through the FOV which made the measurement unusable (Fig. A.1).
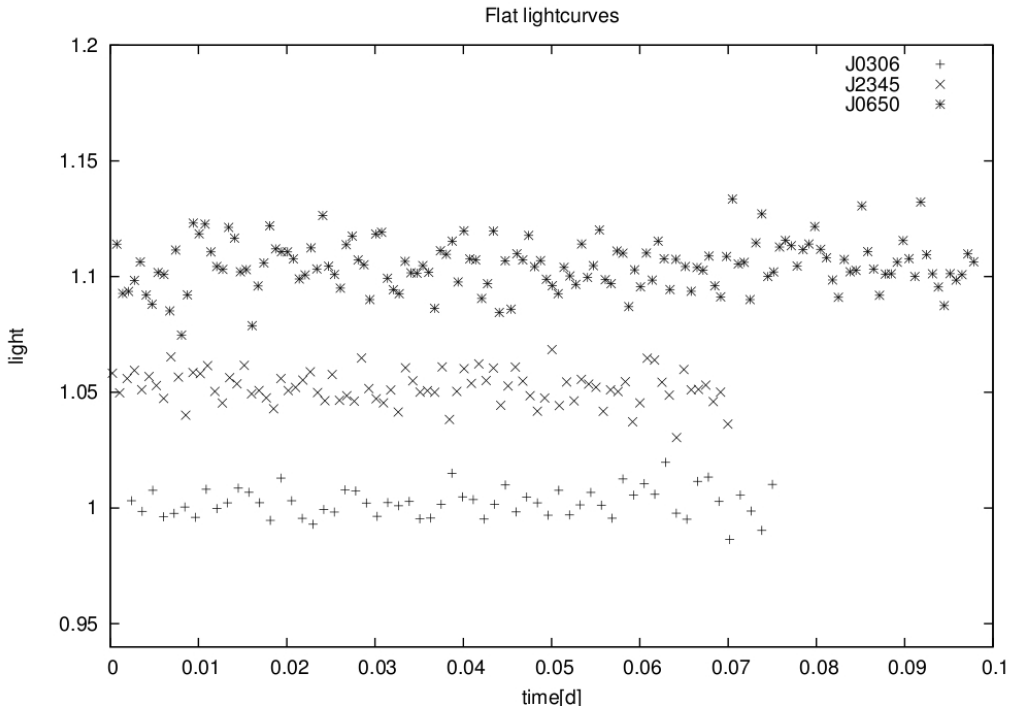
Figure 6.7.: Flat light curves of J0306, J2345 and J0650 in the R_B *channel*. For a better separation a vertical offset of 0.05 was applied.

J1920 light curve

J1920 was already recorded by V. Schaffenroth once in June 2011 for 2 hours. That light curve contained a nice reflection effect without any eclipses. This target had high priority and could be measured on the fifth night for 4.33 hours with S/N of 240. During the observation, a temporary light curve without flat field and bias corrections was reduced to see the progress. After 2 hours a small secondary eclipse occurred and the flux began to decrease. It was decided to extend the measurement for the complete period. After 4 hours the primary eclipse occurred and the measurement was shortly stopped thereafter since the star reached an altitude of only 25 degrees. Nevertheless, the complete orbital period of this eclipsing close binary system could be recorded. The orbital period is around 0.17 days and was calculated by doubling the time difference between primary and secondary eclipse. The final light curve of J1920 in the R_B channel with an exposure time of 25 seconds is shown in figure 6.8. The earlier observed reflection effect is clearly visible, the light rises by 12 percent. The reflection effect occurs when the surface of the cooler companion that is heated up by the hot sdB star points towards the observer. At the light maximum, a grazing secondary eclipse occurs since only a part of the surface is eclipsed by the sdB star. If the eclipse would be full, the light during the secondary minimum would decrease until the level where no reflection effect is visible (shortly before the primary eclipse at light level 1). At the end, when the cooler companion passes in front of the hot sdB star a primary eclipse occurs. The reflection effect indicates a big difference between the surface temperatures of the stars. In figure 6.9, the other three channels of J1920 are plotted. As expected, the quality of the infrared curve is bad. In this channel, the sdB was not bright enough to contribute enough to the signal within the 25 seconds exposure time. The ultraviolet channel has a small trend to lower light. Since extinction gets stronger with shorter wavelength, the blue sdB suffers more from the low altitude of the star than the comparison stars which leads to this trend. The strength of the reflection effect differs significantly between the channels. It has an amplitude of 0.08 in the ultraviolet and 0.15 percent in the infrared channel.

The companion is probably a low-mass main sequence star or even a brown dwarf. Follow-up spectroscopy is necessary to determine the orbital parameters of this system. Altogether, this system is very interesting and a candidate for an eclipsing binary system composed of a sdB star and a brown
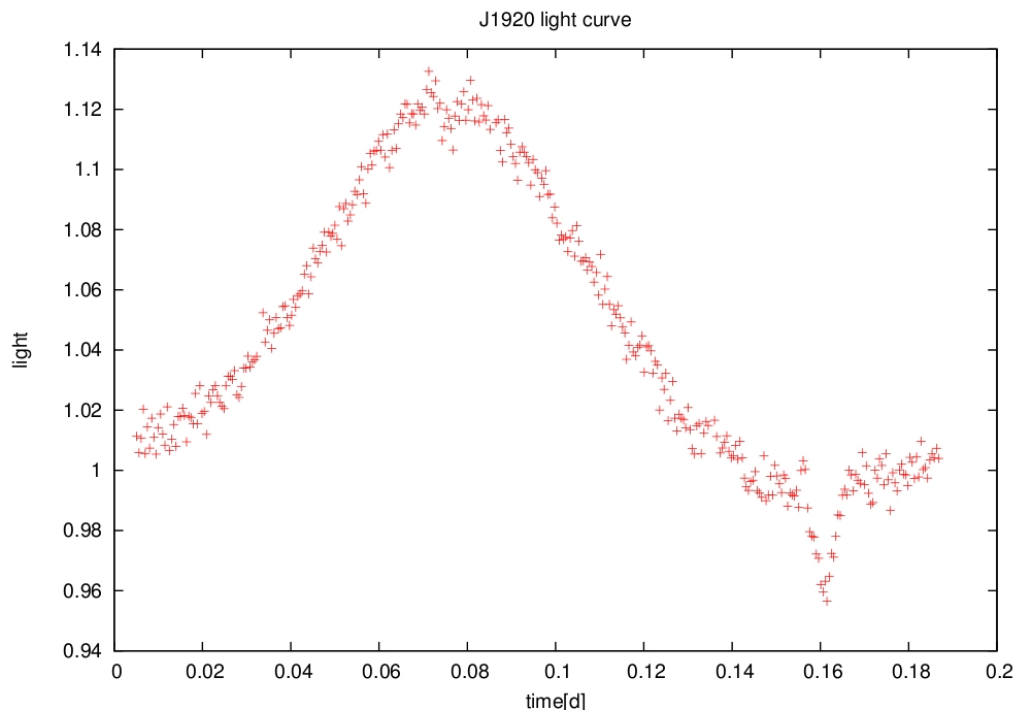
Figure 6.8.: Light curve of J1920 with the deeper primary at 0.16 d and smaller secondary eclipse at 0.07 d in the R_B *channel*.
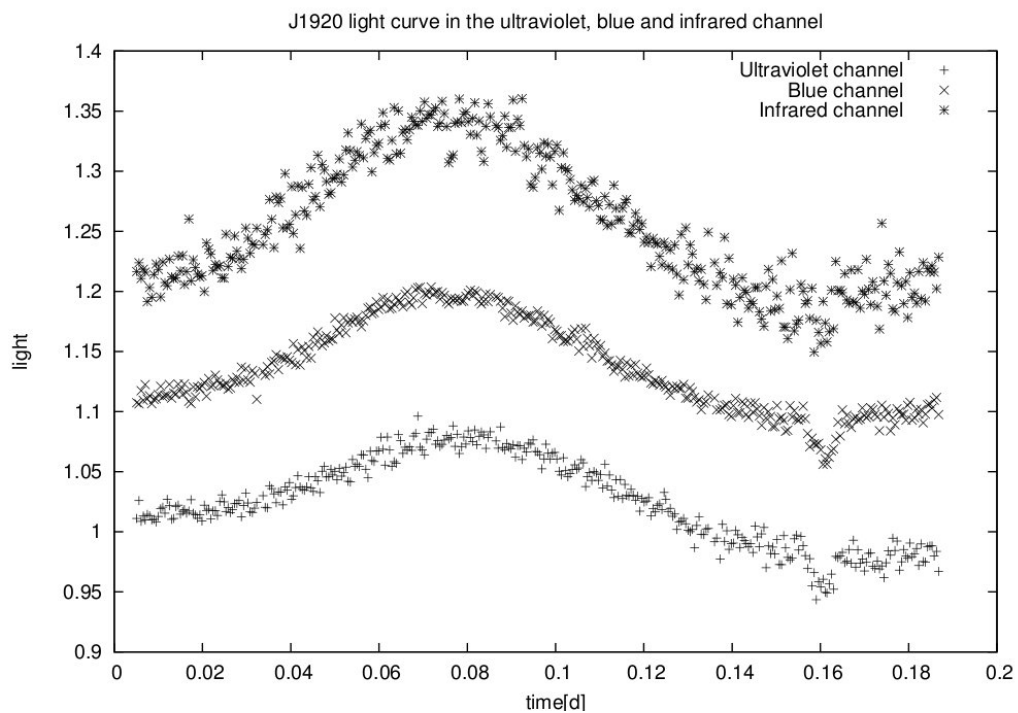

Figure 6.9.: J1920 light curves in the ultraviolet, blue and infrared channel. An offset of 0.1 was applied to separate the curves

dwarf.

7. Summary and outlook

The observation at the Calar Alto observatory revealed a new and rare HW-Virginis system with a period of 0.17 days. Because of the large reflection effect (12%) the system is a promising candidate for a binary system consisting of a sdB star and a substellar companion. Further investigations are planned and the next step would be a time series of radial velocity measurements to specify the type of the companion. Additional light curves would also help to specify the orbital period with a higher accuracy.

In the investigation of the CoRoT fields 146 oscillating stars and 45 eclipsing binary systems could been detected. Additionally, 13 targets showed very shallow eclipses and were classified as stars with possible planetary companions. The orbital period, the eclipse depths and the duration of the eclipse of the eclipsing binary systems were measured. The binary sample contained eclipse depths ranging from 1% to 47%, orbital periods from 0.36 days to 45.9 days and eclipse durations from 0.07 days to 10.8 days.

The work revealed very interesting binary systems. For example, CoRoT 110666679 had the shortest orbital period (0.36 days) among the binary systems. Systems with such short orbital periods are very rare and the processes leading to them are not completely understood yet. With the help of the spectroscopic parameter fit, T_{eff}=8.300 K and $log\ g$=4.4 dex could be determined. Moreover, calculations showed that the system can not be consisted of two main sequence stars because they would not fit into their corresponding Roche lobes. Additionally, the system has a strong decrease of the primary and secondary eclipse depths in the green and blue band compared to the red band. This puzzle could not be solved yet, neither was it possible to determine the exact types of the components. Another outstanding system was CoRoT 102714427 with a period of 1.89 days, T_{eff}=20,000 K, and $log\ g$=4.3 dex. The light curve showed a large ellipsoidal effect in combination with a shallow primary eclipse. A huge B-type companion would lead to deep eclipses, but a small star of later spectral type could not create the strong ellipsoidal effect. Therefore, a compact object for example a white dwarf companion could be a possible explanation of the system. The system CoRoT 102634660 (P=0.85 d, T_{eff}=8000 K, and $log\ g$=4.4 dex) had unequal maxima after the primary and after the secondary eclipse. This effect is called O'Connell effect and occurs in close binary systems with lower effective temperatures. The components are probably exchanging mass and are surrounded by a circumstellar material disc.

Further investigations are needed to understand the detected systems better. High resolution spectra would increase the accuracy of the determination of the stellar parameters. In many cases, the fit of the parameters did not result in reliable parameters because the components in the binary system had similar brightness contributions but could not be resolved in the used spectrum. Therefore, the measured parameters are weighted mean parameters of both stars. High resolution spectra could additionally enable to resolve the spectrum of each star. Moreover, radial velocity curves could reveal more properties of the systems. With their help it would be possible to calculate the masses and to perform reliable light curve fits to calculate the stellar radii. Unfortunately the light curves of the planetary candidates had a high contamination with light from closely located stars. Only radial velocity curves would be able to approve these systems and to decide whether the companions are stars, substellar objects, or even planets.

At the end it is worth to note, that CoRoT offers an immense dataset. The IRa01, LRa01 and LRa02 fields investigated in this work are only a small fraction of these dataset. Unfortunately, until today, there are no spectra available for the other fields. But it is save to say that the not inspected measured fields or the actual measured fields contain many interesting objects which are waiting to be discovered.

A. Appendix

A.1. List of Acronyms

CoRoT **Co**nvection, **Ro**tation and planetary **T**ransits

LEO Low earth orbit

MEDOC Multiple Experiment Data and Operation Center

LTA Long Term archive

CCD Charge coupled device

HRD Hertzsprung-Russell diagram

RV Radial velocity

sdB Subdwarf B star

WD White dwarf

MS Main sequence

EGB Extreme horizontal branch

SPAS Spectrum plotting and Analysis Suite

FAMIAS Frequency Analysis And Mode Identification for Astroseismology

EB Eclipsing Binary

O Oscillating star.

ZAMS Zero age main sequence

TAMS Terminal age main sequence

ZAHB Zero age horizontal branch

TAHB Terminal age horizontal branch

MUCHFUSS Massive Unseen Companions to Hot Faint Underluminous Stars from SDSS

SAA South Atlantic Anomaly

BUSCA Bonn University Simultaneous Camera

FOV Field of view

SDSS Sloan digital sky survey

IRAF Image Reduction and Analysis Facility

A.2. Data and additional figures

Table A.1.: Light curve classification

Field	Total	O	EB	O fraction	EB fraction
LRa02	689	71	22	0.1	0.03
LRa01	529	35	10	0.07	0.02
IRa01	436	40	13	0.09	0.03
Total	1654	146	45	0.09	0.03

Table A.2.: Classification results in Cologne

Field	Total	O	EB	O fraction	EB fraction
LRa02	780	218	24	0.28	0.03
LRa01	1002	266	35	0.27	0.03
IRa01					
Total	1782	484	62	0.27	0.03
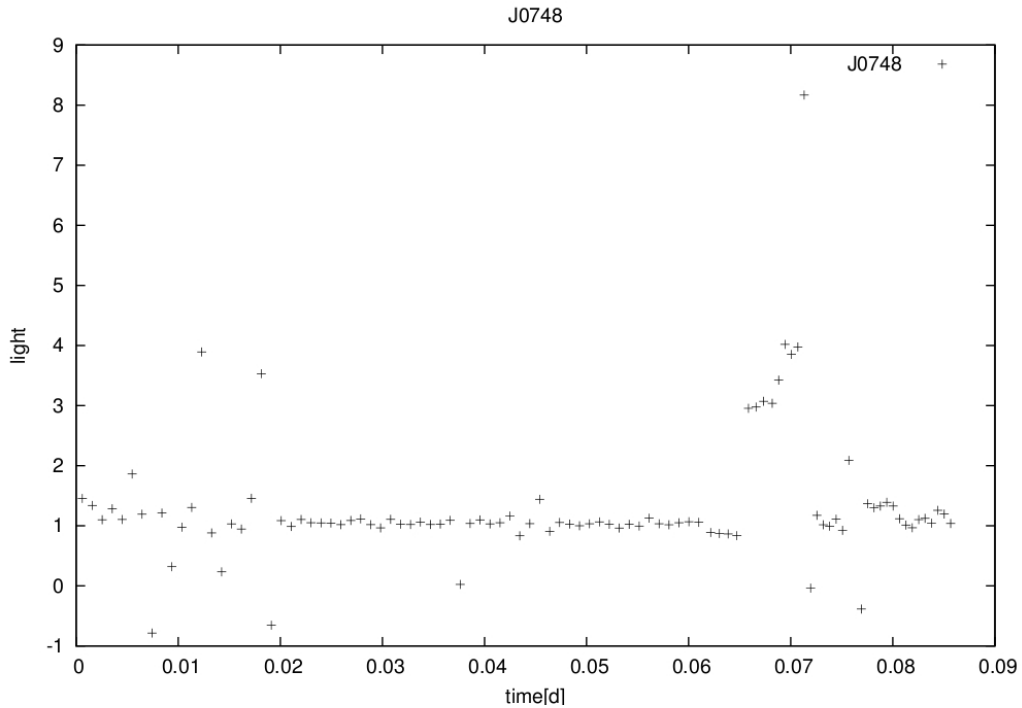
Figure A.1.: Light curves of J0748 in the R_B *channel*. Several clouds passed into the observed sky area and it was not possible to correct them out with the reference stars.

Table A.3.: Contamination of stars

CoRoT ID	Period[d]	Contamination [0,1]
LRa02		
110666679	0.35835	0.08
110856005	0.66154	0.22
110858300	1.19559	0
110659009	1.26616	0.05
102938526	1.43	0
110660662	1.84	0.3
110762262	1.88	0
110656145	1.89358	0
110764867	2.61	0
110749182	2.99	0
110684140	3.36	0.21
110750062	3.84	0
110677259	6.8	0.21
102926060	7.04	0.01
110678020	7.61	0.02
102966594	7.69	0
110671067	15.4	0.03
110856404	16.03	0
110676884	17.24	0.07
110841556	20.83	0
110857632	22.08	0.35
110826503	45.87	0
LRa01		
102725895	0.736	0.02
102634660	0.85	0.01
102631435	1.300	0.02
102648472	1.857	0.06
102714427	1.89	0.29
102717012	3.546	0
102576377	6.579	0.01
102785539	8.4	0.01
102709152	18.832	0.19
102590741	30.4	0.14
IRa01		
102912741	1.245	0.08
102858100	1.311	0.01
102982347	1.489	0
102853429	1.639	0.07
102943073	1.644	0.05
102811578	1.669	0
102776386	2.207	0.05
102806377	3.817	0.01
102918586	4.425	0.13
102852229	6.061	0.01
102870613	7.143	0.02
102943300	20.16	0
102874481	one eclipse	0.06

Table A.4.: Transit candidates

CoRoT ID	Period [d]	Visible	Why overseen
LRa02			
110858446	0.78	No	Not in sample
110756834	2.11	No	Pulsations
110666175	8.76	Yes	To shallow
103006736	1.5	No	Pulsations
110840641	8.79	No	To shallow
110853363	9.1	Yes	To shallow
110836689	0.58	No	To shallow
110774430	0.57	No	To shallow
Lra01			
102659999	0.84	–	Not in sample
102694263	1.21	Yes	To shallow
102697736	2.11	–	Not in sample
102714746	2.75	–	Not in sample
102776522	1.89	No	To shallow

Table A.5.: Detected oscillating stars in the three fields of CoRoT with their observed frequencies

CoRoT ID	f[$\frac{1}{d}$]	CoRoT ID	f[$\frac{1}{d}$]	CoRoT ID	f[$\frac{1}{d}$]	CoRoT ID	f[$\frac{1}{d}$]
Lra02		110682001	0.5	102598395	3.33	102787409	0.32
110845108	3	110682404	0.14	102599358	4.2	102797587	0.59
110846028	10	110683112	1	102604639	2.5	102800481	0.76
110848746	2.5	110683959	1.5	102674076	0.8	102803179	1.23
110854560	0.9	110688151	3.33	102678621	0.56	102804522	1
110855239	1.2	110688167	1	102682158	1	102807286	0.22
110855744	1	110688556	0.9	102684757	0.33	102812302	0.5
110864725	5	110689498	0.07	102700437	0.69	102815542	1.53
110829941	0.9	110741084	0.7	102703184	0.3	102819647	0.31
110830242	0.4	110742289	0.6	102705089	1.5	102824452	2.5
110831716	1	110742521	10	102713596	0.59	102826085	1.66
110833565	1	110744406	12	102717409	1.1	102829365	0.25
110834237	0.71	110663254	1	102744947	0.14	102831410	0.11
110835073	2	110664515	0.84	102748440	0.24	102833285	0.96
110835547	1.2	110666606	2	102749128	0.22	102840875	0.08
110839290	2	110669714	1.28	102762109	0.48	102850502	5
110840796	1.1	110670881	1	102765700	0.7	102854684	1.42
110842370	0.5	110670892	0.37	102765865	0.38	102859384	1.24
110760937	1.67	110675293	1	102765999	0.71	10287910	0.75
110765087	2	110675866	1	102766566	0.59	102880818	10
110769107	0.33	110676186	5	102768672	0.61	102911685	2
110772899	0.5	110676906	0.91	102776185	4	102913667	1.33
110826323	0.5	102902244	–	102780040	0.55	102924517	6.8
110826586	1	103006736	0.71	102794331	0.52	102945921	20
110828013	1.1	103020601	2	102795463	0.14	102956146	10
110745387	0.5	103022765	1.3	102564536	10	102956197	1
110746835	1	103042370	0.83	102573994	0.68	102960155	1
110749624	0.5	110657121	0.66	102751354	2	102963971	0.56
110749874	5	110658805	3.2	102778350	0.17	102967281	10
110750161	1	110661089	1.5	102590836	1	102973761	2.86
110752883	20	110662847	1.7	102583455	16.7	102975791	2.5
110756881	10	110843960	0.5	IRa01		102777301	2.5
110756991	2	110742626	0.66	102732363	1.03	102778314	0.92
110758142	1	110681955	7.7	102739246	1.1	102778136	0.64
110745943	0.07	Lra01		102743727	1.57	102781511	1.65
110746249	0.1	102574156	2.31	102744621	1.4	102785976	2.5
110678020	0.13	102577020	13	102754851	0.73		
110679227	1.4	102581137	1	102776418	5		

Table A.6.: Eclipsing binaries: Light curve analysis

CoRoT ID	Ra	De	Mag.	Period[d]	Rel pri.	Rel sec.	Duration [d]	Class
LRa02								
110666679	102.75	-3.72043	12.486	0.35835	0.05	0.05	0.15	EW
110856005	103.175	-3.54841	14.327	0.66154	0.2	0.14	0.31	EW(total)
110858300	103.353	-5.52384	12.63	1.19559	0.02	invis	0.08	EW
110659009	102.335	-5.44833	14.145	1.26616	0.22	0.16	0.28	EW(total)
102938526	102.327	-3.28809	11.58	1.43	0.02	0.01	0.6	EB
110660662	102.514	-4.55034	13.25	1.84	0.05	0.05	0.14	EW
110762262	103.07	-3.5987	13.653	1.88	0.3	0.15	0.29	EW
110656145	102.291	-4.41512	13.9	1.89358	0.44	0.25	0.4	EB
110764867	103.091	-4.18349	11.899	2.61	0.12	0.04	0.2	EB
110749182	102.643	-5.30851	13.78	2.99	0.06	0.04	0.07	EB
110684140	103.217	-4.07001	11.747	3.36	0.02	0.02	0.3	EB
110750062	102.656	-4.74803	12.713	3.84	0.15	0.03	0.2	EA
110677259	103.002	-3.44242	13.817	6.8	0.47	0.33	0.28	EA
102926060	102.264	-3.21895	13.217	7.04	0.05	invis	4.02	EB
110678020	103.008	-5.6381	12.019	7.61	0.44	0.33	0.4	EA
102966594	102.47	-3.19732	13.098	7.69	bad	bad	bad	EA
110671067	102.796	-4.96592	13.484	15.4	bad	bad	0.1	EA
110856404	103.179	-3.32088	13.962	16.03	0.1	0.08	0.23	EA
110676884	102.999	-3.49651	14.15	17.24	0.31	0.29	0.4	EA
110841556	102.893	-3.79848	13.796	20.83	bad	bad	bad	EA
110857632	103.19	-3.41123	14	22.08	0.13	0.11	10.8	EA
110826503	102.228	-5.51583	12.65	45.87	0.13	0.02	0.48	EA
LRa01								
102725895	101.058	0.49835	13.738	0.736	0.02	0.01	0.14	EB
102634660	100.568	-1.181	13.7	0.85	0.2	0.13	0.25	EW(total)
102631435	100.548	-1.27862	13.531	1.300	0.08	0.02	0.14	EW(total)
102648472	100.643	-0.57276	14.308	1.857	0.23	0.03	0.15	EB(total)
102714427	100.989	0.35167	12.349	1.89	0.01	invis	0.12	EW
102717012	101.004	0.1464	13.97	3.55	0.01	0.01	bad	EA(activ)
102576377	100.193	-0.65223	13.083	6.58	bad	bad	bad	EA
102785539	101.393	-0.28442	14.193	8.4	0.08	0.01	0.25	EA
102709152	100.959	-1.54322	13.736	18.83	0.05	0.03	0.5	EA(total)
102590741	100.296	-0.97935	13.42	30.4	0.02	invis	0.4	EA
IRa01								
102912741	102.196	-2.89809	13.198	1.25	0.11	0.09	0.1	EB(puls)
102858100	101.892	-3.07796	14.314	1.31	0.05	0.02	0.1	EB
102982347	102.563	-2.97465	13.728	1.49	0.12	invis	0.2	EA
102853429	101.865	-2.79528	13.361	1.64	0.01	invis	0.1	EA
102943073	102.349	-2.48166	12.691	1.64	0.04	0.01	0.12	EB(puls)
102811578	101.582	-1.98315	12.469	1.67	0.03	invis	0.09	EB
102776386	101.342	-2.86191	13.191	2.21	0.04	invis	0.17	EW
102806377	101.541	-2.0321	13.094	3.82	0.11	0.01	0.17	EA
102918586	102.226	-0.873	12.244	4.43	0.03	invis	0.1	EA(puls)
102852229	101.858	-2.77432	13.093	6.06	0.1	0.03	0.18	EA(total)
102870613	101.964	-2.68863	12.392	7.14	0.36	0.35	0.4	EA
102943300	102.351	-2.32753	13.061	20.16	0.25	0.23	0.62	EA
102874481	101.988	-2.93636	13.839	one eclipse	0.03	invis	0.32	EA

Table A.7.: Eclipsing binaries: Spectral analysis

CoRoT ID	Class[Exo]	Period[d]	$v_{rad}[\frac{km}{s}]$	$\sigma\ v_{rad}[\frac{km}{s}]$	$T_{eff}[K]$	$\sigma\ T_{eff}[K]$	$log\ g$	$\sigma\ log\ g$	Lines
				LRa02					
110666679	A5	0.35835	49	34	8300	200	4.5	0.31	4
110856005	F8	0.66154	13	14	7362	133	5.92	2	4
110858300	A5	1.19559	29	11	8100	1200	4.94	0.2	6
110659009	A5	1.26616	-3	30	15187	280	3.98	0.5	5
102938526	A0	1.43	-11	17	12883	552	3.91	0.32	6
110660662	A5	1.84	57	14	9000	1134	3.8	0.23	4
110762262	A2	1.88	54	37	18100	357	4.3	0.25	4
110656145	A5	1.89358	117	14	21300	89	4.62	0.17	3
110764867	A0	2.61	139	12	7800	573	5.02	0.19	4
110749182	A0	2.99	11	18	7500	830	5.8	0.4	4
110684140	A5	3.36	23	34	6500	1000	4	2	5
110750062	A5	3.84	-2	20	10030	91	4.16	0.5	4
110677259	F0	6.8	25	30	7588	351	5.9	0.87	4
102926060	A5	7.04	56	12	12284	1900	3.96	0.15	5
110678020	B1	7.61	39	29	8600	60	4.11	0.4	4
102966594	A5	7.69	85	30	12251	420	4.45	0.19	5
110671067	A0	15.4	62	32	8455	1900	5.22	0.22	5
110856404	A5	16.03	133	11	23200	2800	4.23	0.4	3
110676884	F6	17.24	47	53	6947	1500	4.5	0.25	4
110841556	A5	20.83	65	18	25600	1370	4.26	0.13	3
110857632	G0	22.08	30	32	–	–	–	–	1
110826503	A0	45.87	46	15	9500	2184	4.15	0.18	5
				LRa01					
102725895	K7	0.736	–	–	–	–	–	–	–
102634660	G4	0.85	23	16	8000	1000	4	1	4
102631435	G0	1.300	41	23	6900	500	4	1	4
102648472	F5	1.857	29	16	7600	600	4	1	3
102714427	A8	1.89	71	17	20000	1000	4.3	0.2	7
102717012	G0	3.55	6	2	6000	600	4	1	1
102576377	K5	6.58	62	20	6600	500	4	1	1
102785539	F5	8.4	23	10	8200	700	4	1	3
102709152	G1	18.83	65	22	7500	500	4	1	5
102590741	F5	30.4	10	–	–	–	–	–	2
				IRa01					
102912741	F6	1.25	14	10	7000	500	4	0.5	5
102858100	A5	1.31	98	7	8700	2000	4	0.5	5
102982347	A5	1.49	36	20	6300	200	4	1	4
102853429	A5	1.64	36	13	7800	300	4	1	4
102943073	F8	1.64	70	3	6800	300	4	1	2
102811578	A5	1.67	44	10	11600	900	4.6	0.4	4
102776386	A5	2.21	-5	15	7000	500	4	1	2
102806377	A0	3.82	-18	33	10000	800	4.4	0.2	4
102918586	F3	4.43	64	1	7200	2000	4	1	3
102852229	A5	6.06	17	15	7100	500	4.5	1	3
102870613	F6	7.14	13	8	7900	500	3.9	0.3	4
102943300	A0	20.16	44	7	8000	2000	4	1	4
102874481	A0	one eclipse	58	7	9000	600	3.63	0.3	4

Table A.8.: Target list for the McDonald observatory

CoRotNumber	Period[d]	Mag	Ra	De
LRa02				
110666679	0.35835	12.49	102.75000	-3.72043
110856005	0.66154	14.33	103.17500	-3.54841
110858300	1.19559	12.63	103.35300	-5.52384
110659009	1.26616	14.15	102.33500	-5.44833
110656145	1.89358	13.90	102.29100	-4.41512
LRa01				
102725895	0.73578	13.738	101.05800	0.49835
102634660	0.85035	13.7	100.56800	-1.18100
102648472	1.85773	14.31	100.64300	-0.57276
IRa01				
102858100	1.31125	14.31	101.89200	-3.07796

Table A.9.: Final list of targets for the Calar Alto observation

Name	Ra and De	V[mag]
J1920	19 20 59 +37 22 20	15.7
J1622	16 22 56 +47 30 51	16
J0150	01 50 26.10 -09 42 26.9	15.9
J0306	03 06 07 +38 23 35	16.6
J0307	03 07 49 +41 14 01	17.5
J0748	07 48 11 +43 52 39	16.8
J0830	08 30 06 +47 51 50	15.8
J1838	18 38 40 +40 02 26	17.5
J1851	18 51 29 +18 23 58	16.7
J1919	19 19 08 +37 14 23	17
J2104	21 04 54 +11 06 45	17.2
J2150	21 50 53 +13 16 50	16.9
J2219	22 19 20 +39 46 03	17
J2228	22 28 50 +39 19 17	16.1
J2345	23 45 28 +39 35 05	17.1
J2030	20 30 17 +13 18 49	16.6
J0321	03 21 38 +05 38 40	14.9
J2245	22 45 18 +22 07 46	16.3
J2339	23 39 14 +13 42 14	17.3
J2334	23 34 06 +46 22 49	17.4
J0650	06 50 44 +38 31 33	17.1
J1807	18 07 57 +23 01 33	16.9
J1844	18 44 34 +41 21 58	17.1
J2023	20 23 13 +13 12 54	17
J2208	22 08 10 +11 59 13	17.2

Table A.10.: Results Calar Alto 28.09.2011

Name	Duration[h]	Exp time[s]	S/N	Result
J1920	4.33	25	240	eclipsing
J0306	1.74	90	251	flat
J0748	1.9	70	–	–
J2345	1.67	55	179	flat
J0650	2.33	40	123	flat

List of Figures

List of Tables

Bibliography

Auvergne M., Bodin P., Boisnard L., et al., 2009, A&A506, 411

Baglin A., Auvergne M., Barge P., et al., 2002, In: B. Battrick, F. Favata, I. W. Roxburgh, & D. Galadi (ed.) Stellar Structure and Habitable Planet Finding, Vol. 485. ESA Special Publication, p.17

Baudin F., Baglin A., Orcesi J.L., et al., 2006, In: M. Fridlund, A. Baglin, J. Lochard, & L. Conroy (ed.) ESA Special Publication, Vol. 1306. ESA Special Publication, p. 145

Caroll B., Ostlie D., 2006, Introduction to Modern Astrophysics, Pearson Education, second edition

Carone L., Gandolfi D., Cabrera J., et al., 2011, ArXiv e-prints

Cordes O., 2004, Dissertation, Rheinische Friedrich-Wilhelms-Universität Bonn

Deca J., Marsh T.R., Østensen R.H., et al., 2011, ArXiv e-prints

Deleuil M., Meunier J.C., Moutou C., et al., 2009, AJ138, 649

Dorman B., Rood R.T., O'Connell R.W., 1993, ApJ419, 596

Geier S., Edelmann H., Heber U., Morales-Rueda L., 2009, ApJ702, L96

Geier S., Hirsch H., Tillich A., et al., 2011, A&A530, A28

Han Z., Podsiadlowski P., Maxted P.F.L., Marsh T.R., 2003, MNRAS 341, 669

Han Z., Podsiadlowski P., Maxted P.F.L., et al., 2002, MNRAS 336, 449

Hatzes A.P., Fridlund M., Nachmani G., et al., 2011, ApJ743, 75

Heber U., 2009, ARAA47, 211

Heber U., Drechsel H., Østensen R., et al., 2004, A&A 420, 251

Hilditch R., 2001, Introduction to Close Binary Stars, Cambridge University Press, first edition

Hirsch H., 2009, Dissertation, Friedrich Alexander Universität Erlangen Nürnberg

Lammer H., Dvorak R., Deleuil M., et al., 2010, Solar System Research 44, 520

Lee J.W., Kim S.L., Kim C.H., et al., 2009, AJ137, 3181

Maxted P.f.L., Heber U., Marsh T.R., North R.C., 2001, MNRAS326, 1391

Mayor M., Queloz D., 1995, Nature378, 355

Morales-Rueda L., Maxted P.F.L., Marsh T.R., et al., 2003, MNRAS338, 752

Munari U., Sordo R., Castelli F., Zwitter T., 2005, A&A442, 1127

Napiwotzki R., Karl C.A., Lisker T., et al., 2004, APSS291, 321

Østensen R.H., Van Winckel H., 2011, ArXiv e-prints

Pont F., Aigrain S., Zucker S., 2011, MNRAS411, 1953

Richard O. Gray, Christopher J.C., 2009, Stellar Spectral Classification, Princeton University Press

S. SöderhjelmJ. Dischler 2005, A&A 442, 1003

Schaller G., Schaerer D., Meynet G., Maeder A., 1992, A&AS96, 269

SDSS, http://www.sdss.org/

Sebastian D., Guenther E.W., 2011, In: S. Schuh, H. Drechsel, & U. Heber (ed.) American Institute of Physics Conference Series, Vol. 1331. American Institute of Physics Conference Series, p.329

Zima W., 2008, Communications in Asteroseismology 155, 17

Acknowledgements

DECLARATION

Hereby I declare that I wrote this diploma thesis autonomously and that I have not used other resources than those quoted in this work.

ERKLÄRUNG

Hiermit erkläre ich, dass ich die Diplomarbeit selbstständig angefertigt und keine Hilfsmittel außer den in der Arbeit angegebenen benutzt habe.

Bamberg, Februar 2012 ⎯⎯⎯⎯⎯⎯⎯⎯⎯⎯⎯⎯⎯⎯⎯

(Raoul Gerber)